

The role of sensorimotor afferent feedback in mediating functional recovery after spinal cord injury

Thèse N° 9227

Présentée le 7 mars 2019

à la Faculté des sciences de la vie

Unité du Prof. Courtine

Programme doctoral en neurosciences

pour l'obtention du grade de Docteur ès Sciences

par

Kay Alexander BARTHOLDI

Acceptée sur proposition du jury

Prof. B. D. McCabe, président du jury

Prof. G. Courtine, directeur de thèse

Prof. A. Levine, rapporteuse

Prof. S. Arber, rapporteuse

Prof. P. Ramdya, rapporteur

2019

Abstract

Spinal cord injury (SCI) leads to permanent deficits in sensory and motor function due to the physical disruption of descending and ascending pathways. As a consequence, spinal circuits below the level of lesion remain in an intact, but inactive state. A number of studies have shown that epidural electrical stimulation (EES) of the lumbar spinal cord can reactivate these spinal circuits after SCI. EES reversed paralysis of lower limbs in rodent and primate models of SCI as well as in a number of clinical case studies. However, although the positive effects of EES have been documented, little is known about the neural circuits through which EES enables motor pattern formation after SCI.

In the first part of this thesis, we examined the neural circuits activated by EES. In the past, modeling experiments highlighted a pivotal role for large-diameter, myelinated afferent circuits in mediating the facilitating effects of EES after SCI. Using calcium imaging and chemogenetic inactivation experiments, we confirmed that EES primarily recruits proprioceptive and low-threshold mechanoreceptor feedback circuits. We next sought to exploit this knowledge to specifically enhance the effects of EES. We found that $\alpha 2a$ receptors are prominently expressed on proprioceptive afferent neurons in DRGs, whereas $\alpha 2c$ receptors are located on low-threshold mechanoreceptor interneurons in the dorsal spinal horn. Based on this knowledge, we built a computational model that identified beneficial and detrimental interactions between EES and noradrenergic circuits. This understanding guided the design of a circuit-specific, electrochemical neuromodulation that specifically gated the effects of EES towards proprioceptive feedback circuits and re-established locomotion in paralyzed mice and rats.

The second part of this thesis uncovers the impact of movement on sensory afferent pathways. For this, mice were exposed to environmental enrichment (EE) or standard housing (SH). We found that EE primed sensory dorsal root ganglia neurons, inducing a lasting increase in their regenerative potential after SCI. This EE-mediated increase in regenerative potential was confined to proprioceptive afferent neurons and characterized through increased calcium signalling and CBP-dependent histone acetylation which is associated with enhanced gene expression. In a next step, we mimicked the exposure to EE using pharmacology. The pharmacological activation of CBP after injury enhanced axonal growth of proprioceptive afferent fibers and enhanced the recovery of sensory and motor functions.

Here, we provide direct and conclusive experimental evidence for the mechanistic understanding of EES and EE and how they mediate functional recovery after SCI. Based on this knowledge, we identified specific receptors and epigenetic mechanisms for pharmacological modulation. Our findings demonstrate the importance of large-diameter afferent fibers in mediating functional recovery and will be important in establishing a framework for the design of targeted neuromodulation therapies after SCI in human patients.

Keywords: spinal cord injury, epidural electrical stimulation, proprioceptive afferent fibers, noradrenergic α_2 receptors, enriched environment

Zusammenfassung

Verletzungen des Rückenmarks führen zu permanenten Defiziten von sensorischen und motorischen Funktionen aufgrund der Durchtrennung von auf- und absteigenden Faserbahnen zwischen Gehirn und Rückenmark. Als Konsequenz verbleiben neuronale Rückenmarksschaltkreise unterhalb einer Läsion zwar in einem intakten, aber inaktiven Zustand. Mehrere Studien in Nagern und Primaten als auch in menschlichen Patienten haben gezeigt, dass epidurale elektrische Stimulation (EES) des lumbosakralen Rückenmarks diese neuronalen Schaltkreise nach einer Rückenmarkserletzung wieder aktivieren kann. Obwohl die positiven Effekte von EES seit mehreren Jahren bekannt sind, ist bis heute nicht klar, welche neuronalen Strukturen durch EES aktiviert werden.

Im ersten Teil dieser These haben wir neuronale Strukturen, welche durch EES aktiviert werden, untersucht. Simulationsmodelle haben gezeigt, dass vor allem sensorische Neurone von Muskeln und Haut, welche in den Hinterwurzelganglionen lokalisiert sind, durch EES aktiviert werden. Durch die genetische Inaktivierung dieser Neurone konnten wir dies in Mäusen und Ratten zeigen. Dieses Wissen haben wir dann verwendet, um die Effekte von EES nach einer Rückenmarksverletzung zu potenzieren. Wir haben herausgefunden, dass noradrenerge $\alpha_2\alpha$ Rezeptoren auf propriozeptiven Neuronen lokalisiert sind, währenddem $\alpha_2\gamma$ Rezeptoren auf Neuronen im dorsalen Rückenmark exprimiert sind, welche Berührungsinformationen übermitteln. Basierend auf diesem Wissen haben wir ein Computermodell generiert, welches die Interaktion zwischen EES und noradrenergen Rezeptoren untersuchte. Durch dieses Wissen konnten wir eine spezifische, elektro-chemische Neuromodulation erzielen, welche die Effekte von EES potenzierte und das Laufmuster von Mäusen und Ratten mit einer Rückenmarksverletzung wiederherstellte.

Im zweiten Teil dieser These haben wir den Einfluss von Bewegung auf sensorische afferente Faserbahnen untersucht. Dazu wurden Mäuse entweder in grossen Käfigen mit Spielzeug und Laufrädern oder in kleineren Standardkäfigen platziert. Dadurch konnten wir aufzeigen dass mehr Bewegung das regenerative Potential von propriozeptiven Neuronen in Hinterwurzelganglionen erhöht. Das erhöhte regenerative Potential dieser Neurone führte zu erhöhtem axonalem Wachstum durch erhöhten Kalziumtransport und CBP-abhängiger Histoneazetylierung. In einem nächsten Schritt konnten wir die neuronalen Veränderungen, welche durch Bewegung in den propriozeptiven Neuronen induziert wurde, durch die Verabreichung eines Acetyltransferase CBP/p300 Aktivators imitieren. Dieser Aktivator

förderte das axonale Wachstum von propriozeptiven Fasern nach einer Rückenmarksverletzung in Ratten, was mit einer funktionellen Verbesserung einherging.

Mit diesen Studien liefern wir erstmals direkte Beweise für das mechanistische Verständnis von EES und Bewegung und über welche Strukturen diese Therapien funktionelle Verbesserungen nach einer Rückenmarksverletzung erzeugen. Basierend auf diesen Erkenntnissen haben wir Rezeptoren und epigenetische Mechanismen identifiziert, welche wir pharmakologisch moduliert haben. Diese Resultate zeigen die Wichtigkeit von afferenten Faserbahnen der Muskeln und dienen dem Design von spezifischeren Therapien für Patienten mit einer Rückenmarksverletzung.

Schlüsselwörter: Rückenmarksverletzung, epidurale elektrische Stimulation, Rehabilitation, propriozeptive afferente Fasern, noradrenerge α_2 Rezeptoren, körperliche Aktivität

Acknowledgements

I would like to thank Grégoire Courtine for giving me the opportunity to perform my PhD in his lab as well as the scientific guidance to realize this project. I learned a lot during the last four years and I will be eternally grateful for the personal and professional experiences I could make in your lab.

I would like to thank Quentin Barraud for being a scientific mentor over the last years but also a valuable friend at the same time. I was really glad to have your support and appreciated working with you, including all the low-level jokes we shared together.

A very special thank goes to Laetitia Baud for her contribution to all the functional experiments of my study. I admire your endurance, strength as well as your professionalism. I would further like to thank you for being a true friend when a true friend was needed.

I would like to thank Marco Capogrosso, Emanuele Formento and Andreas Rowald for the performed modeling experiments and the scientific contribution to my study.

I would like to thank my committee members Prof. Brian McCabe, Prof. Pavan Ramdya, Prof. Ariel Levine and Prof. Silvia Arber for taking time out of their busy schedules to serve on my committee.

During the last 4 years, I have been surrounded by a truly amazing lab team which I would like to thank for making this time a memorable period of my life. A special thank goes to Newton Cho for being a close friend and for sharing all the ups and downs during my PhD; to Nick James for the scientific guidance and the G&T sessions in Carouge; to Pavel Musienko for scientific support and discussions; to Claudia Kathe for helping out with virus-related experiments; to Jean-Baptiste Mignardot for bringing me out of my comfort zone and for the Hamperokken skyrace; to Selin Anil for her craziness and the 30km from Liddes to Verbier. Thanks to all the other lab members, as each of them contributed to the great times in this lab.

Lastly, I am truly grateful to everyone outside the lab who made this journey possible, my family in particular. A very special thank goes to my mom who supported me during good but also during bad times. I would also like to thank my brother for the great times and trips we had together.

Table of Content

Abstract	3
Zusammenfassung	5
Acknowledgements	7
I. Background and state of the art	10
1.1 Introduction to spinal cord injury	10
1.2 Disruption of descending pathways after SCI	11
1.3 Dorsal root ganglia and sensory afferent pathways	13
1.4 Locomotor training to facilitate stepping after SCI	18
1.5 Epidural electrical stimulation to activate spinal cord circuits	19
1.6 Pharmacological modulation of spinal cord circuits	20
1.7 The noradrenergic descending system	21
1.8 Direct interactions between noradrenergic receptor modulation and reflex circuits	24
1.9 The mechanism through which EES enables motor pattern formation	26
1.10 Enriched environment	28
1.11 Clinical relevance of the performed research	30
II. Synopsis and aims of the thesis	31
III. Deconstruction of the sensorimotor circuits engaged by electrical spinal cord stimulation that restore locomotion after paralysis	35
3.1 Abstract	35
3.2 Introduction	36
3.3 Results	38
3.4 Discussion	54
3.5 Materials and methods	59

IV. Activity-dependent recovery after spinal cord injury involves a druggable epigenetic mechanism	78
4.1 Abstract	78
4.2 Introduction	79
4.3 Results	80
4.4 Discussion	92
4.5 Materials and methods	96
V. Integration and perspectives	109
5.1 Refined strategies to modulate proprioceptive feedback after SCI	110
5.2 The role of low-threshold mechanoreceptors in mediating the effects of EES	110
5.3 The problematic of noradrenergic receptor modulation	111
5.4 Activity-dependent mechanisms mediated by enriched environment	112
5.5 The detailed mechanistic understanding of the applied neuromodulation allows the design of more precise clinical interventions	113
Publications and contributions	114
List of Abbreviations	116
References	117
Curriculum vitae	131

I. BACKGROUND & STATE OF THE ART

1.1 Introduction to spinal cord injury

Severe lesions of the spinal cord lead to a range of disabilities that seriously diminish the patient's quality of life. Spinal cord injuries (SCI) occur with an estimated incidence of 500'000 cases per year, and to date, more than 2 million people worldwide are affected by SCI (1). In about 90% of all cases, SCIs are the result of traumatic events such as car accidents, forms of violence, and falls (2). The degree of functional impairment mainly depends on the level of injury as well as on the extent (size) of a lesion. Injuries at the cervical spinal cord level result in upper and lower limb paralysis, whereas lesions at thoracic and lumbosacral regions lead to lower limb paralysis. In addition to the loss of motor and sensory functions, SCI can cause a large range of other functional impairments including bladder dysfunction, dysregulation of the autonomic nervous system, hyperalgesia or respiratory complications (3).

Injuries of the spinal cord are generally classified as 'complete' or 'incomplete'. The extent of a lesion and the resulting functional impairment is defined by the American Spinal Injury Association (ASIA) impairment scale (<http://asia-spinalinjury.org>). Based on the remaining sensory and motor functions, 4 different severity categories can be defined based on the ASIA impairment scale (AIS):

AIS-A Motor and sensory complete. Complete sensorimotor loss below the lesion including absent sacral sensation.

AIS-B Motor complete and sensory incomplete. Some sensory sensation is present but there is no motor function below the lesion level, i.e. no clinical evidence of voluntary control of any muscle below the lesion.

AIS-C Motor incomplete. Some motor preservation, but the majority of key muscles below the level of injury are graded 3 or less (muscle grading is out of 5, taking into account volitional movement, range of motion against gravity and capacity of resistance).

AIS-D Motor incomplete. Muscle grade is 3 out of 5 or greater in the majority of muscles below the lesion.

To date, patients with motor-complete spinal cord injuries (AIS-A and B) demonstrate very limited recovery. In these patients, the amount of spontaneous recovery is limited to preserve muscle functionality rather than motor recovery. Rehabilitation strategies are mainly designed to learn how to compensate for functional disabilities and to become independent in daily life. This includes sessions where patients learn how to use external assistive devices (4), techniques for muscular facilitation to reduce muscle atrophy (5) and ways to manage bowel and bladder problems (3). In contrast, patients with residual sensation or motor control (AIS-C and D) undergo rehabilitation procedures which include activity-based rehabilitation like daily stand-training or stepping or electrical stimulation of the spinal cord (6) or muscles (7). About 60% of these patients even regain the ability to walk with assistive devices (2).

1.2 Disruption of descending pathways after SCI

The motor system is a complex communication network dispersed over the central and peripheral nervous system. Within this system, movement is generated through the precise and orchestrated interaction between supraspinal centers (i.e. motor cortex, midbrain and brainstem), spinal circuits and sensory inputs originating from the periphery (**Figure 1A**). Supraspinal input is mediated by several descending tracts including reticulospinal, vestibulospinal, rubrospinal and corticospinal tract which convey motor commands from the brain to the spinal cord. At the same time, peripheral inputs derived from a variety of receptors located in muscles, joints or skin converge on the spinal cord where final integration and processing of these inputs take place (8). Ultimately, the spinal cord implements these incoming inputs to precisely time and control muscle contraction. Overall, these three networks are in relative balance to each other in order to adapt and

shape ongoing motor behavior. The neuronal network involved in the generation of movement has previously been described as the "motor-circuit communication matrix" (9).

A severe SCI leads to the disruption of essentially all descending fiber tracts and disrupts the balance between brain, spinal cord and sensory afferent inputs. Motor impairments after SCI are the consequence of the physical interruption of descending connections to spinal circuitries located below the level of lesion. Shortly after injury, axons retract and pathophysiological events such as demyelination and axonal dieback lead to a loss of fibers. As a consequence, spinal motor circuits below the lesion are isolated from the brain and the production of movement thus requires compensatory changes (**Figure 1B**).

After the loss of supraspinal input due to SCI, the importance of spinal neuronal networks and sensory input in controlling and maintaining locomotion is dramatically increased. A critical feature of the spinal networks is their ability to receive, interpret and process sensory information that in turn can generate the appropriate motor output. Pioneering experiments by Brown and Sherrington provided important insights into the physiological understanding of movement production at the spinal cord level. Using transected cats and dogs attached over a treadmill belt, Sherrington demonstrated that sensory information can flexibly control a range of stepping behaviours even in the total absence of supraspinal input (10). He assumed that sensory information originating from the moving treadmill belt engages sensory afferent pathways which in turn activate motor circuits in the spinal cord. The activation of spinal circuits ultimately led to an alternating stepping pattern. Moreover, Sherrington proposed that a specific type of sensory afferent fiber must be involved in the generation of the observed stepping pattern and that these afferents are innervating the responding hindlimb muscle executing the stepping movement. He termed these afferent fibers 'proprioceptive' (fibers involved in sensing the perception and control of body position and balance, **Figure 1C**). Altogether, these experiments provided first evidence that sensory information mediated by proprioceptive afferent fibers can serve as a partial compensation for the loss of brain-derived information and is capable of steering the activity of spinal circuits after injury.

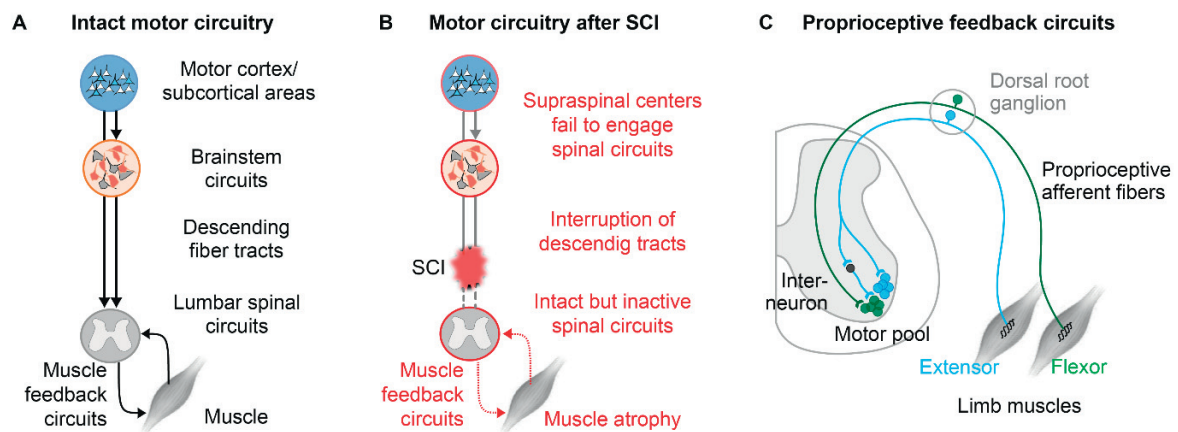


Figure 1 Disruption of motor circuitry following spinal cord injury (A) Schematic showing the different elements of the motor circuitry involved in the generation of movement. The spinal circuits integrate neuronal information from supraspinal centers and from the periphery. (B) A spinal cord injury at the thoracic level disrupts the communication between the brain and the lumbosacral spinal cord leading to hindlimb paralysis. (C) After SCI and the loss of supraspinal inputs, proprioceptive afferent input from muscles becomes very important in providing information to spinal circuits. Panel C adapted from Imai and Yoshida, 2017.

1.3 Dorsal root ganglia and sensory afferent pathways

During locomotion, the lumbosacral spinal cord receives sensory inputs from a variety of peripheral receptors located in skin, joints and muscles. These sensory afferent pathways provide the spinal cord with a dynamic representation of the limbs during stepping, first to elaborate the locomotor pattern itself and second, to rapidly adapt motor outcomes in response to unpredicted perturbations occurring during gait.

After SCI, the spinal network critically relies on the integration of sensory input to generate appropriate motor outcomes. To date, several studies have demonstrated the importance of sensory afferent feedback involved in functional recovery after SCI (11–13). Sensory neurons involved in the transmission of afferent information are located in dorsal root ganglia (DRG). DRG are assemblies of sensory cell bodies located within the spinal subarachnoid space between adjacent vertebrae. The pseudounipolar anatomy of DRG neurons allows them to convey afferent information from the periphery to the spinal cord and from there to supraspinal structures for sensorimotor integration. DRGs thus provide a direct link between the periphery and the CNS and are ideally positioned to be influenced by environmental stimuli.

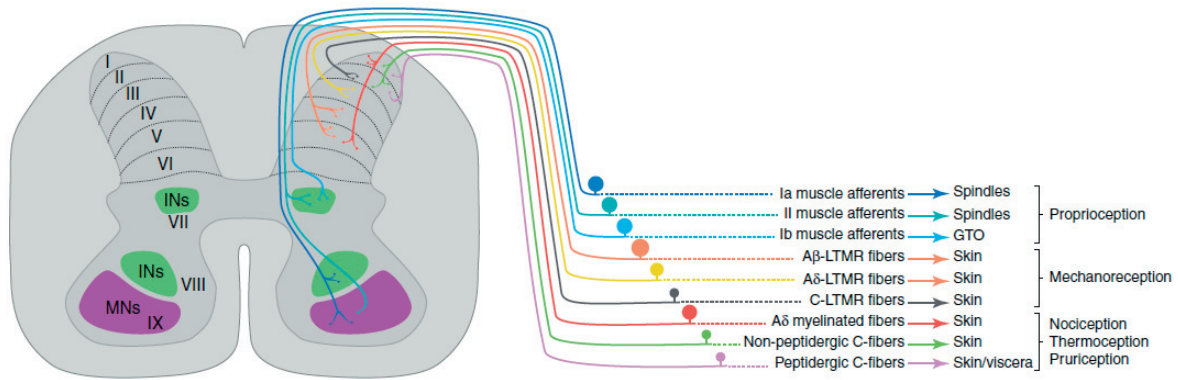


Figure 2 Sensory afferent pathways Schematic showing the different peripheral streams of sensory afferents projecting towards the central nervous system. Figure from Lallemand and Ernfor, 2012.

Sensory afferent pathways are highly segregated and the ability to discriminate between diverse types of sensation is reflected by the existence of functionally and morphologically specialized sensory neurons (14) (**Figure 2**). For example, proprioceptive afferents are large-diameter, myelinated fibers that transmit information about muscle length to the CNS (14–16). Their influence on the activity of central circuits is essential for the modulation of motor output such as the appropriate adjustment of muscle contractions during movement. Changes in the length of a muscle, i.e. induced by stretch, are primarily detected by intramuscular receptors, the muscle spindles. Muscle spindles lie within an independent capsule, parallel to the main muscle. Therefore, the muscle spindles are stretched when the muscle lengthens and shortened when the muscle contracts. Muscle spindles are located throughout the muscle and consist of specialized muscle fibers called intrafusal fibers. Two types of intrafusal fibers are located within a muscle spindle, nuclear bag fibers and nuclear chain fibers. Nuclear bag fibers are located more centrally along the fiber. Instead, nuclear chain fibers are shorter and thinner and have less centrally-located nuclei (17). Once activated by muscle stretch, these afferents convey sensory information via type Ia and type II sensory fibers to the spinal cord. Type Ia sensory afferents are the largest and fastest-conducting sensory fibers and respond to the rate of change in muscle length (stretch). As soon as the muscle stops changing its length, Ia fibers stop firing and adapt to the new muscle length. Ia fibers thus supply information about the rate of change of the respective muscle. In contrast, type II afferents provide a position sense of a still muscle, meaning that they are activated when the muscle itself is not active. A third type of proprioceptive receptor, the Golgi tendon organ (GTO), is located on musculotendinous junctions and measure the tension on a tendon induced by the contracting muscle. GTOs convey information to the spinal cord via Ib afferent fibers. Proprioceptive fibers project to intermediate and ventral spinal cord laminae where they

establish direct and indirect synaptic contacts with motor neurons and various classes of interneurons implicated in motor control (14,18). As proprioceptive sensory afferents convey information about body position, they are vital for the modulation of motor output in healthy subjects but also after SCI (12,19). A number of studies have demonstrated the importance of proprioceptive afferent fibers involved in the recovery of locomotor function after SCI.

A second stream of sensory feedback includes cutaneous afferent pathways involved in the transmission of touch information. A variety of receptors located in the dermis and epidermis of the skin detects a wide range of tactile stimuli and thus endow us with a remarkable capacity for object recognition, texture discrimination or sensory-motor feedback (20) (**Figure 3**). Each mechanoreceptor thereby displays unique response properties elicited by distinct tactile stimuli. This wide range of tactile discrimination is reflected by the qualitative difference between the sensory neurons that sense and transmit cutaneous information.

Generally, two families of mechanoreceptors involved in the perception of touch can be distinguished: low-threshold mechanoreceptors (LTMRs) and high-threshold mechanoreceptors (HTMRs). LTMRs sense innocuous light-touch and vibration and contain a broad number of receptors such as Merkel cells, Ruffini organs, Meissner and Pacinian corpuscles as well as longitudinal lanceolate endings located in the dermis. Once activated, these receptors transmit sensory information via large-diameter, myelinated A β fibers that project to laminae III/IV of the dorsal spinal cord (14,21,22). The activity of LTMRs strongly interacts with the spinal locomotor circuitry, assuming the existence of direct intraspinal connections from the laminae III/IV interneurons onto the motor system. In contrast, HTMRs sense harmful mechanical stimuli activated by mechanical pressure and stretch. They mainly include free nerve endings and convey sensory information via afferent fibers classified as A δ or C to the dorsal horn of the spinal cord.

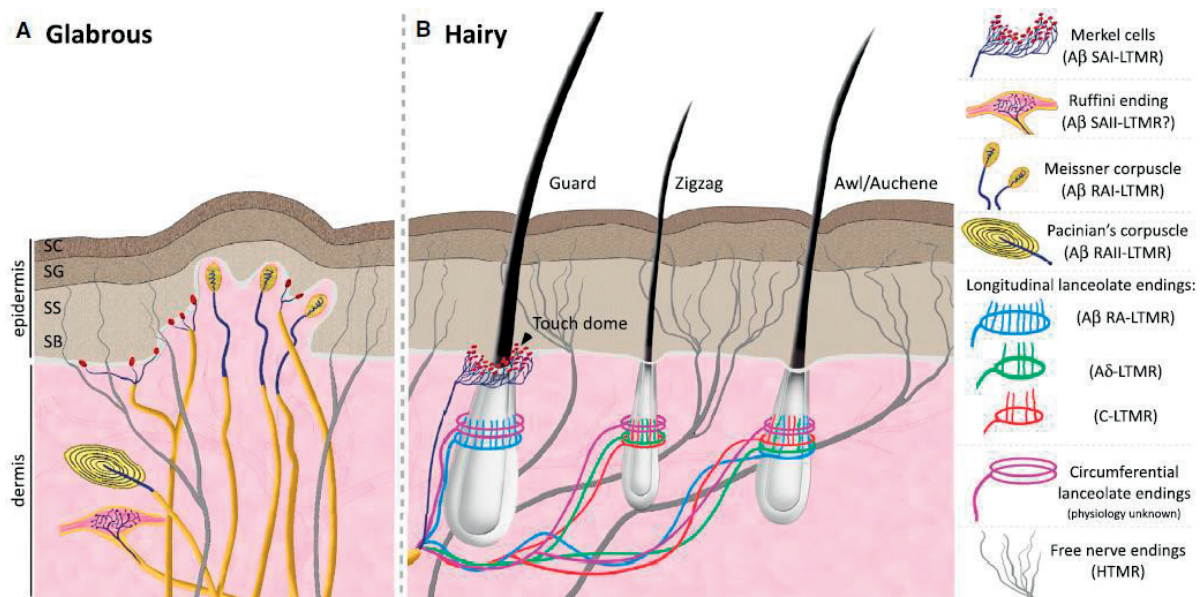


Figure 3 The organization of cutaneous mechanoreceptors in the skin (A) In glabrous (nonhairy) skin, innocuous touch is mediated by four types of mechanoreceptors (Merkel cells, Meissner corpuscles, Ruffini endings and Pacinian corpuscles). **(B)** In hairy skin, tactile stimuli are transduced through three types of hair follicles (guard, awl/auchenne and zigzag). Figure from Abraira and Ginty, 2013.

Compared to proprioceptive feedback, little is known about the influence of cutaneous afferent inputs on spinal motor circuits. Cutaneous LTMRs located on the plantar surface of the foot are not necessary for the production of basic stepping movements. In cats, the elimination of cutaneous inputs from the hindpaws did not affect the animal's ability to walk. Instead, the kinematics of hindlimb movements were altered when compared to intact cats (23). A similar altered gait pattern was observed in experiments where pulses of electrical stimulation were applied to the plantar surface of the foot in cats. Electrical stimulation during stance phase enhanced extensor muscle activity and consequently prolonged the stance phase in cats (24). Altogether, inputs from LTMRs may play a critical role in shaping normal motor function as well as in correcting motor outcomes, i.e. in response to unpredicted perturbations.

During intact stepping, cutaneous LTMRs are activated throughout the entire stance phase of the leg whereas they are inactive during swing phase (25). Cutaneous afferent feedback is thus modulated in a phase-dependent manner. In non-injured subjects, this phase-dependent inactivation of cutaneous afferent pathways is directly regulated by the brain. A recent study in monkeys demonstrated the existence of direct supraspinal connections onto cutaneous interneurons within lamina III/IV (26). These supraspinal connections are mediated by corticospinal tract (CST) fibers and control the activity of laminae III/IV interneurons by direct and phase-specific inhibition during movements. Besides this phase-dependent inactivation controlled by the brain, modulation of cutaneous information is achieved by a process called 'sensory gating'. Sensory gating occurs at the spinal cord level and has been described for different streams of somatosensory information like innocuous touch (21), itch (27) or pain (28). In monkeys, sensory gating was demonstrated by applying electrical stimulation to nerves containing either cutaneous or proprioceptive afferents during the execution of forearm reaching movements (29). Whereas cutaneous inputs were suppressed regardless of the type of movement, muscular (proprioceptive) inputs were specifically facilitated during relevant movements. This implies that, even at the spinal cord level, different streams of sensory information are modulated and gated in an input-specific process (29) and that interneurons in the dorsal horn seem to be organized into discrete functional modules that gate different streams of somatosensory information (27). Despite these recent findings, little is known about the mechanisms on how cutaneous afferents influence locomotion nor about their intraspinal connectivity scheme.

Lastly, small-diameter, non-myelinated C-fibers and lightly myelinated A δ afferents relay nociceptive and thermoceptive stimuli. These afferents are small in diameter (0.2-1-5 μ m) and project to laminae I/II of the dorsal horn (14) where they arborize locally but also project across several segments within the spinal cord (30). **Table 1** summarizes the different streams of sensory pathways involved in the transmission of afferent information.

Sensory fiber type	Class/ Group	Fiber diameter (μm)	Receptor supplied	Myelination
A α	Ia and Ib	12-20	Primary muscle spindle afferents, Golgi tendon organ	Myelinated
A β	II	6-12	Secondary muscle spindle afferents, skin mechanoreceptors	Myelinated
A δ	III	1-5	Skin mechanoreceptors, thermo- and nociceptors	Lightly myelinated
C	IV	0.2-1.5	Thermo- and nociceptors	Non-myelinated

Table 1 Sensory afferent pathways Table showing different streams of sensory pathways involved in the transmission of afferent information.

1.4 Locomotor training to facilitate stepping after SCI

Even though there have been promising therapy interventions for neuronal regeneration in animal models (31), clinical evidence demonstrating the capacity to repair the human spinal cord after SCI is still lacking. So far, the only proven effective interventions after SCI are activity-based rehabilitation strategies such as locomotor training. To date, repeated activity is the most common practice for humans with neuromotor disorders. Based on the knowledge obtained by Sherrington, the benefits of daily locomotor training to regain stepping after SCI were evaluated in a number of studies. Training as a rehabilitative strategy focuses on the reorganization of neuronal networks in the spinal cord and has been shown to be an effective possibility to regain the ability to walk in chronic, incomplete SCI patients (32). However, in patients with clinically complete lesions classified as AIS-A or B, locomotor training showed no or very limited efficacy to improve function. Nevertheless, these patients can still generate locomotor movements during assisted stepping on a treadmill with body weight support. These automatically evoked stepping movements after SCI are controlled by neuronal networks located at lumbosacral levels that coordinate the alternating activity of flexor and extensor muscles in the legs. This indicates that following SCI, the spinal circuitry below the lesion continues to maintain active and functional neuronal properties (8); however, without any therapeutic intervention it remains in an inactive state with the excitability insufficient to evoke any spontaneous movements. Several interventions to enhance and control the activity of these

neuronal networks have been described in the past years. The most promising strategies include electrical and pharmacological stimulation of the denervated spinal cord (11,33,34).

1.5 Epidural electrical stimulation to activate spinal cord circuits

The therapeutic potential of epidural electrical stimulation (EES) has been widely used to improve life quality and functionality of patients suffering from various diseases or injuries of the CNS. For example, deep brain stimulation of basal ganglia to regulate dysfunctional circuits have become common medical practices to alleviate many of the cognitive and motor symptoms of Parkinson's disease (35,36). Similarly, dorsal column stimulation has been applied for more than five decades to a wide variety of pain disorders like chronic, intractable pain or phantom limb pain (37). Moreover, several studies have shown that EES contributes to the improvement of motor function and recovery after SCI. When applied over the dorsal aspect of lumbosacral segments, EES promotes weight-bearing standing and step-like movements in experimental animals and human patients with severe SCI (33,38,39). For example, locomotor-like flexion and extension activity in the paralyzed legs in human patients with complete SCI was observed during continuous, electrical stimulation within a frequency range of 20-60 Hz (40). Recently, clinical studies reported that even human patients with severe SCI regained voluntary movements after 7 months of electrically enabled stand training (41). Animal studies have shown similar benefits of EES during treadmill stepping or standing in rats (13) and cats (42). Stimulation applied during standing induced muscle activity in the recruited muscle, whereas tonic electrical stimulation induced alternating bursts of flexor and extensor muscles during weight-bearing locomotion on a treadmill. Additionally, when applied at different sites along the lumbosacral segments, EES has been shown to promote specific patterns of locomotion; stimulation at spinal level L2 encouraged flexion of the hindlimb whereas stimulation at S1 favored limb extension. These distinct stepping features can be combined synergistically when EES is applied in a spatially and temporally controlled manner during the gait cycle using a closed-loop control system (43). Within the framework of this spatiotemporal approach, EES was applied at specific spinal levels and at specific timepoints during the gait cycle. For example, stimulation at S1 spinal level was only applied during the stance phase of the gait cycle whereas L2 stimulation was applied during swing phase. Using this approach, hindlimb movements could be controlled and modified in real time in a very detailed manner during stepping.

1.6 Pharmacological modulation of spinal cord circuits

Another strategy to increase neuronal activity after SCI consists of pharmacological stimulation of specific monoaminergic receptor subtypes. In the intact state, midbrain and brainstem neurons mediate tonic input through the release of dopamine (DA), serotonin (5HT) and noradrenaline (NA) within most laminae of lumbosacral segments during locomotion (44). The release of monoamines from these supraspinal centers acts as a slow modulatory system which increases the neuronal activity of spinal circuits through the modulation of specific receptor subtypes. Compared to excitatory signaling systems, the monoaminergic system follows a slow signaling transduction pathway that alters cell properties over a longer timescale (45). These monoaminergic inputs primarily operate peri-synaptically through diffusion, which is termed volume neurotransmission.

After SCI, descending monoaminergic fibers from brainstem areas are cut and degenerate. However, postsynaptic receptors below the lesion remain intact and can still be modulated when administering specific monoaminergic agonists or antagonists. This enabled the design of various monoaminergic therapies as a replacement strategy for the lack of neuromodulators after SCI (**Figure 4A**). Pharmacological activation of several serotonergic (5HT₁, 5HT_{2A}, 5HT₇) and dopaminergic (D₁) receptor subtypes has been tested for the efficacy to engage denervated spinal circuits in rats. Results showed that quipazine (a 5HT₂ agonist), 8-OHDPAT (a 5HT_{1A/7} agonist), and SKF-82197 (a D₁ receptor agonist), each modulated specific aspects of locomotion. The combination of these agonists further improved stepping outcomes and even potentiated the effects of EES (46). When applying EES at L2 and S1 spinal levels in combination with the administration of the serotonergic agonists quipazine and 8-OHDPAT, a number of studies has shown coordinated hindlimb stepping with plantar foot placement as early as 1 week after severe SCI in rats (11,34). In the absence of these stepping-enabling factors, no or limited stepping was observed (**Figure 4B**).

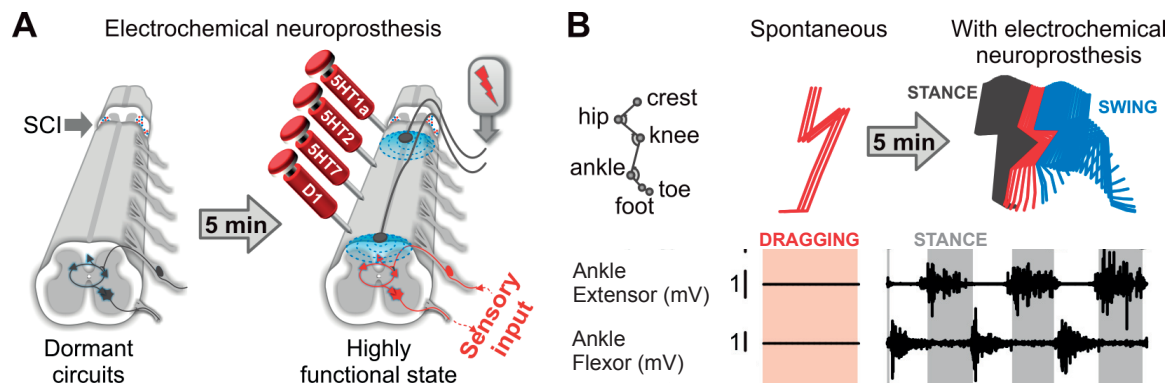


Figure 4 Electrochemical modulation of spinal circuits. (A) Electrochemical neuroprosthesis that transforms lumbar locomotor circuits from dormant to highly functional states. (B) Stick diagram decomposition of hindlimb movements and EMG activity from ankle muscles during locomotion without and with electrochemical stimulation in a rat with complete SCI. Figure from van den Brand et al., 2015.

1.7 The noradrenergic descending system

Even though noradrenergic receptors have been among the first ones targeted to restore locomotion after SCI, these receptors recently have received minimal attention as a means to pharmacologically modulate spinal circuits after injury. This might be due to the fact that the modulation of noradrenergic receptors yielded conflicting functional outcomes among different species. For example, in combination with tail pinching, the administration of clonidine (a broad noradrenergic α_2 agonist) led to a facilitation of stepping in spinal cats (47). In contrast to this, intrathecal application of the same pharmacological agent abolished all remaining muscle activity in paraplegic AIS-C patients (48). As a result, functional stepping capacities on the moving treadmill belt were abolished 25 minutes after clonidine injection.

The noradrenergic system uses noradrenaline as a hormone and neurotransmitter to exert a broad range of effects within the body. The noradrenergic system originates in the locus coeruleus located in the brainstem from where descending fibers project to several spinal cord levels. Outside the central nervous system, noradrenaline is released directly into the bloodstream by the adrenal glands where it mainly acts on the sympathetic nervous system. Noradrenaline belongs to the catecholamine family and acts on target cells by binding to and activating noradrenergic receptors located on the cell surface. The general function of noradrenaline is to mobilize the body during situations of stress and danger (fight or flight). In the brain, noradrenaline increases arousal and alertness, promotes vigilance, and focuses attention. In the rest of the body, noradrenaline affects heart rate and blood pressure or regulates the blood flow to skeletal muscles (49,50).

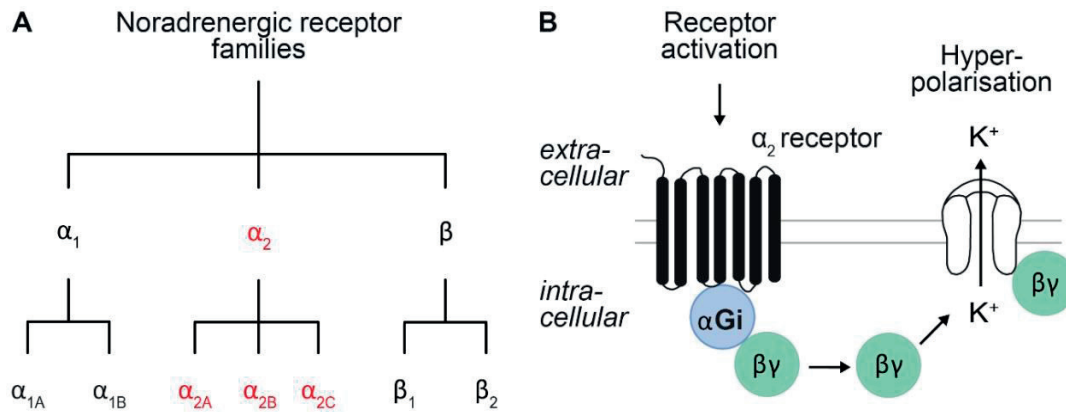


Figure 5 The noradrenergic receptor families. (A) 3 receptor families (α_1 , α_2 and β) can be differentiated among the noradrenergic receptor superfamily. Within each receptor family, several receptor subtypes exist. For the α_2 receptor family, three receptor subtypes (α_{2A} , α_{2B} and α_{2C}) can be defined. (B) Once activated, all α_2 receptor subtypes mediate a decrease of neuronal activity, i.e. by opening inwardly rectifying potassium channels (inhibitory G_i -protein signaling).

Within the noradrenergic system, three receptor families can be differentiated (α_1 , α_2 and β) based on sequence similarity, receptor pharmacology and signalling mechanisms (51,52) (**Figure 5**). Historically, α_2 receptor subtypes have been among the first ones targeted to restore locomotion after SCI in cats (47,53,54). This receptor family can be further subdivided into three receptor subtype classes (α_{2A} , α_{2B} and α_{2C}) (55). Each subtype, once activated, induces a G-protein mediated decrease of neuronal activity by opening inwardly rectifying potassium channels (56,57). α_2 receptors are found in the central and the peripheral nervous system (58). Peripheral tissues mostly express the α_{2A} and α_{2B} subtypes, with little α_{2C} . In contrast, within the CNS, radioligand (59) and *in situ* hybridization (60) experiments revealed that α_{2A} and α_{2C} receptors are predominantly expressed, whereas there is little α_{2B} receptor expression (59–61). *In situ* hybridization studies further reported α_{2A} receptor mRNA labelling in the superficial dorsal horn of the rat spinal cord (62) as well as in DRG (63). Instead, α_{2C} receptor labelling was detected in the ventral spinal cord (64) and in DRG neurons (65). In a more recent paper, the location of α_{2A} and α_{2C} receptor subtypes was examined immunohistochemically (66). Both receptor subtypes were found in superficial dorsal horn layers of the rat spinal cord as well as in DRG (**Figure 6A and C**). The primary location of α_{2A} receptors was found on laminae I/II terminals of capsaicin-sensitive, substance P-containing primary afferent fibers. This implies that the α_{2A} receptor subtype is likely to play a role in the modulation of nociceptive information at the spinal level (66). In contrast, α_{2C} receptor labelling in the dorsal horn did not appear to co-localize with nociceptive markers. Instead, some co-localization was found between α_{2C} receptors and enkephalin, suggesting that the

alpha2c receptor subtype may be expressed by a subset of spinal interneurons. These results imply that alpha2a and alpha2c receptor subtypes are likely expressed on different neuronal subpopulations and therefore may serve different physiological functions in the spinal cord.

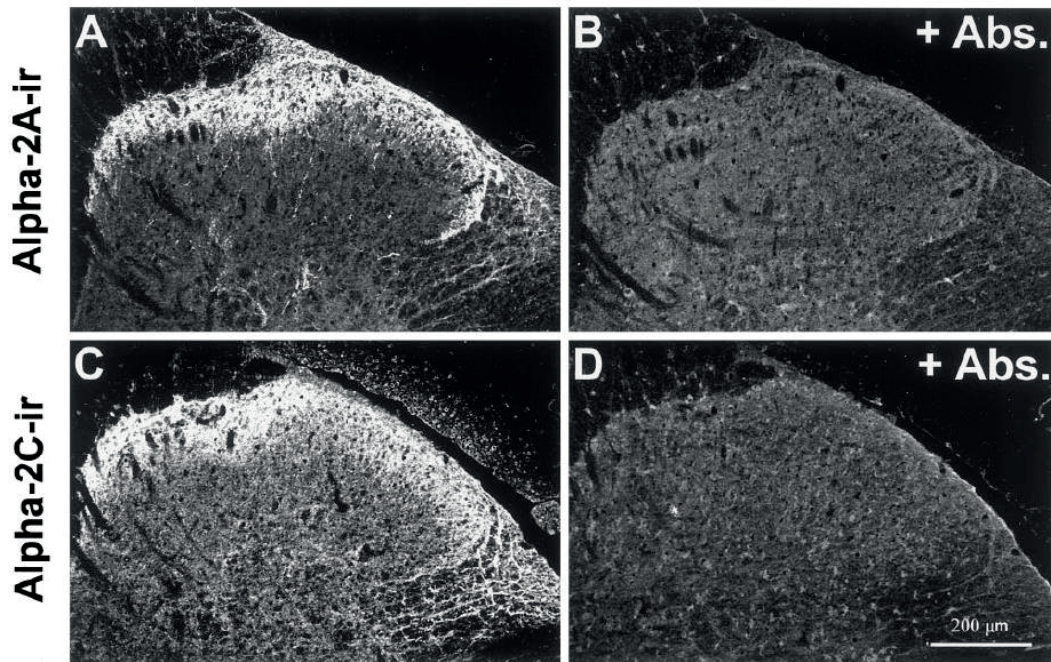


Figure 6 Characterization of alpha2a and alpha2c receptors in the rat spinal cord. Immunoreactivity for alpha2a (A) and alpha2c (C) receptors were observed in the superficial dorsal horn. Alpha2a immunoreactivity was observed in the area surrounding the central canal. Alpha2c labelling was more prevalent in deeper layers of the dorsal horn than alpha2a labelling. (B,D) Staining was blocked in both cases by pre-incubation of antiserum with the cognate peptide. Figure from Stone et al., 1998.

The detailed physiological roles and effects mediated by each of the three alpha2 receptor subtypes are still largely unknown. This is partially due to the fact that the three receptor subtypes are genetically seen highly homologous as well as due to a lack of subtype-selective drugs (67). Transgenic mouse lines carrying deletions in the genes encoding for the individual alpha2 receptor subtypes gave first insights on the physiological roles of the different adrenergic receptors (49). For example, alpha2b receptors are required for the vascular development of the placenta (placenta angiogenesis) during embryonic development. Alpha2a receptors are involved in presynaptic feedback inhibition of noradrenaline release from sympathetic nerves. Furthermore, they play an important role in the mediation of analgesic and sedative effects. Lastly, alpha2c receptors serve as feedback regulators of catecholamine release from the adrenal gland (68).

1.8 Direct interactions between noradrenergic receptor modulation and reflex circuits

Experiments in cats have shown that descending noradrenergic fibers essentially modulate the transmission in spinal reflex pathways. For example, by applying electrical stimulation to the locus coeruleus/subcoeruleus in cats, a profound depression of transmission in group II reflex pathways was observed (69). This is in line with pharmacological experiments in cats using the broad noradrenergic alpha2 agonist clonidine. The activation of noradrenergic alpha2 receptors markedly depressed the excitability of mono- and polysynaptic reflex circuitries (54,70) (**Figure 7A**), which play an important role in enabling locomotion with epidural electrical stimulation (13,71). Indeed, when combined with EES, clonidine led to a depression of locomotor states in spinal rats (72), whereas the activation of serotonergic and dopaminergic receptor subtypes enabled stepping.

In line with the above mentioned experiments in cats and rats, clonidine induced a depression of locomotor states in human patients (48). In AIS-C patients, electrophysiological testing revealed that the administration of this pharmacological agent abolished all remaining muscle activity. To date, clonidine is frequently used in the clinic to reduce over excitability of reflex circuits after SCI, i.e. spasticity.

In contrast to the activation of alpha2 receptors, the activation of alpha1 receptors through methoxamine did not induce significant changes in measured reflex outcomes or the currents needed to elicit a muscle response compared to the pre-drug testing (**Figure 7B**).

Overall, these findings imply that noradrenergic alpha2 receptors are located on the same neuronal structures that are also recruited by EES and point towards a direct interaction between noradrenergic circuits and spinal reflex pathways.

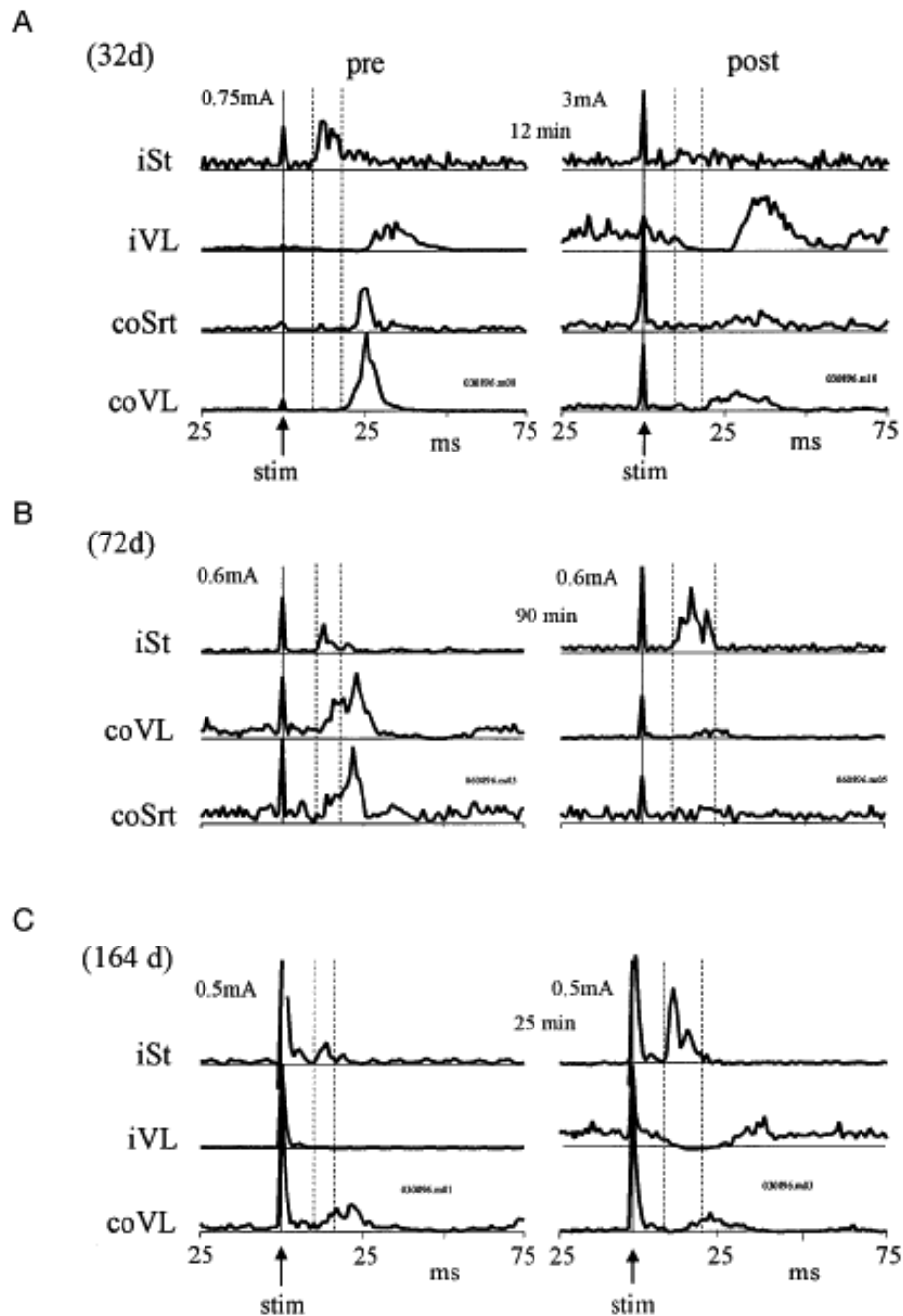


Figure 7 Comparison of responses to electrical stimulation of the superficial peroneal nerve in a cat at rest (standing). (A) Averaged response of 20 and 10 stimuli before and after clonidine injection, respectively. Electrical current delivered before clonidine injection was 0.75mA and was 3.0mA after injection. No response can be seen even at this current. (B) Averaged response of 9 and 10 stimuli before and after methoxamine injection, respectively. Current of the stimulation stayed the same (0.6mA) before and after drug injection. (C) Averaged response to 10 and 15 stimuli before and after NE injection, respectively. Current before and after drug injection was 0.5mA. Figure from Chau et al., 1998.

1.9 The mechanism through which EES enables motor pattern formation

Despite having been applied successfully over the last 50 years, little is known about the underlying mechanism through which EES enables motor pattern formation. In the past, a broad number of computational modeling studies tried to investigate the mechanisms through which EES facilitates locomotion. Computational modeling provides a tool which allows the examination of complex neural systems and the neural interactions within these systems. These experiments highlight a pivotal role for large-diameter afferent fibers in mediating the facilitating effects of EES after SCI (73–75). Based on these experiments, electrical currents flow around the spinal cord and recruit large myelinated afferent fibres in the DRG (**Figure 8A**). These afferent fibers include proprioceptors (type Ia/II and Ib afferents), and to a lesser extent, cutaneous low-threshold mechanoreceptors (LTMRs, A β afferents). The current understanding is that the recruitment of these fibers activates motoneurons through mono- and di-synaptic pathways, thereby increasing the excitability of the whole spinal locomotor network through the integration of these afferents in the spinal cord (75,76). In turn, the increased in excitability increases the spinal circuit sensitivity to sensory feedback, presumably allowing the emergence of locomotor behaviors.

Computational models were able to replicate spinal reflex curves elicited by EES. These reflexes are mainly mediated by type Ia/II afferents (**Figure 8B** and **C**). The simulations were verified by electrophysiological experiments in rats showing that each pulse of stimulation elicited well-defined mono- and polysynaptic reflex responses in hindlimb muscles (74). Additionally, the integration of inhibitory networks (Ia inhibitory interneurons) into the neuronal network steered the reciprocal activation of extensor and flexor motoneurons during specific phases of gait.

Altogether, these studies provide evidence that EES enables motor control through the specific recruitment of proprioceptive feedback circuits. However, this hypothesis has not been addressed with mechanistic tools that allow causal, unequivocal demonstration.

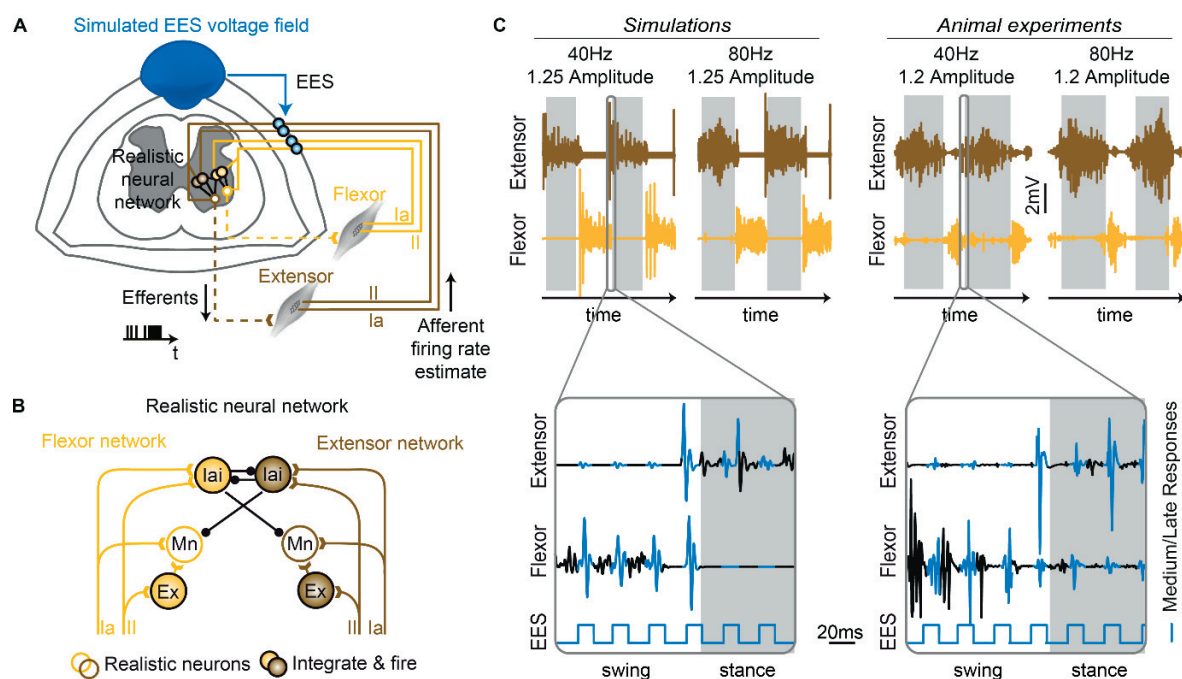


Figure 8 Computational model of muscle spindle feedback circuits (A) Biologically realistic neural network of muscle spindle feedback circuits of two antagonist muscles involved in the reciprocal recruitment of agonist muscles. This neural network includes Ia-inhibitory interneurons, group-II excitatory interneurons, and group-Ia and group-II afferents. (B) Musculoskeletal model of the rat hindlimb, prediction of the muscle stretch during locomotion for antagonist ankle muscles, and resulting firing rates using a muscle spindle model. (C) Simulations based on type Ia/II afferents were able to replicate the spinal reflex recruitment curves. This was verified by electrophysiological experiments in rats showing that each pulse of stimulation elicits well-defined mono- and polysynaptic reflex responses in hindlimb muscles. Figure adapted from Moraud et al., 2016.

1.10 Enriched environment

Besides motor training, exposure to enriched environment (EE) represents another activity-based rehabilitation strategy that has been shown to induce plasticity in the adult CNS of experimental animals. By definition, EE is 'enriched' in comparison to standard laboratory housing conditions (77). This includes animal housing in larger cages and in larger groups of animals where they have the opportunity for more social interaction. At the same time their environment is enriched by tunnels, nesting material, toys and varying food locations. Additionally, animals are often given the opportunity for voluntary physical activity on running wheels (77). EE thus represents a complex interaction between physical and social stimulation where the environment is varied over the period of the experiment (**Figure 9A**).

EE as an experimental concept was first described by Donald Hebb in the late 1940s. He reported that rats, when exposed to an enriched environment, showed behavioural improvements over rats kept at standard laboratory housing conditions. Besides the observed behavioural improvements, EE was found to have profound anatomical effects on the structure and function of neurons in various supraspinal areas such as the cortex and hippocampus (78) (**Figure 9B**). A richer and more stimulating environment has been shown to elicit various plastic responses such as increased neurogenesis or synaptogenesis (79–81). These structural changes mainly take place at a young age and, to a lesser degree, during adulthood. Ultimately these structural changes lead to increased memory and cognitive performance such as improved learning. Due to these positive effects on brain function, EE may serve as a treatment or recovery strategy for various brain-related dysfunctions like Alzheimer's disease or to counteract the symptoms of aging-related diseases like dementia. Additionally, these findings show the importance of physical exercise and learning mediated by EE at the behavioral and neurobiological level.

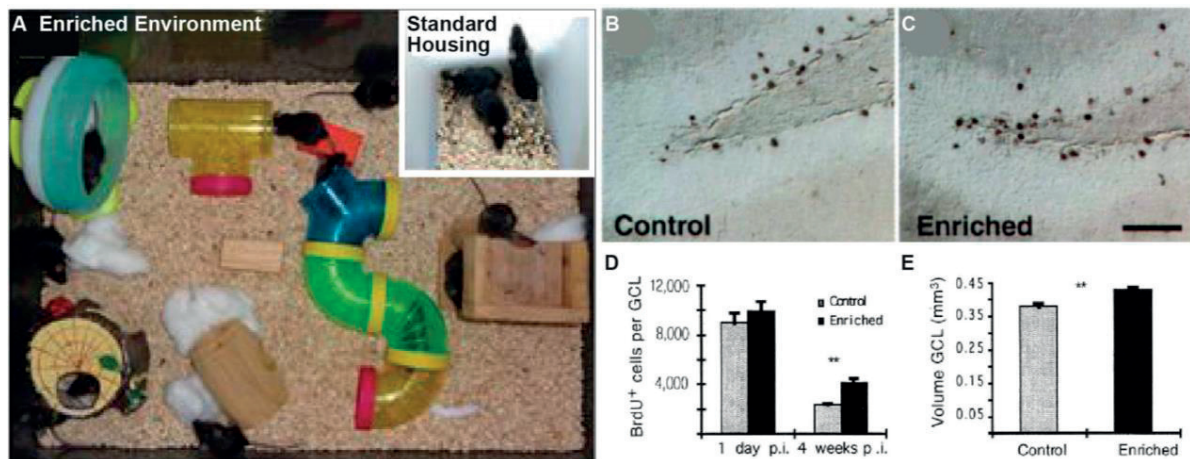


Figure 9 The concept of enriched environment and its anatomical consequences (A) Enriched environment is defined by a bigger cage size with more toys and nesting material compared to standard housing conditions. (B,C) Comparison of BrdU labelling in the hippocampus of control (SH) and enriched mice after 4 weeks of SH or EE. (D) Number of BrdU-positive cells per hippocampal granule cell layer (GCL) (E) Volume of the dentate gyrus. After 4 weeks of EE, the volume of the hippocampal dentate gyrus was significantly increased in the enriched group ($P < 0.005$). Panels adapted from Kempermann et al., 1997.

So far, research on EE mainly focused on anatomical changes at the supraspinal level whereas changes at the spinal cord level have received little or no attention. Taking into account the importance of spinal circuits and afferent pathways in processing and transmitting sensory information involved in the generation of movement, neuronal plasticity in response to EE might also occur at these levels. For example, DRG neurons are ideally positioned to be influenced by environmental stimuli as they are located at the interface between the peripheral and the central nervous system. The location of DRG neurons allows them to convey afferent information from the periphery to the spinal cord and supraspinal structures for sensorimotor integration. Specifically, proprioceptive neurons have been shown to be heavily involved in steering lumbosacral neuronal networks and in modulating motor output (12,19). This implies that increasing sensory input through different rehabilitation strategies like motor training or exposure to EE may force structural changes within proprioceptive afferent pathways and ultimately lead to functional improvements. To date, the underlying mechanisms accompanying proprioceptive plasticity in response to EE are not well understood and need further investigation.

1.11 Clinical relevance of the performed research

Several studies in the past have shown the promising effects of EES and EE in modulating neuronal circuits and improving functional outcomes after various diseases of the CNS. However, the molecular mechanisms responsible for this plasticity and recovery remain obscure and a more in-depth understanding is missing. So far, this lack of mechanistic understanding might have been due to the lack of scientific tools that allow specific targeting of neuronal populations and circuits. Over the last 5-6 years this situation has changed dramatically. Along with the development of techniques such as optogenetics or DREADDs (Designer receptor exclusively activated by designer drugs) that allow the reversible manipulation of specific neuronal circuits and populations, the identification of networks controlling behavior and/or disease has become possible.

The research conducted in this thesis aims to identify the underlying circuits activated by EES and EE. In order to improve current therapeutic interventions in human patients, there is a critical need to understand the underlying mechanisms of the applied therapy. For example, in most clinical settings, inadequate resources combined with the increased fatigability of spinal cord injured patients, means the intensity of physical rehabilitation is limited (82,83). This increases the importance of understanding the underlying mechanisms to further optimize stimulation protocols and training sessions to ultimately enhance rehabilitation outcomes. One possibility to further optimize therapy-mediated effects may lie in the application of more refined electrical stimulation parameters to specifically recruit the structures of interest or in the identification of pharmacological targets in order to enhance the effects of EES or EE. Thus, findings presented in this thesis may lead to the design of more precise and more economic interventions for human patients in the future.

II. SYNOPSIS & AIMS OF THE THESIS

Over the past decade, the Courtine lab has developed a neuroprosthetic rehabilitation strategy to reactivate lumbosacral spinal cord circuits with the goal to restore locomotion in rodents, non-human primates and human patients after a paralyzing SCI. An important aspect of this rehabilitation strategy is the use of EES to reactivate lumbar spinal circuits. Several studies over the past years have shown that EES, when applied over the dorsal aspect of lumbosacral segments, promotes weight-bearing standing and step-like movements in experimental animals and human patients with a severe SCI. Despite the successful application of EES, the underlying mechanisms of this treatment are not well understood. Even though modeling studies point towards the importance of large-diameter afferent fibers in mediating the effects of EES, this finding has not been demonstrated directly and conclusively at the anatomical level. Therefore, I thoroughly investigated the mechanisms mediating recovery of hindlimb control due to EES by employing a series of experiments in rats and transgenic mice.

Similarly, little is known about the structural changes on sensory afferent pathways induced by enriched environment. In collaboration with Prof. Simone di Giovanni and Dr. Thomas Hutson from Imperial College London, I provided help to establish some experimental techniques as well as to manage transgenic mouse lines needed to conduct these experiments.

AIM 1. Demonstrating the importance of proprioceptive afferent fibers in mediating the effects of electrical spinal cord stimulation

There is growing evidence that EES contributes to the improvement of motor function and recovery after SCI. However, the neuronal structures through which EES enables motor pattern formation remain poorly understood. The first aim of this thesis was to demonstrate unequivocally the neuronal structures activated by EES. Using calcium imaging and chemogenetic inactivation experiments in transgenic mice and rats, we show that EES recruits proprioceptive and low-threshold mechanoreceptor afferent circuits. This aim is fully addressed in the first part of this thesis and sets the research framework for the following aims.

AIM 2. Targeted modulation of noradrenergic alpha2a and alpha2c receptor subtypes facilitates locomotion enabled by EES

We next reasoned that pharmacological agents could potentiate the activity of large-diameter afferent circuits to augment the facilitation of locomotion during EES. Several studies in the past have shown a direct interaction between noradrenergic alpha2 receptor modulation and mono- and polysynaptic reflex circuitries which are mediated by large-diameter afferent fibers.

At the spinal cord level, the alpha2 receptor family is mainly represented by alpha2a and alpha2c receptor subtypes. To study the contribution of these alpha2 receptors to the production of locomotion by EES, we conducted clonidine experiments in mice lacking alpha2a or alpha2c receptors. The combination of EES and Clonidine failed to facilitate locomotion in mice lacking alpha2c receptors, whereas mice lacking alpha2a receptors exhibited alternating locomotor movements under the same stimulation paradigm.

We confirmed the opposing role of alpha2a and alpha2c receptors in rats by injecting a dual alpha2a antagonist/alpha2c agonist. This agent allows the inactivation of alpha2a receptors while inactivating alpha2c receptors at the same time. The injection of this pharmacological agent significantly increased reflex responses compared to the pre-drug condition.

We next evaluated the functional impact of this noradrenergic agent in combination with EES to restore walking in rats whose spinal cords were completely transected. When positioned bipedally over a moving treadmill belt, the administration of the dual alpha2a antagonist/alpha2c agonist alone exerted no visible influence on muscle activity. Rats essentially dragged both hindlimbs along the treadmill belt. Strikingly, as soon as EES was switched on, all tested rats displayed robust, weight-bearing locomotor movements with

clearly alternating EMG bursts in antagonist muscles. Locomotion arrested immediately when EES was switched off, but resumed as soon as EES was reintroduced.

Based on these functional outcomes, we suggested that alpha2a and alpha2c receptors are located on distinct circuits that are both engaged by EES. They further implied that alpha2a and alpha2c receptors play opposite roles in the regulation of locomotion enabled by EES.

AIM 3. Alpha2a and alpha2c receptors are expressed on proprioceptive and low-threshold mechanoreceptor feedback circuits

By using transgenic mouse lines expressing GFP under the alpha2a or alpha2c promotor (alpha2a^{GFP} and alpha2c^{GFP} mice), we found that noradrenergic alpha2 receptors are expressed on large-diameter, myelinated feedback circuits. While alpha2a receptors are prominently expressed on proprioceptive neurons located in DRGs, alpha2c receptors are mainly found on excitatory interneurons in laminae III/IV of the spinal cord gray matter. These alpha2c^{ON} interneurons co-localized with ROR α , a marker for interneurons involved in the transmission of cutaneous low-threshold mechanoreceptor afferent information.

These results confirmed the distinct distribution and phenotypes of neurons expressing alpha2a or alpha2c receptors within the spinal cord and DRGs, including PV^{ON} and ROR α ^{ON} interneurons that are both activated by EES.

AIM 4. Computational modeling to study intraspinal circuits involved in the transmission of low-threshold mechanoreceptor feedback

To disentangle the structural and functional properties of proprioceptive and LTMR circuits and their responses to the modulation of alpha2 receptors, we modeled the interactions between these two feedback circuits during locomotion enabled by EES. For this, we reconstructed intraspinal pathways of proprioceptive and LTMR afferents and their downstream connections onto motoneurons. Based on this knowledge, simulations showed that EES interacts synergistically with natural sensory feedback mediated by proprioceptive afferents.

In contrast, as LTMR feedback is activated in a phase-dependent manner during the step cycle, simulations showed that the continuous activation of these feedback circuits interacts negatively with proprioceptive feedback circuits, suggesting that down-regulating their excitability would augment muscle responses elicited by EES.

These simulations confirmed that upregulating proprioceptive circuits in conjunction with an inactivation of LTMR feedback circuits engages hindlimb motoneurons underlying locomotion produced by EES.

AIM 5. Intrathecal delivery of the dual alpha2a antagonist/alpha2c agonist facilitates locomotion in rats with clinically relevant SCI

Finally, we sought to test whether this targeted intervention could reestablish functional interactions between residual supraspinal pathways and the spinal cord located below a clinically relevant contusion injury. To evaluate the supraspinal (*voluntary*) control of leg movements, contused rats were positioned bipedally in a robotic body weight support assisting overground locomotion (84). Surprisingly, the systemic (I.P.) delivery of the dual alpha2a antagonist/alpha2c combined with EES failed to facilitate locomotion in all tested rats. Our lab previously demonstrated that a severe contusion spares a subset of descending projections from glutamatergic neurons located in the ventral gigantocellular nucleus, and that these neurons relay the cortical command to the lumbar spinal cord to produce voluntary locomotor movements after SCI (85). We found that alpha2c receptors are frequently expressed on neurons in the brain and brainstem, including glutamatergic neurons located in the ventral gigantocellular nucleus. We thus surmised that the activation of alpha2c receptors may inactivate these neurons, thus preventing the transmission of the supraspinal command to the lumbar spinal cord. To test this hypothesis, we administered the dual alpha2a antagonist/alpha2c agonist intrathecally over the lumbar spinal cord. Using this route, all tested rats exhibited voluntary leg movements that allowed them to cross the entire extent of the runway.

AIM 6. Environmental enrichment induces a lasting increase in the regenerative potential of proprioceptive afferent neurons

The second part of this thesis uncovers the impact of movement on sensory pathways. For this, mice were exposed to enriched environment (EE) or standard housing (SH) prior to injury. In contrast to SH, EE primed sensory DRG neurons and induced a lasting increase in their regenerative potential. This EE-mediated increase in regenerative potential is specifically linked to the increased activity of proprioceptive afferent neurons. Within these neurons, EE induced an increase in calcium signalling and epigenetic reprogramming via CREB Binding Protein (CBP)-dependent histone acetylation, associated with enhanced gene expression. This resulted in gene expression changes selectively found in proprioceptive neurons, accompanied by an increased, intrinsic growth potential.

Lastly, the exposure to EE was mimicked pharmacologically. The pharmacological activation of CBP by TTK21 (a CBP activator) after injury was performed in rats after contusion injury. When injected after injury, the pharmacological activation of CBP enhanced axonal growth of proprioceptive afferent fibers and enhanced the recovery of sensory and motor functions.

III. CHAPTER I

Deconstruction of the sensorimotor circuits engaged by electrical spinal cord stimulation that restore locomotion after paralysis

3.1 Abstract

Epidural electrical stimulation (EES) targeting the human lumbosacral posterior roots restored locomotion after spinal cord injury (SCI). However, the circuits engaged by EES remain unknown, despite the importance of this knowledge to refine and disseminate this therapy clinically. Here, we demonstrate that EES recruits proprioceptive and low-threshold mechanoreceptor afferents within the dorsal roots. Targeted silencing of proprioceptive feedback circuits revealed that EES modulates these pathways to produce motor patterns. In contrast, the non-physiological recruitment of low-threshold mechanoreceptor feedback circuits diminished the functional outcomes enabled by EES. Computational simulations then steered the design of a pharmacological intervention targeting the identified circuits to enhance the beneficial effects of EES. This intervention amplified the facilitation of walking with EES in a clinically-relevant model of severe SCI, opening perspectives for designing precise neuromodulation therapies in humans.

Adapted from manuscript in preparation. **Deconstruction of the sensorimotor circuits engaged by electrical spinal cord stimulation that restore locomotion after paralysis.**

Kay Bartholdi*, Quentin Barraud*, Andreas Rowald, Emanuele Formento, Nicholas D James, Thomas Hutson, Newton Cho, Claudia Kathe, Jordan Squair, Laetitia Baud, Nathalie Mestdagh, Eric Jnoff, Silvestro Micera, Simone Di Giovanni, Pavel Musienko, Marco Capogrosso & Grégoire Courtine.

*Equally contributing authors

3.2 Introduction

The regulation of dysfunctional brain and spinal cord circuits with electrical stimulation using implantable neural interfaces has broadened the spectrum of therapeutic options to treat or alleviate symptoms associated with various neurological disorders. The most common treatments involve the surgical placement of deep brain stimulation electrodes within the basal ganglia of individuals with Parkinson's disease (35,36), and the insertion of electrode arrays over the posterior spinal cord of individuals suffering from chronic pain (86,87). However, the number of neurological conditions that may be addressed with electrical neuromodulation therapies is expanding quickly.

One noticeable example is the recovery of walking after spinal cord injury (SCI). Three independent studies showed that epidural electrical stimulation (EES), when applied over the lumbar spinal cord, enabled voluntary control of locomotion in a patients who had sustained a SCI leading to severe or motor complete paralysis (41,88,89). These proof-of-concept studies stress the importance of uncovering the underlying mechanisms that mediate the facilitation of movement with EES.

Mounting evidence suggests that the application of EES over the dorsal aspect of the spinal cord recruits large-diameter afferent fibers (73,74,90,91). These afferent fibers primarily innervate muscle proprioceptors (type Ia/Ib/II) that transmit information about the length of a muscle as well as the tension applied to its tendon. Albeit to a lesser extent, afferent fibers recruited by EES also include low-threshold mechanoreceptors ($A\beta$ afferents) that convey information about innocuous light touch sensation (21). These two types of afferent feedback circuits strongly modulate the activity of motoneurons, both directly and indirectly through the recruitment of spinal interneurons involved in motor control. These sensorimotor circuits are essential for the modulation of motor output and play a critical role during locomotion (12,16,92).

However, the mechanisms through which EES recruits these afferent fibers, their respective contribution to the production of locomotion, and the spinal circuits engaged by their recruitment remain unclear. This understanding has far-reaching implications, since the identification of the recruited neural structures and intraspinal circuits may support the design of more precise stimulation protocols that are more efficacious and can be applied to a broader population of patients.

Here, we establish causality between the recruitment of proprioceptive afferent fibers with EES and the formation of motor patterns through the resulting activation of proprioceptive feedback circuits. However, we also show that the recruitment of low-threshold mechanoreceptors diminishes functional outcomes enabled by EES.

Consequently, we designed a pharmacotherapy that amplifies the activation of proprioceptive feedback circuits with EES, while reducing the activity of circuits linked to low-threshold mechanoreceptors. This pharmacotherapy led to the immediate production of locomotion in a clinically relevant model of paralysis in rats.

3.3 Results

EES engages proprioceptive neurons within dorsal root ganglia

Parvalbumin (PV) is expressed by the majority of proprioceptive neurons (93). To visualize proprioceptive feedback circuits, we cleared the dorsal roots, DRGs and lumbosacral spinal cord of PV^{Cre}:R26^{LSL-tdTomato} mice. CLARITY-optimized light-sheet microscopy revealed large bundles of proprioceptive afferent fibers located within the dorsal roots that emerged from dense populations of PV^{ON} neurons concentrated within the DRGs. These bundles penetrated the spinal cord through a continuum of rootlets distributed along the entire extent of the dorsal lumbosacral spinal cord (**Figure 10A**).

Computational modeling studies suggested proprioceptive feedback circuits are the primary neural structures engaged by EES, but the recruitment of proprioceptive neurons located in the dorsal root ganglia (DRG) with EES has never been visualized directly.

To validate these predictions and to assess whether EES activates proprioceptive feedback circuits, we imaged intracellular calcium levels in the L2 DRG of PV^{Cre}:R26^{LSL-tdTomato} mice in response to continuous EES applied over the midline of the L2 spinal cord segment for 30 minutes (**Figure 10B**). We first parametrized EES at the intensity (1.2x muscle response threshold) and frequency (40 Hz) that are commonly employed to facilitate walking after SCI. This stimulation led to a robust increase in the levels of calcium released from intracellular stores of PV^{ON} neurons (**Figures 10C and 10D**). In contrast, PV^{OFF} neurons required stimulation intensities as large as three times the muscle response threshold to exhibit a similar increase in calcium levels. At this intensity, EES did not recruit additional PV^{ON} neurons compared to EES applied at 1.2x threshold stimulation. This indicates that PV^{ON} cells activated by EES were nearly all recruited at lower intensities commonly delivered to facilitate walking with EES (1.2x motor threshold).

These results showed that EES robustly activates proprioceptive neurons concentrated in the DRGs through the recruitment of their large-diameter, myelinated proprioceptive afferent fibers. In contrast, EES delivered at threshold intensity had no detectable influence on non-proprioceptive DRG neurons whose afferent fibers encompass small- to medium-size diameters and are often lacking myelin.

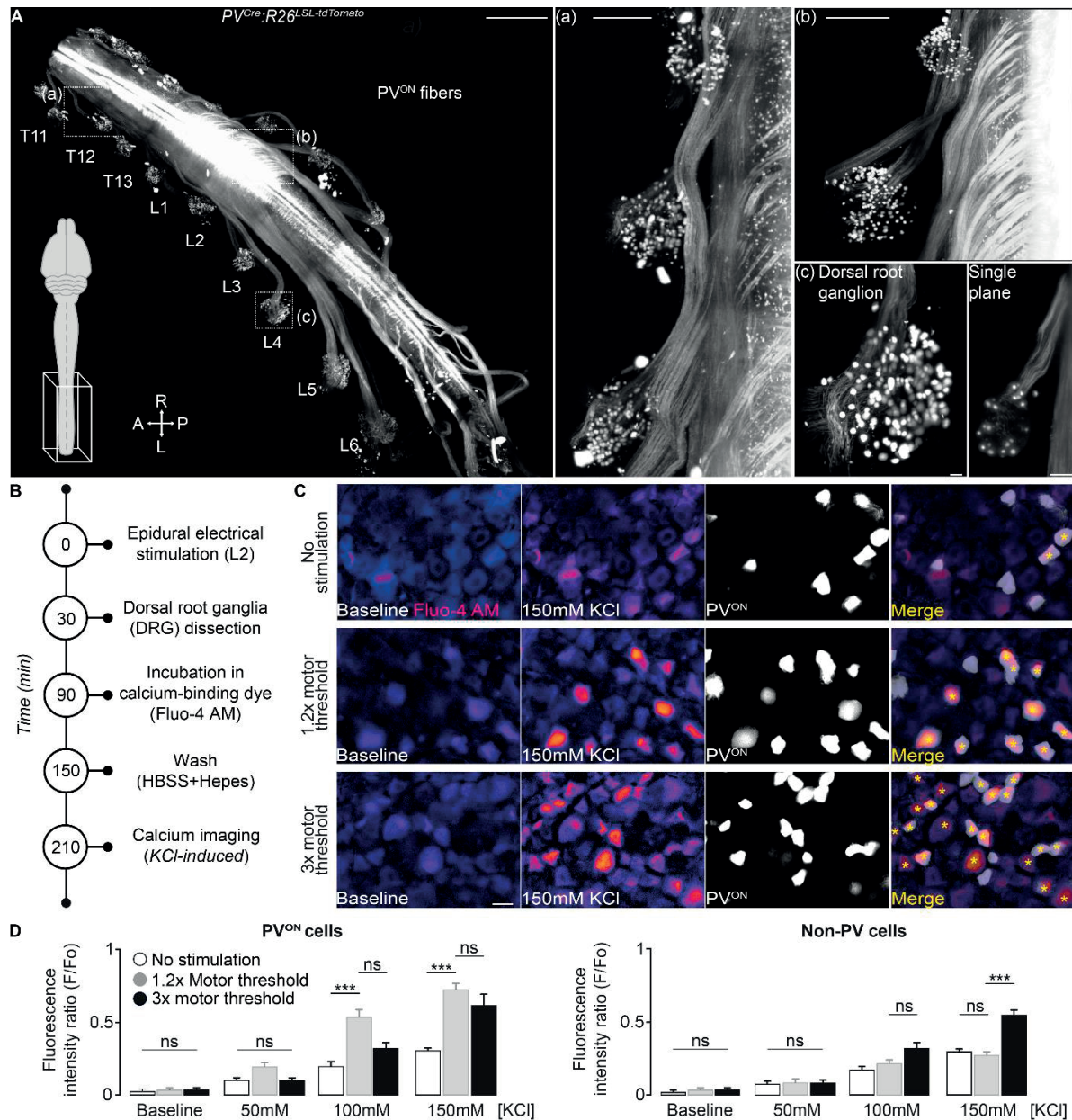


Figure 10 Epidural electrical stimulation (EES) recruits proprioceptive neurons in DRG (A) Cleared lumbar spinal cord with attached DRGs of a $PV^{Cre};R26^{LSL-tdTomato}$ mouse. Insets show proprioceptive afferent fibers and neurons in DRGs. Scale bars, 2mm (overview), 500 μ m (a), 500 μ m (b), 50 μ m (c) and 25 μ m (single plane) for the insets, respectively. (B) Timeline summarizing calcium imaging experiments. Experiments were conducted on $PV^{Cre};R26^{LSL-tdTomato}$ mice under three experimental conditions: no stimulation (n=5), EES at 1.2x motor threshold (n=5) and EES at 3x motor threshold (n=5). (C) Representative images of intracellular calcium release in L2 DRG for each experimental condition. Asterisks indicate double-labelling between the released intracellular calcium and PV^{ON} and/or PV^{OFF} neurons. Scale bar, 50 μ m. (D) Bar plots reporting calcium release in L2 DRGs for each experimental condition. EES at 1.2x motor threshold led to an increase in calcium release in PV^{ON} neurons. In contrast, PV^{OFF} neurons did not release significantly more intracellular calcium at this stimulation intensity. **P = 0.0031. ns, not significant. Two-way ANOVA followed by Tukey's post-hoc test.

EES engages proprioceptive feedback circuits to facilitate walking after SCI

We next sought to establish a causal link between the recruitment of proprioceptive feedback circuits and the recovery of locomotion with EES after SCI.

For this, we performed targeted silencing of PV^{ON} neurons using chemogenetics (DREADDs). We injected AAV2/5-flex-h4mDi-mCherry into both sciatic nerves of PV^{Cre} rats (n = 4, **Figure 11A** and **11B**). Post-mortem quantifications of the L4 DRGs revealed that $44 \pm 4.3\%$ of PV^{ON} neurons expressed DREADDs (**Figure 11C**). One week after sciatic nerve injections, rats received a severe contusion of the mid-thoracic spinal cord (250 kdyn, **Figure 11D**). In the same surgery, they were implanted with EES electrodes over the L4 spinal cord segment and with bipolar electrodes in leg muscles to record EMG signals.

Previous studies provided evidence that a single pulse of EES elicits short- and medium-latency reflex responses into leg muscles that have been linked to the recruitment of mono- and polysynaptic proprioceptive circuits, respectively (94). A single pulse of EES elicited these reflex responses into the tibialis anterior muscles of all the tested rats. The administration of the DREADD agonist clozapine N-oxide (CNO) near completely abolished these reflex responses in PV^{Cre} rats expressing DREADDs, whereas CNO had no influence on the reflex responses in wild-type animals (**Figure 11E** and **11F**).

We next tested whether this inactivation of proprioceptive feedback circuits altered the ability of EES to facilitate locomotion after SCI. Three weeks after contusion, the rats were positioned bipedally over a treadmill belt while supported in a robotic body support system. Without EES, all tested rats exhibited complete paralysis of both legs associated with an absence of muscle activity (**Figure 11G**). Continuous EES enabled coordinated locomotion with alternating bursts of EMG activity in antagonist muscles of the ankle that were elaborated from a succession of reflex responses linked to each pulse of EES (**Figure 11G**). The inactivation of proprioceptive feedback circuits following CNO administration led to a pronounced decrease of reflex responses elicited in leg muscles, which resulted in diminished locomotor outcomes in PV^{Cre} rats expressing DREADDs ($P < 0.001$). In contrast, CNO had no influence on the locomotor outcomes of wild-type rats (**Figure 11G**).

To quantify locomotor performance, we applied a principal component (PC) analysis onto a set of 129 parameters calculated from kinematic recordings (**Figure 11H**). PC1 (40% of explained variance) segregated the experimental groups and experimental conditions. Consequently, locomotor performance was quantified based on the scores of each rat onto PC1 (**Figure 11H**). This analysis showed that EES enabled contused rats to display continuous, coordinated locomotor movements that shared many features underlying the gait patterns of non-injured rats. In turn, inactivation of proprioceptive feedback circuits

induced a significant decline in locomotor performance with EES, leading to gait patterns nearly equivalent to those measured without EES ($P < 0.001$, **Figure 11H** and **11I**).

These results demonstrate that EES activates leg muscles through the recruitment of proprioceptive feedback circuits, and that this recruitment is essential to facilitate locomotion during EES after SCI.

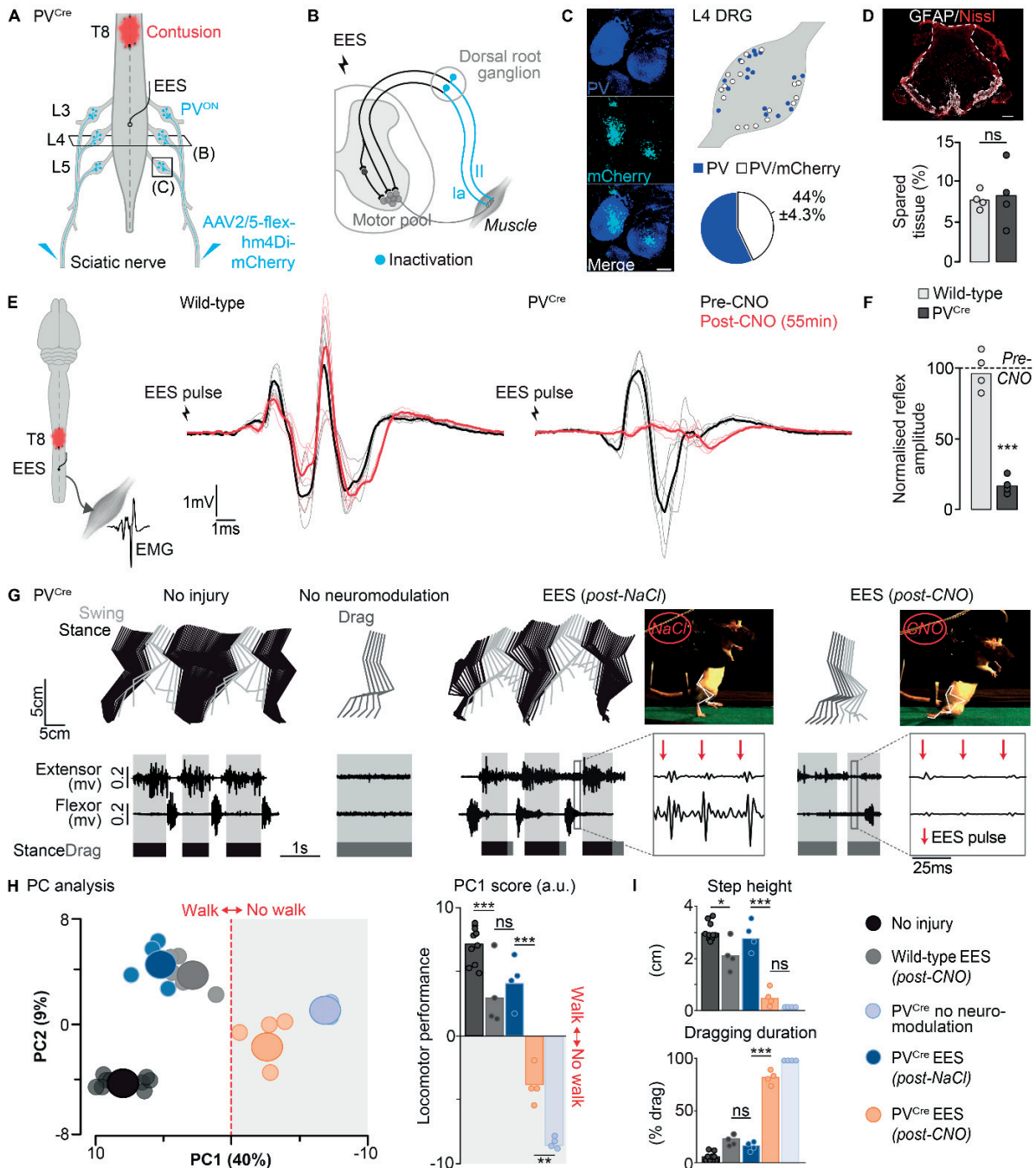


Figure 11 EES engages proprioceptive feedback circuits to facilitate walking after SCI (A) Scheme summarizing chemogenetic inactivation of proprioceptive neurons in DRG. (B) Functional and electrophysiological experiments were performed before and after CNO-mediated silencing of PV^{ON} neurons. (C) Photograph showing DRG neurons double-labelled for PV and mCherry. Scale bar 10 μ m. DRG reconstruction displaying the ratio of PV^{ON}/mCherry^{ON} labelled neurons. $44 \pm 4.3\%$ of all PV^{ON} neurons were infected by mCherry. (D) Image showing a representative coronal section through a contusion epicenter (GFAP, Glial fibrillary acidic protein). Scale bar 200 μ m. Bar plot reporting the area of spared tissue at the lesion epicenter for PV^{Cre} (n=4) and wild-type (n=4) rats. ns, not significant. Non-paired Student's t-test. (E) Scheme illustrating reflex recordings in leg flexor muscles in response to EES at L4 spinal level. Representative reflex curves of a wild-type and a PV^{Cre} rat, pre- and 55 minutes post-CNO. (F) Bar plot showing normalized reflex responses 55 minutes post-CNO in PV^{Cre} and wild-type rats. CNO injection led to a decrease of reflex responses in PV^{Cre} rats. CNO had no influence on reflexes in wild-type rats. ***P = 0.0004, Two-way ANOVA followed by Bonferroni's post-hoc test. (G) PV^{Cre} and wild-type rats were tested during bipedal locomotion on a treadmill. Stick diagram decompositions of the right leg movements and activity of extensor and flexor muscles of the ankle. The grey and white backgrounds correspond to stance and swing phases of gait, respectively. Snapshots showing a PV^{Cre} rat walking bipedally under EES 55 minutes after NaCl-injection and dragging 55 minutes after CNO administration. EMG insets show motor responses evoked in extensor and flexor muscles at distinct moments of the gait cycle. (H) PC analysis applied on 129 gait parameters averaged for each rat and condition (small circle). Large circles show the average per group. Bar plot showing average scores on PC1, which quantifies locomotor performance of PV^{Cre} rats (n=4) and wild-type rats (n=4) compared to non-injured rats (n=10). Inactivating proprioceptive feedback circuits following CNO resulted in diminished locomotor outcomes in PV^{Cre} rats. CNO had no influence on locomotor outcomes in wild-type rats. ***P < 0.0001. Two-way ANOVA followed by Bonferroni's post-hoc test. (I) Bar plots showing average values of single gait parameters extracted from the PCA for each experimental condition. ***P = 0.0003 for step height, ***P < 0.0001 for dragging duration. Two-way ANOVA followed by Bonferroni's post-hoc test.

Targeted modulation of large-diameter afferent circuits to enhance the effects of EES

We reasoned that pharmacological agents could potentiate the activity of large-diameter afferent circuits, which would augment the facilitation of locomotion during EES. Several studies in the past have demonstrated a direct interaction between noradrenergic receptor modulation and reflex pathways, which are mediated by large-diameter afferent fibers (54).

For example, experiments in cats have shown that descending noradrenergic fibers essentially modulate the transmission in spinal reflex pathways (69). Furthermore, the activation of noradrenergic α_2 receptors by the broad α_2 agonist Clonidine markedly depressed the excitability of mono- and polysynaptic reflex circuitries in cats (54).

The α_2 receptor family can be subdivided into three receptor subtype classes (α_2a , α_2b and α_2c) (**Figure 12A**). In the spinal cord, *in-situ* hybridization experiments revealed that α_2a and α_2c receptors are predominantly expressed, whereas there is little α_2b receptor expression (60). The activation of α_2 receptor subtypes induces a G-protein mediated decrease of neuronal activity (56,57).

To study the contribution of α_2 receptors to the facilitation of locomotion during EES, we conducted experiments in mice lacking α_2a or α_2c receptors (95,96).

The combination of EES and Clonidine failed to facilitate locomotion in mice lacking α_2c receptors (**Figure 12B** and **C**). This absence of locomotor movements was not due to defect in the locomotor circuitry, since the combination of EES and agonists to 5HT receptors promoted robust locomotor movements in the same mice. In striking contrast,

mice lacking alpha2a receptors that had received Clonidine exhibited alternating locomotor movements as soon as EES was switched on (**Figure 12B and C**).

These results suggest that alpha2a and alpha2c receptors are located on distinct subsets of circuits that are both engaged when EES is delivered to the spinal cord. Our results further imply that alpha2a and alpha2c receptors play opposite roles in the regulation of locomotion enabled by EES, opening the possibility that these circuits could be targeted specifically to augment the facilitation of locomotion with EES.

Based on these functional outcomes, we sought to identify a noradrenergic pharmacological strategy that targets alpha2a and alpha2c receptors, with the aim to specifically augment the facilitation of locomotion with EES. To achieve this goal, we conceived a pharmacological manipulation that aimed at increasing the excitability of alpha2a receptors and decreasing the excitability of alpha2c receptors.

For this purpose, we administered a dual alpha2a antagonist/alpha2c agonist that was previously synthesized for pain treatment (97,98). The delivery of this pharmacological agent led to a significant increase of reflex responses elicited by a single pulse of EES in rats with a complete spinal transection (**Figure 12D**).

These experiments confirm our hypothesis that alpha2a and alpha2c receptors, when modulated correctly, are directly involved in the regulation of reflex responses underlying locomotion.

We next evaluated the functional impact of this dual alpha2a antagonist/alpha2c agonist to restore walking in rats whose spinal cords were completely transected.

When positioned bipedally over a moving treadmill belt, all tested rats (n=5) exhibited complete paralysis of both hindlimbs, associated with quiescent activity in hindlimb muscles (**Figure 12E**). EES enabled alternating movements of the left and right hindlimbs, but this facilitation was insufficient to promote plantar foot placements associated with weight-bearing locomotion. Administration of the dual alpha2a antagonist/alpha2c agonist alone exerted no visible influence on muscle activity. Rats essentially dragged both hindlimbs along the treadmill belt. Strikingly, as soon as EES was switched on all tested rats displayed robust, weight-bearing locomotor movements with alternating EMG bursts in antagonist muscles and stable coordination between the left and right hindlimb (**Figure 12E**). Locomotion arrested immediately when EES was switched off, but resumed as soon as EES was reintroduced (**Figure 12F and I**). The quantification of locomotor performance using principal component (PC) analysis on a set of 129 parameters confirmed the functional improvements caused by the electrochemical intervention (**Figure 12G and H**).

We then sought to verify that this powerful facilitation of locomotion resulted from the targeted modulation of proprioceptive feedback circuits. For this purpose, we tested whether delivering EES in combination with the dual $\alpha 2a$ antagonist/ $\alpha 2c$ agonist could facilitate walking in *Egr3* mutant mice, which lack functional muscle spindle feedback circuits (**Figure 12I**). While this electrochemical combination promoted robust locomotion in wild-type mice with complete SCI, virtually no hindlimb movements could be observed in *Egr3* mutant mice (**Figure 12J** and **K**). In contrast, the administration of agonists to 5-HT receptors led to alternating leg movements, indicating that the lack of muscle spindle feedback circuits per se was not responsible for the absence of locomotion when delivering EES and noradrenergic modulators.

These behavioral experiments indicate that both, electrical and pharmacological intervention, act on the same neuronal structures to induce a facilitation of locomotion. Based on previously shown experiments, these activated structures may be proprioceptive afferent feedback circuits.

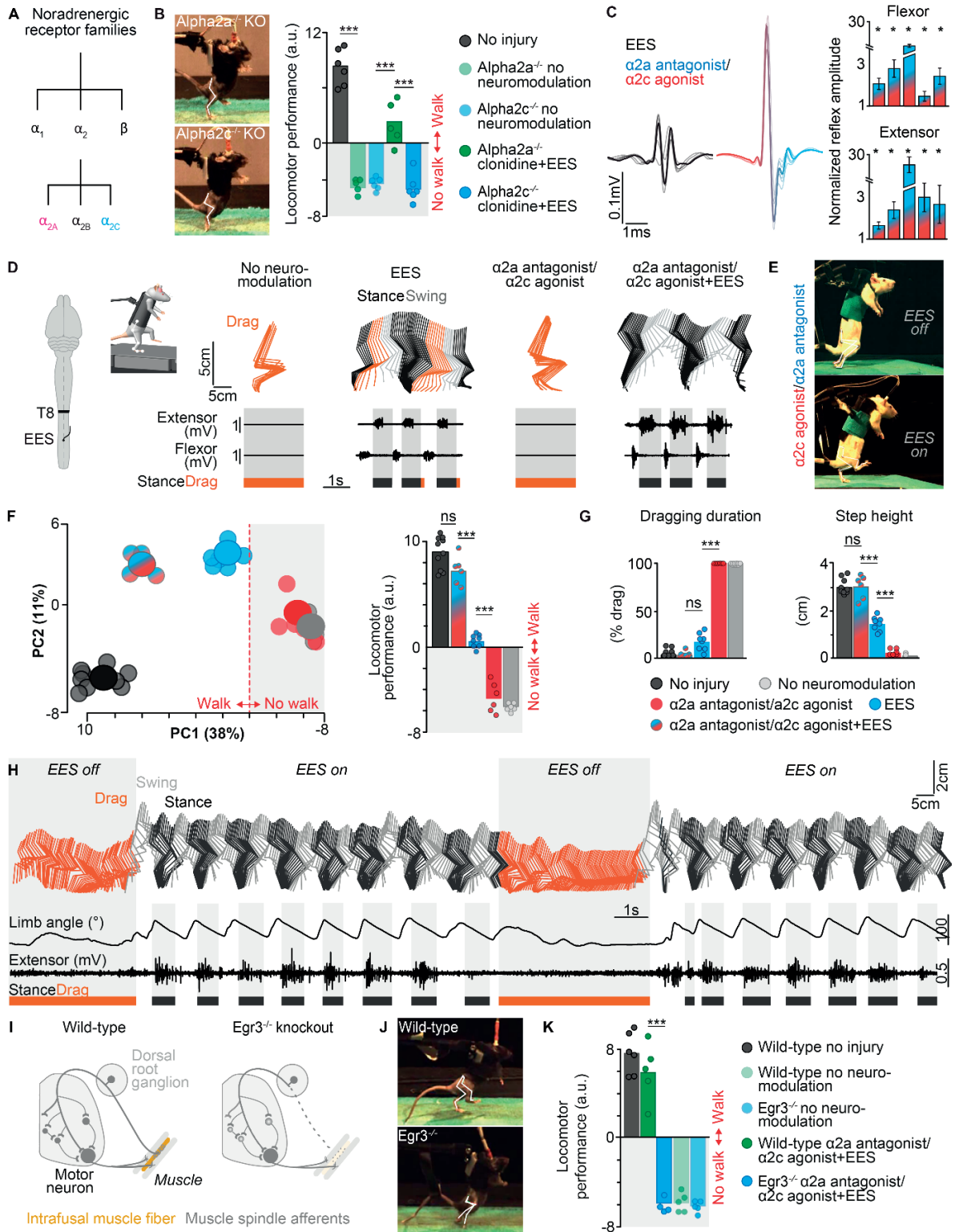


Figure 12 Targeted modulation of noradrenergic alpha2a and alpha2c receptors restores locomotion enabled by EES (A) Noradrenergic receptor families (alpha1, alpha2, beta) and alpha2 receptor subtypes (alpha2a, alpha2b, alpha2c). (B) Snapshots showing alpha2a KO mice stepping in a coordinated manner while alpha2c KO mice dragged both hindlimbs post-clonidine under EES. Bar plot showing the average scores on PC1 for alpha2a (n=5) and alpha2c KO mice (n=5) compared to uninjured mice (n=6). ***P < 0.0001. Two-way ANOVA followed by Tukey's post-hoc test. (C) Inactivation of alpha2a and activation of alpha2c receptors using a dual alpha2a antagonist/alpha2c agonist. Reflex curves showing a significant increase of reflex curves after delivery of this agent. Bar plot reporting increased reflexes for flexor and extensor muscles for all tested animals. *P < 0.05, bootstrapping, two-sided. (D) Rats with a complete SCI were tested on a treadmill during bipedal locomotion under electrochemical neuromodulation. Stick diagram decompositions of right leg movements and EMG activity of ankle extensor and flexor muscles. Grey and white backgrounds correspond to stance and swing phases of gait, respectively. (E) Snapshots showing hindlimb dragging in a rat after injection of the dual alpha2a antagonist/alpha2c agonist. Gait was immediately activated when EES was switched on. (F) PC analysis on 129 gait parameters averaged for each rat and condition (small circle). Large circles show the average per group. Bar plot showing the average scores on PC1, which quantifies the locomotor performance of injured rats (n=6) under different experimental conditions compared to intact (non-injured) rats (n=10). ***P < 0.0001. One-way ANOVA followed by Tukey's post-hoc test. (G) Bar plots showing average values of single gait parameters for each experimental condition extracted from the PCA. ***P < 0.0001 for dragging duration. ***P < 0.0001 for step height. One-way ANOVA followed by Tukey's post-hoc test. (H) Stick diagram decomposition reporting the direct electro-chemical interaction on producing locomotion. (I) Scheme showing mice with (wild-type) and without functional muscle spindle feedback (Egr3KO). (J) Snapshots showing stepping in wild-type mice under the dual alpha2a antagonist/alpha2c agonist and EES. Egr3KO mice were dragging under the same intervention. (K) Bar plot showing the average scores on PC1, which quantifies the locomotor performance of injured wild-type (n=5) and Egr3KO (n=4) mice under different experimental conditions compared to uninjured mice (n=5). ***P < 0.0001. One-way ANOVA followed by Tukey's post-hoc test.

Alpha2a and alpha2c receptors are expressed on proprioceptive and low-threshold mechanoreceptor feedback circuits

To guide the understanding of this targeted intervention and to better understand the sensorimotor circuits engaged by EES, we studied the spatial distribution of alpha2a and alpha2c receptors in the spinal cord and DRG using mice expressing GFP under the alpha2a or alpha2c promoter (99). In these mice, the distribution of neurons expressing alpha2a and alpha2c receptors reproduced the previously documented topologies in brain and brainstem (99).

We found that neurons expressing alpha2a versus alpha2c receptors exhibited different spatial distributions in the spinal cord (**Figure 13A** and **B**). Neurons expressing alpha2a receptors were mostly found within laminae I/II and lamina X of the spinal cord grey matter. In contrast, neurons expressing alpha2c receptors were concentrated within laminae III/IV (**Figure 13B** and **D**). These spatial distributions were preserved along the entire extent of the lumbosacral spinal cord. Additionally, neurons expressing alpha2a and alpha2c receptors were found abundantly in DRGs (**Figure 13B** and **E**).

We next sought to identify the phenotype of these neurons using immunohistochemistry, both in the spinal cord and DRGs.

Within laminae I/II, alpha2a receptors were mainly expressed on inhibitory glycinergic (66%) and GABAergic (27%) interneurons (**Figure 13G**). These interneurons are richly innervated by small-diameter, non-myelinated afferent fibers involved in the transmission

of nociceptive information (14). Around the central canal (lamina X), alpha2a was expressed on glutamatergic, glycinergic and cholinergic interneurons (**Figure 13G**).

In contrast, alpha2c receptors were near-exclusively expressed on excitatory glutamatergic interneurons in the spinal cord (93%, **Figure 13G**). The phenotype and spatial location of these neurons resembled the characteristics of neurons expressing the nuclear orphan receptor ROR α (21). Indeed, double-labelling experiments confirmed that nearly all these glutamatergic interneurons expressed ROR α (90%, **Figure 13I**). ROR α^{ON} interneurons receive light touch information originating from low-threshold mechanoreceptor (LTMR) afferents (21). The large diameter of these fibers (A β) suggest that they could be recruited by EES. We thus asked whether EES led to the activation of alpha2c $^{\text{ON}}$ neurons located in the spinal cord. The delivery of continuous EES during 30 minutes under anesthetized conditions (without movement) led to a robust expression of the activity-dependent marker *cfos* in alpha2c $^{\text{ON}}$ neurons ($P < 0.001$, **Figure 13H**).

A similar distinction between alpha2a $^{\text{ON}}$ and alpha2c $^{\text{ON}}$ neurons was observed in DRGs. The alpha2a receptor subtype was predominantly expressed on proprioceptive PV $^{\text{ON}}$ neurons (67%). Instead, alpha2c $^{\text{ON}}$ neurons mainly expressed markers of nociceptive afferent neurons, including peptidergic (CGRP, 66%) and non-peptidergic (Ib4, 18%) neurons (**Figure 13F**).

To confirm the observed alpha2c/ROR α double-labelling genetically, we performed single-cell sequencing of neurons located in the dorsal horn of the spinal cord. For this, we used a recently published single-cell RNA sequencing database which identified 30 global excitatory and inhibitory cellular subtypes of neurons in the mouse dorsal horn (100) (**Figure 13J**). Based on this database, we examined the relative expression of the key marker genes *Rora* and *Adra2c* across all 30 cell types (21). We found that only one excitatory cell type (Glut_Elavl4_Meis2) robustly expressed both, *Rora* and *Adra2c*, consistent with our hypothesis that this combination of gene expression represents a unique and distinct cell type within the spinal cord. As a control, we additionally examined the expression of glutamate (*Slc17a6*) as well as classical markers including *Cck* and *Cmip*, which have previously been reported to be associated with *Rora* $^{\text{ON}}$ cells in the dorsal horn. Furthermore, we found that these cells expressed very low to negligible levels of *Pkcg* or *Pax2*, consistent with previous work (21) (**Figure 13K**).

Taken together, these results demonstrate the remarkably distinct phenotypes and distributions of neurons expressing alpha2a or alpha2c receptors within the spinal cord and DRG, including PV $^{\text{ON}}$ and ROR α^{ON} neurons that are both activated by EES.

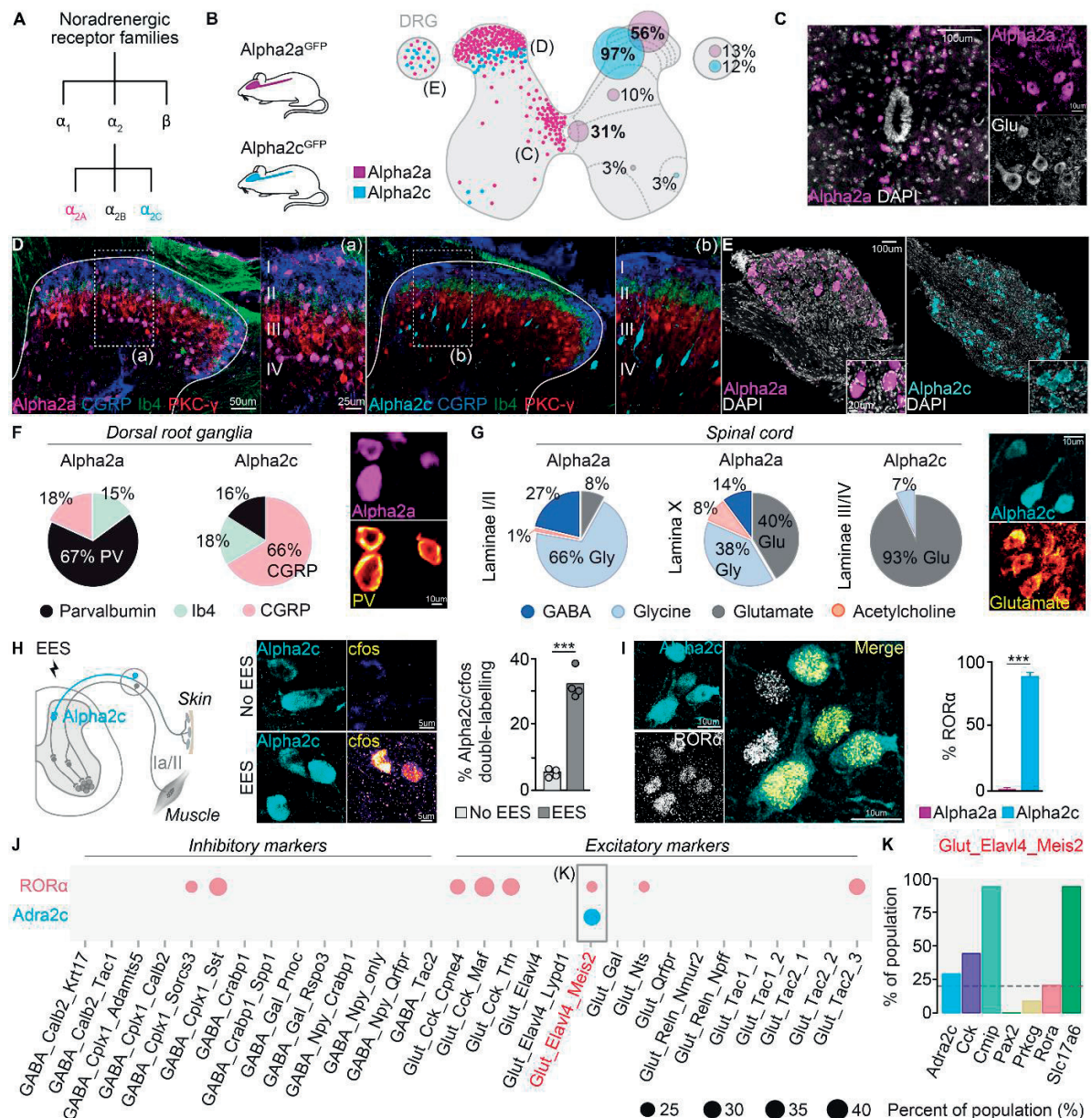


Figure 13 Noradrenergic alpha2a and alpha2c receptors are located on neuronal pathways activated by EES (A) Noradrenergic receptor families (alpha1, alpha2, beta) and alpha2 receptor subtypes (alpha2a, alpha2b, alpha2c). (B) Overview showing the location of cells expressing alpha2a or alpha2c receptor subtypes in spinal cord and DRGs. (C) *In-situ* hybridization. (D) Representative images of GFP, PKC-γ, CGRP and Ib4 labelled dorsal horns display the distinct laminar location of alpha2a^{ON} and alpha2c^{ON} neurons. Scale bar 50μm for the overview, 25μm for the insets. (E) Images showing the expression of alpha2a and alpha2c receptor subtypes in DRGs. Scale bar 100μm for the overview, 20μm for the insets. (F) Phenotype of cells expressing alpha2a or alpha2c receptors located in spinal cord and DRGs. Polar plots displaying overlap of alpha2a^{ON} and alpha2c^{ON} with parvalbumin (PV), Ib4 or CGRP in DRGs. Scale bar 10μm. (G) Polar plots displaying overlap of alpha2a^{ON} and alpha2c^{ON} neurons in the spinal cord with various neurotransmitter markers. Scale bar 10μm. (H) Scheme illustrating the cfos experiment. Images showing alpha2c^{ON}/cfos double-labelling in laminae III/IV after EES. Scale bars 5μm. Bar plot reporting the percentage of alpha2c^{ON} neurons co-localising with cfos after EES versus no EES. ***P < 0.0001. Non-paired Student's t-test. (I) Photographs showing co-localization between alpha2c^{ON} and RORα^{ON} interneurons in laminae III/IV. Scale bars 10μm. Bar plot reporting co-labelling between alpha2c^{ON} and RORα^{ON} interneurons. ***P < 0.001. Non-paired Student's t-test. (J) Single-cell sequencing experiments confirming alpha2c/RORα co-expression (Glut_Elavl4_Meis2). (K) Key molecular markers defining alpha2c and RORα.

Interneurons involved in the transmission of low-threshold mechanoreceptor feedback establish synaptic contacts onto inhibitory pre-motor interneurons

Our results demonstrate that EES recruits proprioceptive and LTMR feedback circuits (**Figure 14A**). Both pathways play opposite roles in the regulation of locomotion enabled by EES. Whereas the activation of proprioceptive circuits enables locomotion, the activation of LTMR feedback circuits by EES diminishes functional outcomes.

Due to the detrimental effects of LTMR activation on locomotor outcomes, we sought to identify the intraspinal circuits involved in the transmission of LTMR feedback in response to EES.

To dissect the structural and functional properties of these circuits and their responses to the modulation of alpha2 receptors, we modeled the interactions between proprioceptive and LTMR feedback circuits in response to single pulses of EES. For this, we combined a finite element model (90) with a static computational model that emulated mono- and di-synaptic connections of proprioceptive neurons onto motoneurons.

In a next step, we expanded this computational model with LTMR feedback circuits (**Figure 14B**). Compared to proprioceptive feedback, pathways transmitting cutaneous LTMR information are poorly characterized. Electrophysiological experiments showed that cutaneous reflexes typically involve two to three interneurons that lead to excitation or inhibition of motoneurons (101–103). In line with this, a recent study showed that $ROR\alpha^{ON}$ interneurons, which receive direct synaptic inputs from LTMR afferents, establish direct synaptic contacts onto several classes of excitatory interneurons involved in motor control, such as $V0c^{ON}$ or $V2a^{ON}$ interneurons (21).

Our electrophysiological and functional experiments have shown that decreasing the excitability of interneurons located on LTMR circuitries significantly augmented reflex responses and locomotor outcomes enabled by EES. This implies that LTMR feedback circuits interact negatively with proprioceptive feedback circuits at the spinal level, suggesting that down-regulating their excitability would augment proprioceptive feedback and ultimately functional outcomes. Such a negative interaction could be explained by the presence of an inhibitory pre-motor interneuron located between $ROR\alpha^{ON}$ interneurons and motoneurons.

Consequently, we modelled LTMR feedback circuits that linked $ROR\alpha^{ON}$ interneurons to both, excitatory and inhibitory premotor interneurons establishing direct synaptic contacts onto motoneurons (**Figure 14B**).

To test the two modeling networks (LTMR network containing an inhibitory interneuron versus no inhibitory interneuron), we evaluated changes in the membrane potential of motoneurons in response to a single pulse of EES (**Figure 14C**). When modeled with the network containing an inhibitory interneuron in the LTMR circuitry, motoneurons displayed a lower resting membrane potential. Consequently, when applying a single pulse of EES, the chance of activating the motoneuron was smaller. In contrast, when no inhibitory interneuron was implemented in the circuitry, the same amplitude of EES led to an activation of motoneurons.

In a next step we performed simulations where we compared the inactivation of proprioceptive or LTMR afferents circuits using the two networks. As anticipated, simulations with both networks revealed that the inactivation of proprioceptive circuits led to a suppression of reflex responses (**Figures 14D** and **E**). In this case, the integration of an inhibitory interneuron in intraspinal LTMR circuits did not change the modeled reflex outcomes.

Instead, when inactivating LTMR feedback circuits, the presence of inhibitory interneurons between $ROR\alpha^{ON}$ interneurons and motoneurons largely increased reflex curves in response to single pulses of EES (**Figure 14E**) and resembled the reflex outcomes obtained in the rat (**Figure 12D**). In contrast, in a network without inhibitory but only excitatory interneurons, a decrease of reflex curves was observed (**Figure 14D**). When inactivating LTMR feedback circuits, the excitation mediated by this interneuron was automatically inactivated as well.

Overall, these simulations suggest that the recruitment of LTMR feedback circuits diminishes functional outcomes and why their down-regulation leads to an increase of reflex responses. Our modeling experiments reveal that such a strong increase in reflex amplitude can be explained by the presence of inhibitory interneurons located between $ROR\alpha^{ON}$ interneurons and motoneurons.

We next performed monosynaptic rabies tracing experiments to visualize direct synaptic connections from $ROR\alpha^{ON}$ interneurons onto inhibitory premotor interneurons.

To reveal premotor interneurons, intramuscular injections of ΔG protein Rab-eGFP together with an AAV expressing rabies glycoprotein (AAV-Gly) were performed in $ROR\alpha^{Cre}:R26^{LSL-tdTomato}$ mice at post-natal day 2 (P2) (**Figure 14F**). Inhibitory interneurons were identified by the marker parvalbumin (PV), which characterizes a subgroup of GABAergic V1 interneurons in the spinal cord (104–106).

$22\pm 4\%$ of rabies^{ON} premotor interneurons co-labelled with PV. Double-labelled interneurons were found in dorsal, intermediate and ventral laminae of the spinal cord

gray matter (**Figure 14G**). In intermediate laminae, vGlut2^{ON} synapses from RORα^{ON} interneurons were found in close contact to rabies^{ON}/PV^{ON} premotor interneurons (**Figure 14H**). On average, each inhibitory premotor interneuron received 6 ± 2 synaptic contacts from RORα^{ON} interneurons (**Figure 14I**).

This experiment demonstrates that RORα^{ON} interneurons establish synaptic contacts with inhibitory premotor interneurons which directly modulate the activity of motoneurons.

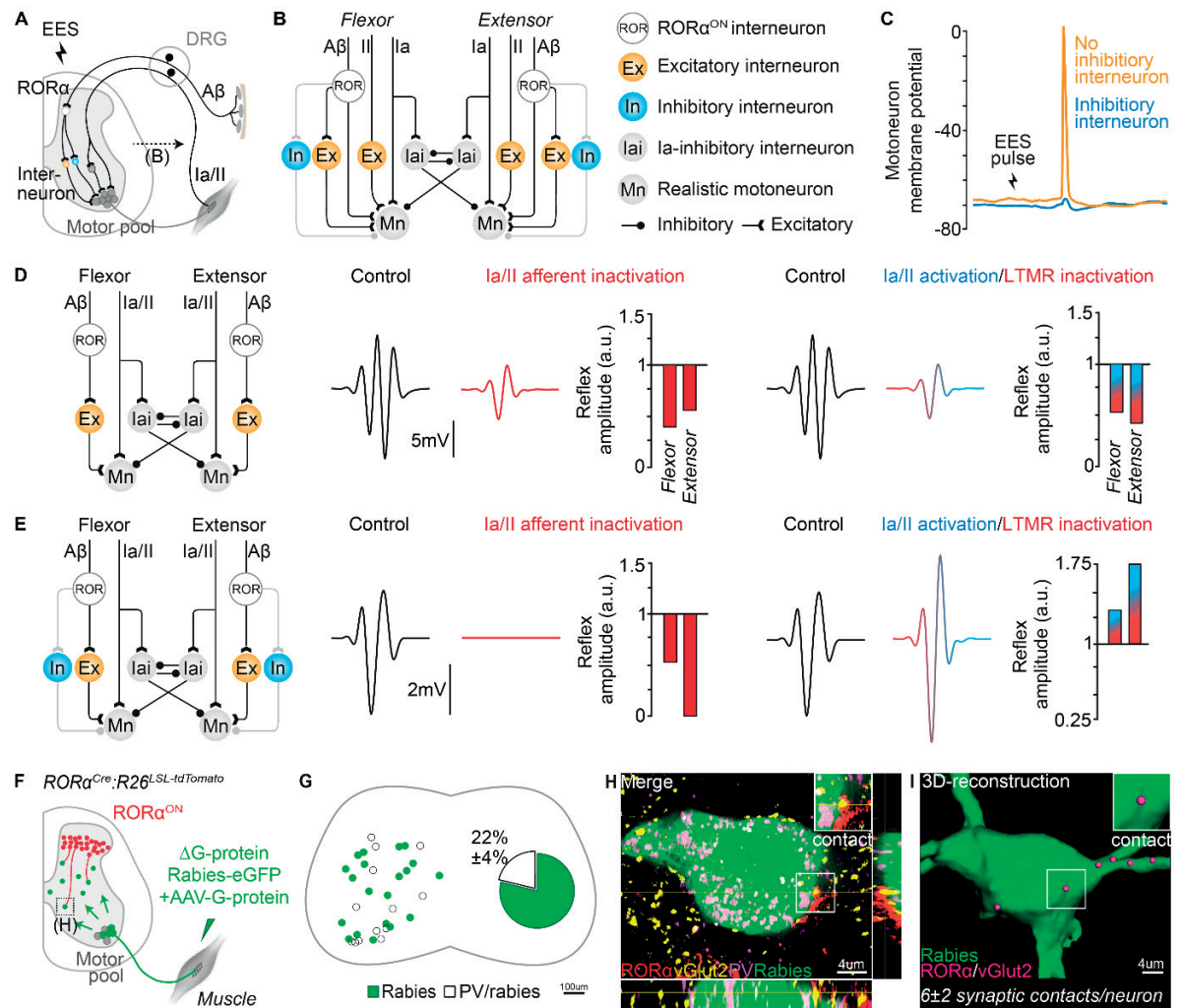


Figure 14 Intraspinal circuits involved in the transmission of LTM feedback in response to EES (A) Scheme illustrating proprioceptive and LTM feedback circuits and downstream connections. (B) Scheme showing the network used for modeling experiments. LTM feedback circuits were modeled either with or without inhibitory interneuron. (C) Modeled motoneuron membrane potential in response to a single pulse of EES, based on a model containing an inhibitory interneuron or not. (D) Modeled muscle reflex curves in response to EES for different experimental conditions, based on a network without inhibitory interneurons located on the downstream pathway of LTMs. Scale bar 5mV. (E) Modeled muscle reflex curves in response to EES for different experimental conditions, based on a network containing inhibitory interneurons located on the downstream pathway of LTMs. Scale bar 2mV. (F) Scheme summarizing the experimental approach to visualize premotor interneurons. (G) Reconstruction showing the location of inhibitory pre-motor interneurons. (H) Image showing a rabies^{ON} pre-motor interneuron co-localizing with parvalbumin (PV). This interneuron receives synaptic inputs (vGlut2) from RORα^{ON} interneurons. Scale bar 4μm. (I) 3D reconstruction of the same inhibitory pre-motor interneuron showing several synaptic contacts from RORα^{ON} interneurons. In average, each rabies^{ON}/PV^{ON} neuron receives 6 ± 2 synaptic contacts from RORα^{ON} interneurons. Scale bar 4μm.

Enabling voluntary control of walking in rats with clinically relevant contusion SCI

Finally, we sought to test whether this targeted modulation therapy could reestablish functional interactions between residual supraspinal pathways and the spinal cord located below a clinically relevant contusion SCI. To model a severe contusion in rats, we delivered a robotically controlled impact (250 kdyn) onto thoracic segments (T8/T9) (85). This lesion spared as little as $8.7 \pm 1.2\%$ of intact cross-sectional tissue. To label the fibers and synaptic projections of descending noradrenergic pathways, we injected AAV-DJ-hSyn-flex-mGFP-2A-Synaptophysin-mRuby into the rostral ventrolateral medulla (RVLM) of TH^{Cre} rats (**Figure 15A**). Visualization of the entire spinal cord using CLARITY-optimized light-sheet microscopy revealed stereotypical projection patterns of TH^{ON} fibers. These fibers primarily extended in the lateral white matter, from which bundles of fibers projected into the spinal cord grey matter at regular intervals along the neuraxis (**Figure 15D**). The severe contusion completely interrupted these fibers, only sparing a subset of TH^{ON} fibers located in the ventral white matter (**Figure 15D and E**).

To evaluate the supraspinal (*voluntary*) control of leg movements, the contused rats were positioned bipedally in a robotic body weight support that provides personalized assistance against gravity during overground locomotion (**Figure 15G**) (84). The systemic (I.P.) delivery of the dual alpha2a antagonist/alpha2c combined with EES failed to facilitate locomotion in all tested rats. The animals fell backward, incapable of initiating locomotor movements. This failure contrasted with the coordinated leg movements observed in response to the delivery of EES and 5-HT agonists.

We previously demonstrated that a severe contusion spares a subset of descending projections from glutamatergic neurons located in ventral gigantocellular nucleus, and that these neurons relay the cortical command to the lumbar spinal cord to produce voluntary locomotor movements (85). We found that alpha2c receptors are expressed on various neurons in the brain and brainstem, such as on glutamatergic neurons located in the ventral gigantocellular nucleus (**Figure 15F**). We thus surmised that the activation of alpha2c receptors may inactivate these neurons, thus preventing the transmission of the supraspinal command to the lumbar spinal cord.

To test this hypothesis, we administered the dual alpha2a antagonist/alpha2c agonist intrathecally to the lumbar spinal cord. Using this route, all the tested rats exhibited voluntary leg movements that allowed them to cross the entire extent of the runway (**Figures 15G, H and I**).

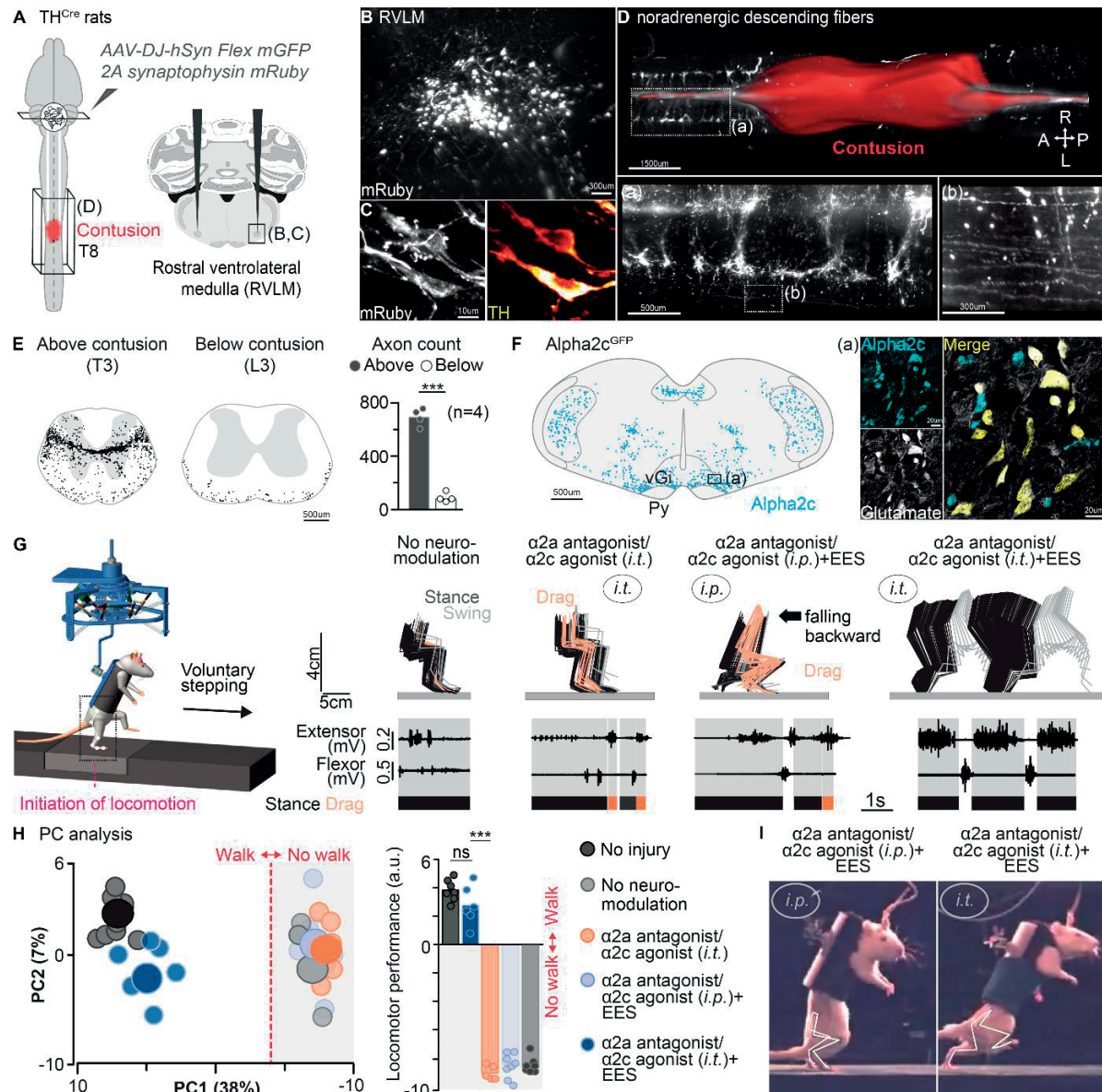


Figure 15 Voluntary control of locomotion in rats with a severe contusion injury (A) Scheme illustrating tracing strategy to label descending noradrenergic axons and synapses in TH^{Cre} rats. (B) 3D image showing the injection site in the ventral brainstem (rostral ventrolateral medulla, RVLM). Scale bar 300μm. (C) Images showing virus-infected neurons (mRuby) co-localising with TH in RVLM. Scale bar 10μm. (D) 3D rendering showing the interruption of noradrenergic descending fibers by the contusion. Scale bar 1.5mm. 3D insets above the contusion showing details about the anatomical arrangement of the noradrenergic tract. Scale bars 500μm and 300μm, respectively. (E) Spinal cord reconstructions of descending projections above (T3) and below (L3) the contusion. Bar plot showing the quantification of axon density of noradrenergic fibers above and below injury (n= 4 rats). Scale bar 500μm. ***P < 0.0001, paired Student's t-test. (F) Reconstruction of alpha2c^{ON} cells at brainstem level. Scale bar 500μm. Images showing alpha2c^{ON} cells co-localising with glutamate in the ventral gigantocellular nucleus (vGi). Scale bars 20μm. (G) Rats with a severe contusion (250kdyn) were tested during bipedal locomotion on a runway with gravity-assist under various experimental conditions. Stick diagram decompositions of the right leg movements and activity of extensor and flexor muscles of the ankle. The grey and white backgrounds correspond to the stance and swing phases of gait, respectively. (H) PC analysis applied on 129 gait parameters averaged for each rat and condition (small circle). Large circles show the average per group. The bar plot shows the average scores on PC1 (locomotor performance) of injured rats (n=6) under different experimental conditions compared to uninjured rats (n=7). ***P < 0.0001. One-way ANOVA followed by Tukey's post-hoc test. (I) Snapshots showing a rat unable to initiate stepping after systemic injection of the dual alpha2a antagonist/alpha2c agonist in combination with EES. In contrast, after intrathecal injection of the same pharmacological agent, rats exhibited voluntary leg movements that allowed them initiate locomotion along the runway.

3.4 Discussion

Several studies in animal models and human patients showed that EES, applied over the dorsal aspect of lumbar segments, leads to improved functional recovery (34,107). However, the limited understanding of the identity of neural structures activated by EES have prevented more precise and refined stimulation interventions so far. Here, we provide direct anatomical evidence that EES recruits proprioceptive and LTMR feedback circuits. Whereas the activation of proprioceptive afferent circuits engaged motor pattern formation, the activation of LTMR circuits diminished the production of locomotion enabled by EES. We discuss our findings with an emphasis on the role of sensory feedback involved in the generation of locomotion after SCI as well as the therapeutic potential of such circuit-specific interventions for human patients.

Targeting proprioceptive feedback circuits after SCI

Our study shows that EES robustly activates proprioceptive neurons concentrated in DRGs through the recruitment of their large-diameter, myelinated fibers. These findings demonstrate the importance of exploiting muscle spindle feedback in the design of rehabilitative strategies after SCI. This includes the specific modulation of proprioceptive feedback circuits during rehabilitation to enhance the effect of rehabilitation therapies after SCI.

One possibility to specifically recruit proprioceptive neurons in DRG consists in applying electrical currents within a defined range of stimulation frequencies at low amplitudes (41,76). Based on modeling experiments, spatiotemporal EES patterns applied with a frequency envelope resembling the firing rates of Ia afferent fibers is 'in-phase' with the natural firing pattern of proprioceptive afferent fibers during locomotion. This 'in-phase' stimulation paradigm led to improved motor and sensory outcomes in SCI patients when combined with daily locomotor training over 5 months (41).

Another possibility to enhance the activity of proprioceptive feedback circuits consists in the specific modulation of this afferent circuit, i.e. by pharmacological agents. Pharmacological receptors expressed on proprioceptive DRG neurons may serve as a possible target for pharmacological agents to directly influence the activity of this circuit. As demonstrated in this study, noradrenergic receptor subtypes could serve as a possible target to achieve this goal.

Activation of LTMRs diminishes locomotor outcomes generated by EES

Besides proprioceptive afferents, LTMR feedback circuits involved in the transmission of light-touch information are recruited by EES. Compared to muscle spindle feedback, little is known about the impact of LTMRs on the motor system and how their activation by EES affects motor outcomes.

During stepping, cutaneous LTMRs are activated throughout the entire stance phase of the leg whereas they are inactive during swing phase (25). In contrast to proprioceptive circuits, LTMRs are thus activated in a phase-dependent manner. Our modeling experiments showed that the continuous activation of LTMR feedback circuits by continuous EES interferes with the natural activation pattern of LTMR feedback circuits. Indeed, down-regulating the excitability of LTMRs in combination with an up-regulation of proprioceptive circuits during EES-enabled stepping immediately enhanced locomotor outcomes in spinal rats.

A similar, sensory-specific modulation of proprioceptive and cutaneous afferent pathways has recently been described in monkeys (29). During the execution of forearm reaching movements, electrical stimulation was applied to nerves containing either cutaneous or proprioceptive afferents. Whereas cutaneous inputs were suppressed regardless of the type of movement, muscular inputs were specifically facilitated during relevant movements. These outcomes imply that different streams of sensory information are modulated in an individual manner and are in line with the results we present here.

In the intact state, this sensory-specific modulation may be directly controlled by the brain. A recent study in monkeys demonstrated the existence of direct supraspinal connections onto cutaneous interneurons within lamina III/IV (26). Supraspinal inputs were mediated by corticospinal tract (CST) fibers which controlled the activity of lamina III/IV interneurons by direct and phase specific inhibition during movements. Similarly, direct CST connections from the brain to interneurons located in laminae III/IV of the spinal cord have been shown in mice (21,108).

Until recently, little was known about the anatomical properties of intraspinal pathways involved in the transmission of LTMR afferent information. A recent study gave first anatomical insights into the intraspinal connectivity pattern of LTMR circuits. LTMRs, defined by the expression of the molecular marker ROR α , were found to establish direct synaptic contacts onto several classes of molecularly identified, excitatory interneurons involved in motor control, such as V0c or V2a interneurons (21).

In our study, by using the same experimental approach, we found inhibitory PV^{ON} premotor interneurons located in intermediate laminae, receiving synaptic input from

ROR α ^{ON} interneurons. Previous studies reported that PV^{ON} neurons located in intermediate spinal cord regions are derived from the V1 class of spinal interneurons, and show the characteristics of Ia-inhibitory interneurons (105). Ia-inhibitory interneurons receive synaptic input from Ia afferent fibers of one muscle and in turn provide inhibitory input onto motoneuron pools innervating antagonist muscles (109). These interneurons play a pivotal role in the alternating recruitment of antagonist motoneuron pools during locomotion by providing the main source of rhythmic inhibition to flexor and extensor motoneuron pools (109,110). Based on the location of the identified, inhibitory premotor interneurons in intermediate laminae, our findings suggest that LTMR may establish synaptic contacts with Ia-inhibitory interneurons. The continuous activation of LTMRs by EES would lead to a non-physiological activation of Ia-inhibitory interneurons, which, in turn, would cause a disruption of the naturally occurring left-right activity pattern during locomotion. To confirm this hypothesis, more anatomical evidence will be needed though.

Similarly, a recent paper investigating crossed reflex pathways in mice assumed the existence of an inhibitory interneuron along intraspinal pathways involved in the transmission of cutaneous information (111).

Clonidine-mediated alpha2 receptor modulation after SCI

Historically, noradrenergic alpha2 receptors have been among the first ones targeted to restore locomotion after SCI. In cats with a complete transection of the spinal cord, clonidine, usually in combination with tail pinching, has been shown to reliably enhance stepping function after SCI (47,54,70). In contrast, when delivering clonidine in human patients, a depression of locomotor states was observed (48). A similar functional outcome was reported in spinal rats when clonidine was administered in combination with EES (72).

These conflicting functional outcomes among different species may explain why noradrenergic receptor stimulation only received minimal attention over the last years as a means to pharmacologically modulate spinal circuits after SCI. So far, there was no explanation for the observed differences in functional outcomes between the species after clonidine injection. By using transgenic mouse lines, we found that noradrenergic alpha2a and alpha2c receptor subtypes, which are activated by clonidine, are expressed on proprioceptive and LTMR feedback circuits, respectively. The inactivation of proprioceptive afferent pathways by clonidine through the activation of alpha2a receptors explains why this pharmacological agent abolished locomotion enabled by EES in rats. Similarly, it also explains the diminished stepping outcomes in human patients after clonidine

administration, taking into account the importance of proprioceptive circuits in generating locomotion after SCI.

Overall, these findings demonstrate why clonidine alone or in combination with EES failed to induce stepping after SCI. Nevertheless, it is still unknown why clonidine enabled locomotion in cats. In order to induce stepping in cats, tail pinching was often applied after the injection of clonidine. Tail pinching is primarily activating cutaneous afferent pathways and is thus acting on different sensory circuits compared to EES. Another explanation for the observed differences could be that cats display a different ratio of alpha2a and alpha2c receptors compared to rats and humans.

The expression of noradrenergic alpha2a and alpha2c receptors on proprioceptive and LTMR afferent circuits suggests that we modulate neuronal circuits involved in the transmission of fight and flight responses. The noradrenergic system is known to be involved in mobilizing the body during situations of stress and danger (fight and flight). The modulation of noradrenergic receptors located on proprioceptive and cutaneous reflex pathways can trigger an immediate escape in a situation of sudden danger or fear. Our findings imply that EES exerts its effects on the same reflex pathways.

Having the detailed knowledge about the expression pattern of alpha2a and alpha2c receptor subtypes, together with the evidence that EES modulates proprioceptive and LTMR afferents, we used this knowledge to tailor a targeted neuromodulation strategy to produce stepping after SCI. Within this targeted neuromodulation strategy, electrical and pharmacological stimulation both exert their effects on the same neuronal structures. The direct interaction between the two interventions was observed in functional testing. The electrical or pharmacological intervention alone did not induce plantar and weight-bearing stepping. In contrast, only when both interventions were applied simultaneously, all tested rats displayed robust, weigh-bearing locomotor movements. This is in contrast to serotonergic or dopaminergic receptor modulation. Even though serotonergic agonists (5HT₁, 5HT_{2A}, 5HT₇) have been shown to potentiate the effects of EES, such a direct interaction as observed between EES and the dual alpha2a antagonist/alpha2c agonist cannot be achieved.

Limitations of the current study

To visualize activated DRG neurons in response to the application of EES, we performed *ex-vivo* calcium imaging experiments. Even though a previous study has demonstrated the feasibility of *in-vivo* DRG recordings (112), we here used an *ex-vivo* approach to visualize activated neurons in response to the application of EES. Due to the

isolated location of DRGs within the spinal subarachnoid space between adjacent vertebrae and thus the difficult accessibility, *in-vivo* DRG recordings are difficult to achieve from a technical point of view. Besides this technical aspect, additional problems such as induced movements (i.e. by breathing) have to be taken into account when recording DRG activity *in-vivo*. Nevertheless, despite some minor limitations, *ex-vivo* calcium imaging as our method of choice worked reliably and provided stable outcomes.

To label interneurons expressing alpha2a or alpha2c receptor subtypes we used transgenic mouse lines engineered by a bacterial artificial chromosome (BAC) insertion into their genome. Even though in most cases the labelling outcomes obtained by such transgenic mouse lines have been shown very reliable (113), the random insertion of such BAC-cassettes into the genome of mice can lead to aberrant and non-specific labelling. To verify the correct transgenic labelling obtained by the alpha2a^{GFP} and alpha2c^{GFP} mouse lines, we will thus perform alpha2a and alpha2c mRNA labelling by performing *in-situ* hybridization in the spinal cord and DRGs.

In this study we have shown that EES primarily engages large-diameter myelinated fibers, in particular muscle spindle and LTMRs feedback circuits. Therefore, we restricted our model to these pathways. However, our model does not include the activation of Ib afferent fibers by EES. Based on their diameter and myelination, it is very likely that Ib afferent fibers, which transmit information from Golgi tendon organs (GTOs) to the spinal cord, are also recruited by EES. At this point, only little is understood about the exact role and contribution of Ib afferent fibers during gait and how they modulate functional outcomes. In the future it will thus be important to dissect the role of this sensory afferent pathway and to understand its role in the production of locomotion, with the goal to generate more precise simulations.

Future perspectives

Despite lacking mechanistic understanding about how EES mediates its effects to produce locomotion after SCI, functional improvements in patients with relatively simple stimulation protocols have been reported in the past. Nevertheless, there is critical need for the detailed understanding of the underlying mechanisms of the applied therapeutical intervention (114). The mechanistic understanding of EES presented here has the potential to further optimise current stimulation strategies with the goal to enhance functional improvements after SCI. This knowledge may lead to more specific therapy interventions in the future and establish a framework to design efficient neuromodulation strategies to reverse paralysis in humans one day.

3.5 Materials and methods

Experimental setup

Experiments were conducted on adult female Lewis rats (~220 g body weight), adult Long Evans rats (~240 g body weight) and adult C57BL/6 mice (20-30 g body weight). PV^{Cre} (Jackson Laboratory, JAX# 017320), ROR α ^{Cre} (21), alpha2a^{GFP} (MMRRC, MMRRC:014248-UCD), alpha2c^{GFP} (MMRRC, MMRRC:030098-UCD), alpha2a^{-/-} knockout (115), alpha2c^{-/-} knockout (67), Egr3^{-/-} knockout (12) and R26^{LSL-tdTomato} (Jackson Laboratory, #007909) transgenic mouse strains were used and maintained on a mixed genetic background (129/C57BL/6). PV^{Cre} (RRRC, 773) and TH^{Cre} (Horizon discovery, TGRA8400) rat lines were maintained similarly. Experimental animals used were of both sexes. Housing, surgery, behavioral experiments and euthanasia were performed in compliance with the Swiss Veterinary Law guidelines. Animal care, including manual bladder voiding, was performed twice daily for the first 3 weeks after injury, and once daily for the remaining post-injury period. All procedures and surgeries were approved by the Veterinary Office of the canton of Geneva in Switzerland.

Surgical procedures and post-surgical care

General surgical procedures used have been described previously (34,71). All interventions were performed under general anesthesia and aseptic conditions. Briefly, stimulating electrodes were created by removing a small part (~400 μ m notch) of insulation from Teflon-coated stainless steel wires (AS632, Cooner Wire, USA), which were subsequently secured at the midline overlying spinal cord segments L2 and S1 by suturing the wires to the dura. A common ground wire (~1cm of Teflon removed at the distal end) was inserted subcutaneously over the right shoulder (**Figure 16, step 1**).

Bipolar intramuscular electrodes (Cooner Wire; AS632 and AS632-1 for rats and mice, respectively) were inserted bilaterally in the medial gastrocnemius (MG, ankle extensor, in rats) or vastus lateralis (VL, knee extensor, in mice) and tibialis anterior (TA, ankle flexor) muscles to record electromyographic (EMG) activity. All the wires were connected to a percutaneous amphenol connector (Omnetics Connector Corporation, USA) cemented onto the skull of the animals.

In the same set of surgery, wildtype and transgenic rats (n=10) and mice (n=20) received a complete thoracic (T8) SCI. A subset of n=10 rats received a severe contusion injury (250 kdyn; 1 dyn=10 μ N) using a force-controlled spinal cord impactor (IH-0400 Impactor, Precision Systems and Instrumentation LLC, USA). The spinal cord displacement

induced by the impact was measured for each animal and the extent and location of each lesion was verified postmortem.

Analgesia (buprenorphine Temgesic®, ESSEX Chemie AG, Switzerland, 0.01-0.05mg per kg, s.c.) and antibiotics (Baytril® 2.5%, Bayer Health Care AG, Germany, 5-10mg per kg, s.c.) were provided for 3 and 5 days post-surgery, respectively.

Neurorehabilitation procedures and behavioral testing

Several groups of rats participated to the study. The main groups of rats involved 10 spinal and 6 contused rats. One of the contused rats was excluded due to a lesion extent that largely exceeded the mean variability of the rest of the group. All animals followed a comprehensive rehabilitation program during 2 months, starting 7 days after spinal cord injury, as previously described in detail (34) (**Figure 16, step 3**). Briefly, rats were trained 6 days per week for 30 min per day. To reactivate lumbar motor circuits during training, we applied an electrochemical neuromodulation therapy consisting of a serotonergic replacement therapy and epidural electrical stimulation (34). Five minutes prior to training, the rats received a systemic (i.p.) administration of quipazine (5-HT_{2A/C}, 0.2 - 0.3 mg/kg) and 8-OH-DPAT (5-HT_{1A/7}, 0.05 - 0.2 mg/kg) that was adjusted daily based on locomotor performance. Specifically, quipazine was adjusted to modulate extension components while 8-OH-DPAT was adjusted to modulate flexion components. During training, continuous epidural electrical stimulation (0.2ms, 100-300µA, 40Hz) was delivered through L2 and S1 electrodes. Training was conducted bipedally on a treadmill (11 cm/s) with adjustable robotic bodyweight support against the direction of gravity (Robomedica, USA). Starting 2 weeks after the induced injury, contused rats were additionally trained overground with the robotic bodyweight support system (84). The robotic bodyweight support provided optimal vertical and mediolateral support to the bipedally positioned animals. The forward component of the robot was set to zero force control mode. In this condition, the robot does not facilitate locomotion in the forward direction, i.e. a supraspinal command is necessary to initiate and sustain a forward motion of the body. The content of each training session evolved with the actual capacities of the rats and training objectives. Positive reinforcement was used to encourage the rats to perform the requested tasks.

Leg motor control was evaluated on a treadmill and along a straight runway with robotic assistance. All animals participated in behavioral evaluation 9 weeks post injury (**Figure 16, step 4**). They were tested without neuromodulation, with electrical neuromodulation, and with electrochemical neuromodulation. Experiments with mice did not involve rehabilitation procedures. Instead, leg motor control was evaluated in different testing conditions 4 weeks after spinal cord contusion.

Acute functional experiments in cats

Four cats were decerebrated and received a complete SCI at mid-thoracic level shortly after. Epidural electrodes were acutely implanted over the midline of L5 spinal segment and an intrathecal catheter was implanted at lumbar segments for local administration of pharmacological agents. For functional recordings, a treadmill enabling evaluations of bilateral locomotion in cats was used (116). A custom-made stereotaxic frame was used to fix the animal over the treadmill without impeding leg movements. Force plates located below each belt recorded the ground reaction forces generated by the left and right hindlimb. A video-based system allowed concurrent recording of whole body kinematics. Kinematic and muscle activity recordings were conducted to evaluate the effects of pharmacological interventions on locomotor performance. After baseline recordings of locomotion during continuous epidural electrical stimulation, various pharmacological agents were applied to achieve selective activation/inactivation of noradrenergic receptors in lumbar segments of spinal cats.

Circuit-specific inactivation using DREADDs

In order to reversibly silence proprioceptive afferent neurons in DRG, we used a viral mediated expression of an engineered G protein-coupled receptor exclusively activated by an otherwise inert drug-like small molecule (Clozapine N-oxide, CNO). A total of 2.5 μ L of AAV5-flex-DREADD-hm4Di-mCherry (titer 1.12^{E13} VG/ml) was injected bilaterally into each sciatic nerve under isoflurane anaesthesia (2% isoflurane) in a first surgery in PV^{Cre} rats (n=5). A 5 μ L Hamilton syringe was inserted into the nerve and used to slowly deliver the virus over the course of 90 seconds. The syringe was left in position for 2 minutes following injection to minimise any backflow of tracer. The skin was then sutured separately and animals were administered analgesics and allowed to recover in a heated incubator before being returned to their home cage.

One week after virus injection, stimulating electrodes were implanted at the midline overlying spinal cord segment L4 in PV^{Cre} (n=5) and wild-type (n=4) rats. Intramuscular electrodes (Cooner Wire; AS632) were inserted bilaterally in the tibialis anterior (TA, ankle flexor) muscles to record EMG activity. In the same set of surgery, all rats received a severe contusion injury (250 kdyn; 1 dyn=10 μ N) using a force-controlled spinal cord impactor (IH-0400 Impactor, Precision Systems and Instrumentation LLC, USA). The spinal cord displacement induced by the impact was measured for each animal and the extent and location of each lesion was verified postmortem. Analgesia (buprenorphine Temgesic®, ESSEX Chemie AG, Switzerland, 0.01-0.05 mg per kg, s.c.) and antibiotics (Baytril® 2.5%,

Bayer Health Care AG, Germany, 5-10 mg per kg, s.c.) were provided for 3 and 5 days post-surgery, respectively.

Starting 7 days after spinal cord injury, all animals were trained on 5-6 consecutive days on the treadmill using the above described electrochemical neuromodulation therapy consisting of a serotonergic replacement therapy and epidural electrical stimulation (34). Animals were trained until they showed plantar stepping enabled by electrical stimulation only.

Functional experiments under different experimental conditions were performed 4 weeks after virus injection. Stepping outcomes were evaluated under electrical stimulation at L4 spinal level before and after systemic (i.p.) injection of CNO (5 mg/kg body weight, dilution with saline). For both groups, control (wildtype) and PV^{Cre} rats, functional testing were performed before and over the course of 45-60min after CNO-injection.

For static reflex measurements, rats were anesthetized using urethane (0.5 - 0.6 mg/kg bodyweight, dilution with saline). Single electrical pulses were applied over the dorsal aspect of the L4 spinal cord level while EMG responses were recorded from both tibialis anterior (TA) muscles using acute needle implants (Ambu, Denmark) to detect electromyographic signals. Monosynaptic reflex curves were measured using the TDT system (Tucker Davis Technologies, USA). Testing were performed before and over the course of 60min after CNO-injection. CNO (5 mg/kg body weight, dilution with saline) was injected systemically (i.p.). For all animals, the extent and location of each lesion as well as the DREADD expression in DRG were verified postmortem.

Intrathecal (i.t.) injections

I.t. injections in contused rats were performed according to methods described previously (117,118). Animals were securely held in position while a 30G needle was inserted into the tissues between the dorsal aspects of L5 and L6, perpendicular to the vertebral column. When the needle entered the subarachnoid space, a sudden lateral movement of the tail was observed. This 'tail-flick' reflex was used as an indication of successful needle insertion. For each pharmacological agent tested, a volume of 0.05mL was injected. After injection, the syringe was held in position for a few seconds and progressively removed to avoid any liquid backflow. During the whole procedure, no sign of distress or pain was observed.

Kinematic, kinetic and muscle activity recordings

All procedures used have been detailed previously (34,84). During both treadmill and overground conditions, bilateral leg kinematics were captured using the high-speed

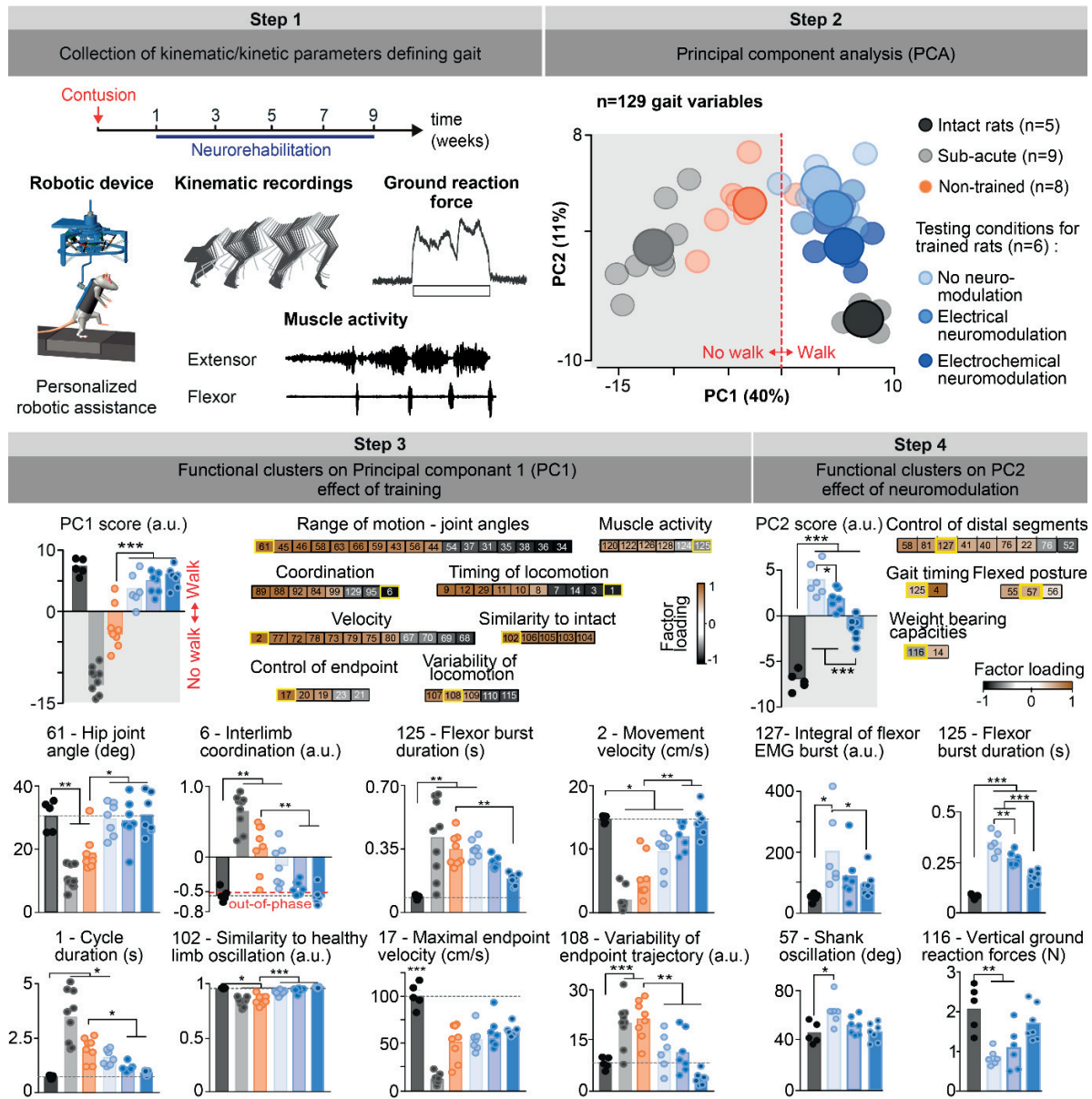
motion capture system Vicon (Vicon Motion Systems, UK), consisting of 12 infrared cameras (T-10, 200 Hz). Reflective markers were attached bilaterally at the iliac crest, the greater trochanter (hip joint), the lateral condyle (knee joint), the lateral malleolus (ankle), the distal end of the fifth metatarsophalangeal (mtp) joint and, for the rats, the tip of the fourth toe was added. The body was modeled as an interconnected chain of rigid segments, and joint angles were generated accordingly. Ground reaction forces were recorded using a biomechanical force plate (2 kHz; HE6X6, AMTI, YSA) located below the treadmill belt or in the middle of the runway. Electromyographic signals (2 kHz) were amplified, filtered (10-1000 Hz bandpass), stored and analyzed offline to compute the amplitude, duration and timing of individual bursts (**Figure 17, step 1**). For both the left and right legs, 10 successive step cycles were extracted over several trials on the runway for each rat under each experimental condition and time point. A 20 second interval was used when no or minimal leg movements were observed. Leg movements were reconstructed as a virtual segment connecting the iliac crest and the MTP marker. Kinematracer (Kissei Comtec Co., Japan) motion tracking software was used to obtain 2-D coordinates of hindlimb movements. EMG- signals were recorded concomitantly to video acquisition.

Analysis of kinematic, kinetic and muscle activity

A total of 104 (mice) and 129 (rats) parameters quantifying kinematics, kinetics, and muscle activity features were computed for each leg and gait/stroke cycle according to methods described in detail previously (34,84). All the parameters are reported in **table 2**. To evaluate differences between experimental conditions and groups, as well as the most relevant parameters to explain these differences, we implemented a multi-step statistical procedure based on PC analysis (72,84) (**Figure 17, step 2**). PC analysis was applied on data from all individual gait cycles or swim strokes for all the rats together. Data were analyzed using the correlation method, which adjusts the mean of the data to 0 and the standard deviation to 1. This method of normalization allows the comparison of variables with disparate values (large versus small values) as well as different variances (**Figure 17, step 3**).

#	Computed parameter	
Rat Mouse	Gait timing	Velocity
1	1 Cycle duration	67 59 Whole limb angle velocity (minimal)
2	2 Movement velocity	68 60 Hip joint angle velocity (minimal)
3	3 Stance duration	69 61 Knee joint angle velocity (minimal)
4	4 Swing duration	70 62 Ankle joint angle velocity (minimal)
5	5 Stance duration in percentage of whole cycle	71 MTP joint angle velocity (minimal)
6	6 Interlimb coordination	72 63 Whole limb angle velocity (maximal)
7	7 Double stance (in percentage of gait cycle duration)	73 64 Hip joint angle velocity (maximal)
8	8 Stride length	74 65 Knee joint angle velocity (maximal)
9	9 Step length	75 66 Ankle joint angle velocity (maximal)
10	10 Step height	76 MTP joint angle velocity (maximal)
11	11 Step height normalized to stance height	77 67 Whole limb angle velocity
12	12 Path length	78 68 Hip joint angle velocity
	Endpoint trajectory shape	79 69 Knee joint angle velocity
13	13 Stance width	80 70 Ankle joint angle velocity
14	Body weight support by the postural prosthesis	81 MTP joint angle velocity
15	14 Maximal backward position of the foot	(Intra-limb) coordination
16	15 Maximal forward position of the foot	82 71 Temporal coupling between crest and thigh oscillation
17	16 Maximal endpoint velocity	83 72 Temporal coupling between thigh and shank oscillation
18	17 Timing of the maximal endpoint velocity	84 73 Temporal coupling between shank and foot oscillation
19	18 Endpoint acceleration	85 Temporal coupling between foot and toe oscillation
20	19 Endpoint velocity	86 74 correlation of crest and thigh oscillation
21	20 orientation of the velocity vector at swing onset	87 75 Correlation of thigh and leg oscillation
22	Drag duration	88 76 Correlation of leg and foot oscillation
23	relative drag duration (percent of swing duration)	89 Correlation of foot and toe oscillation
	Stability	90 77 Correlation of hip and knee oscillation
24	21 Amplitude of lateral trunk position	91 78 Correlation of knee and ankle oscillation
25	22 Sagittal trunk movement	92 79 Correlation of ankle and MTP oscillation
26	23 Sagittal trunk velocity	93 80 Timing of crest-thigh (minimal)
27	24 Variability of vertical hip-midpoint oscillation	94 81 Timing of crest-thigh (maximal)
28	25 Variability of medio-lateral hip rotation	95 82 Timing of thigh-shank (minimal)
29	26 Forward movement of the center of mass	96 83 Timing of thigh-shank (maximal)
30	27 Lateral oscillation of the center of mass	97 84 Timing of shank-foot (minimal)
	Joint angles and limb segment oscillations	98 85 Timing of shank-foot (maximal)
31	28 Crest oscillation (minimal elevation)	99 Degree of linear coupling between joint oscillations (PC1)
32	29 thigh oscillation (minimal elevation)	100 Degree of linear coupling between joint oscillations (PC2)
33	30 Shank oscillation (minimal elevation)	101 Degree of linear coupling between joint oscillations (PC3)
34	31 Foot oscillation (minimal elevation)	Similarity to healthy gait
35	Toe oscillation (minimal elevation)	102 Correlation between limb oscillation of healthy and injured leg
36	32 Whole limb oscillation (minimal elevation)	103 Correlation between hip oscillation of healthy and injured leg
37	33 Crest oscillation (maximal elevation)	104 Correlation between knee oscillation of healthy and injured leg
38	34 thigh oscillation (maximal elevation)	105 Correlation between ankle oscillation of healthy and injured leg
39	35 Shank oscillation (maximal elevation)	106 Correlation between MTP oscillation of healthy and injured leg
40	36 Foot oscillation (maximal elevation)	Variability of gait
41	Toe oscillation (maximal elevation)	107 86 Variability of foot trajectory in the forward direction
42	37 Whole limb oscillation (maximal elevation)	108 87 Variability of foot trajectory in the sagittal plane
43	38 Hip joint angle (maximal)	109 88 Variability of foot trajectory in the 3-dimensional room
44	39 Knee joint angle (maximal)	110 89 Variability of gait cycle duration
45	40 Ankle joint angle (maximal)	111 90 Variability of stride length
46	MTP joint angle (maximal)	112 91 Variability of double stance duration
47	41 Whole limb adduction	113 92 Variability of step height
48	42 Foot adduction	114 93 Variability of path length
49	43 Hip joint angle (minimal)	115 94 Variability of max endpoint velocity
50	44 Knee joint angle (minimal)	Kinetics
51	45 Ankle joint angle (minimal)	116 vertical ground reaction force
52	MTP joint angle (minimal)	Muscle activity parameters
53	46 Whole limb abduction	117 Burst onset of extensor
54	47 Foot abduction	118 Burst end of extension
55	48 Crest oscillation	119 Burst duration of extensor
56	49 Thigh oscillation	120 Mean amplitude of extensor
57	50 Shank oscillation	121 Integral of extensor activity
58	51 Foot oscillation	122 Root mean square of extensor activity
59	Toe oscillation	123 Burst onset flexor
60	52 Whole limb oscillation	124 Burst end of flexor
61	53 Hip joint angle	125 Burst duration of flexor
62	54 Knee joint angle	126 Mean amplitude of flexor
63	55 Ankle joint angle	127 Integral of flexor activity
64	56 MTP joint angle	128 Root mean square of flexor activity
65	57 Whole limb medio-lateral oscillation	129 Co-contraction of the flexor and extensor muscle
66	58 Foot rotation	

Table 2 Kinematic, kinetic and EMG parameters



Virus production

AAV constructs used for central injections were based on a backbone vector from the Allen Institute for Brain Science (AAV-Flex-vector (690) XbaI/HindIII). Briefly, the vector contains a hSyn promoter, a WPRE element for enhanced expression and double inverted loxP elements (flex) flanking complementary DNA sequences (synthetic constructs from Blue Heron) in inverted orientations. DREADD (hM4Di) constructs were also used and detailed sequence information is available upon request. AAV2/5 production was carried out in 293AAV HEK cells following standard procedures, yielding vector suspension with titers $>1 \times 10^{13}$ VG/ml. The following vectors or constructs were obtained commercially: AAV-DJ-hSyn Flex mGFP 2A synaptophysin mRuby (Stanford vector core facility, reference AAV DJ GVVC-AAV-100), AAV2/6-G (The Boston Children's Hospital Viral Core) and Rabies-eGFP (Gene Transfer, Targeting and Therapeutics Core at the Salk Institute). The vectors were used at the concentration indicated for each injection procedures. All flexed AAV vectors used in the present study showed transgene expression only upon Cre-mediated recombination.

Virus and tracer delivery procedures

Spinal cord and brain targeted tracer or viral delivery were performed through stereotaxic injections using high precision instruments (David Kopf) under isoflurane anesthesia.

Monosynaptic rabies virus tracings were performed on $ROR\alpha^{Cre};R26^{LSL-tdTomato}$ neonate mice according to protocols described previously (119). A virus mixture containing equal volumes of AAV6-G (1×10^{14} GC/ml, The Boston Children's Hospital Viral Core) and Rab-eGFP (1×10^9 TU/ml, Gene Transfer, Targeting and Therapeutics Core at the Salk Institute) was injected unilaterally into the tibialis anterior muscle of neonate mice (P2). 3 μ l of virus mixture was injected into each muscle.

Anterograde tract-tracing of axons from rostro ventrolateral medulla (RVLM) projection neurons was performed in a group of four TH^{Cre} rats. A craniotomy was performed bilaterally over the brainstem medulla oblongata and AAV-DJ hSyn FLEX-mGFP 2A Synaptophysin-mRuby (titer 1.15×10^{14} GC/ml) was injected bilaterally into both RVLM. Four injections (250nl per injection) at two different rostrocaudal locations at two depths were made. Coordinates used for targeting this nucleus were -12.12 to -12.62mm anteroposterior from Bregma, 2mm lateral and 8 to 8.3mm ventral from the surface of the cerebellum.

Injections were performed using either a glass pipette driven with the Nanoliter pump (Nanoliter 2010 injector, *World Precision Instruments*) or using the Hamilton injection

system (for brainstem injections in rats). The virus was injected at 3nl/s and the needle was held in place for 2 minutes before being slowly retracted.

After a survival time of 8 (mice) to 18 (rats) days, all animals were deeply anesthetized by an i.p. injection of 0.5ml Pentobarbital-Na (50mg/mL) and transcardially perfused with approximately 80ml Ringer's solution containing 100'000IU/L heparin (Liquemin, Roche, Switzerland) and 0.25% NaNO₂ followed by 300ml of cold 4% phosphate buffered paraformaldehyde, pH 7.4. The brain and spinal cord were removed and postfixed overnight at 4°C in the same fixative before they were transferred to 30% sucrose in phosphate buffer (PB) for cryoprotection. The tissue was embedded in Tissue Tek O.C.T (Sakura Finetek Europe B.V., The Netherlands), frozen at -40°C, and cut to a thickness of 30µm.

Immunohistochemistry

Mounted or free-floating sections (30µm) were washed 3 times in 0.1M PBS and blocked in 5% normal goat serum containing 0.3% Triton (Sigma, USA). Sections were then incubated in primary antibody diluted in the blocking solution overnight at 4°C (CGRP, parvalbumin) or room temperature (GFP, Ib4, PKC-gamma, ChAT, RORα, vGlut2), or 3 nights at room temperature (Glutamate, Glycine, GABA). Primary antibodies used were rabbit anti-Glutamate (1:1000, Sigma, USA), rabbit anti-GABA (1:1000, Millipore, USA), rabbit anti-PKC-gamma (1:500, Santa Cruz Biotechnology, USA), rabbit anti-cfos (1:500, Santa Cruz Biotechnology, USA), rabbit anti-Parvalbumin (1:2000, Swant, Switzerland), rabbit anti-GFAP (1:1000, Dako, USA), rabbit anti-RFP (1:1000, Rockland, USA), chicken anti-GFP (1:500, Life Technologies, USA), goat anti-ChAT (1:500, Chemicon, USA), goat anti-RORα (1:500, Santa Cruz Biotechnology, USA), mouse anti-vGlut2 (1:2000, Millipore, USA), mouse anti-CGRP (1:1000, Abcam, UK), mouse anti-TH (1:500, Millipore, USA) and rat anti-glycine (1:200, Immunosolution, Australia). Sections were again washed 3 times in 0.1M PBS and incubated with the appropriate secondary antibody (Alexa fluor® 405, Alexa fluor® 488, Alexa fluor® 555 or Alexa fluor® 647; Molecular Probes, Life Technologies, USA) in blocking solution. DAPI (Life Technologies, USA) was used as a counterstain at a dilution of 1:1000 in 0.1M PBS for 20 minutes. Slides were washed, air-dried and cover slipped with Mowiol (Calbiochem, USA).

Fluorescent *in-situ* hybridization

To label mRNA of PV^{ON} and alpha2c^{ON} interneurons in the spinal cord, an RNA labeling kit from Molecular instruments (Molecular instruments, USA) was used. After perfusion, tissues were fixed in 4% phosphate buffered paraformaldehyde for 3 hours at

4°C before they were transferred to 30% sucrose in phosphate buffer (PB) for cryoprotection at 4°C for 2 nights. RNA *in situ* hybridization was performed on 40µm spinal cord sections according to a standard protocol. Briefly, samples were placed in 5x SSCT (20x SSC buffer, Invitrogen, USA; 10% Tween 20, Applichem, Germany) for 10min and then pre-hybridized in 30% probe hybridization buffer (Molecular instruments, USA) for 30min at 37°C. Samples were hybridized overnight at 2µM probe concentration in 30% probe hybridization buffer at 37°C. Following hybridization, samples were washed in a solution of 30% probe wash buffer (Molecular instruments, USA) and 5x SSCT four times 15 minutes. Sections were then incubated in an amplification buffer (Molecular instruments, USA) for 30min at room temperature. In the meantime, fluorophore-labeled HCR hairpins (Molecular instruments, USA) were snap-cooled (heating at 95°C for 90sec) and cooled down to room temperature. Amplification was performed overnight at room temperature at a concentration of 120nM per hairpin in the amplification buffer. Following amplification, samples were washed in 5x SSCT for at least 2 times 30min to remove unbound hairpins. Lastly, sections were air-dried and coverslipped using Mowiol (Calbiochem, USA).

Evaluation of spared tissue after spinal cord contusion

The extent and location of spinal cord damage was evaluated in each experimental animal. The lesion cavity was cut in serial coronal sections (40 µm) that were stained using GFAP antibodies (**Figure 18A** and **B**). For each lesion, we calculated the spared spinal cord surface with respect to the distance from the epicenter of the lesion, the spared area at the epicenter, and the total volume of damaged spinal cord tissue. The percentage of spared tissue at the epicenter was calculated using Fiji and normalized using the mean surface of sections rostral and caudal to the contusion, taking into account spinal cord compression (**Figure 18C**).

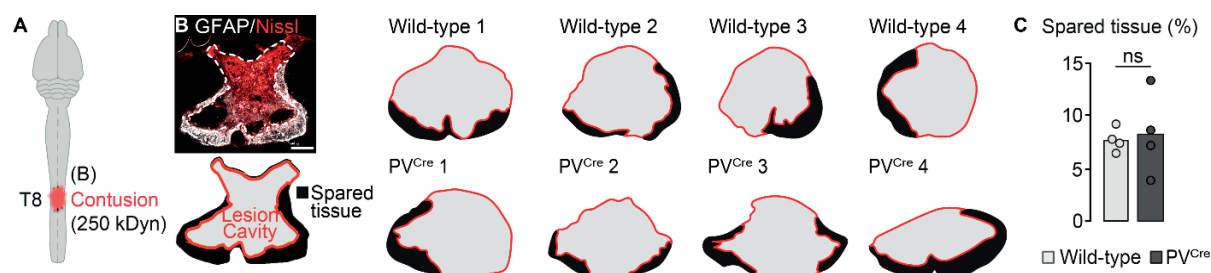


Figure 18 Lesion size quantification. (A) Severe contusion injuries (250 kdyn) were applied at spinal level T8. (B) Photograph of a coronal section at the contusion epicenter (GFAP, Glial fibrillary acidic protein), which was used to trace the contour of the contusion cavity and to measure the spared intact tissue, as illustrated below. Scale bar 250µm. The reconstructions of the lesion cavity at the epicenter are shown for PVCre (n=4) and wild-type (n=4) rats used for behavioral and anatomical evaluations. Scale bar 500µm. (C) The bar graph reports the area of spared tissue at the lesion epicenter for PVCre and wild-type rats. ns, not significant; Non-paired Student's t-test.

Neuromorphological evaluations

The percentage of double-labelled $\alpha 2a^{GFP}$ and $\alpha 2c^{GFP}$ neurons and various neurotransmitters (GABA, Glycine, Glutamate, and Acetylcholine) and sensory afferent markers (Parvalbumin, Ib4, CGRP) was quantified using 5 confocal image stacks per mouse at the L2 spinal cord level or in dorsal root ganglia. Images were acquired with standard imaging settings. Image acquisition was performed using a Leica TCS SPE or SP8 laser confocal scanning microscope (Leica Microsystems, Germany). Images were analyzed manually for double-labelling using the LAS AF interface (Leica Microsystems, Germany).

For $ROR\alpha^{Cre};R26^{LSL-tdTomato}$ mice injected with G-deleted rabies virus, the spinal cords were cut in coronal sections of 40 μ m. Images were acquired with standard imaging settings, using a Leica TCS SPE or SP8 laser confocal scanning microscope (Leica Microsystems, Germany). The number of $ROR\alpha^{ON}/vGlut2^{ON}$ synaptic contacts onto inhibitory pre-motor interneurons were counted manually using the Fiji 3D object counter. Synaptic contacts were quantified on 3 confocal image stacks per mouse. Neurons and synaptic contacts were reconstructed offline using the Imaris software (Bitplane, USA).

Single-cell sequencing data processing

For single-cell sequencing data of the mouse spinal cord, we queried the gene expression omnibus. For this, three studies were identified (100,120,121). Two out of the three studies used droplet-based methodology with relatively low sequencing depth (~50,000 per cell) (120,121), while the third study sequenced up to ~200,000 reads per cell (100). We retrieved the data from the gene expression omnibus (GSE103840, GSE103892) or the processed loom files available at <http://mousebrain.org/downloads.html>. Initial examination of the data revealed that the expression of markers of interest (*Rora*, *Adra2c*) were only robustly expressed with deeper sequencing, so only one dataset was used for further analysis (100).

Cells were classified according to the 30 global excitatory (glutamatergic) and inhibitory (GABAergic) phenotype as described in the publication (100). In a first step, the relative expression of the key marker genes *Rora* and *Adra2c* across all cell types were examined. Cells were defined as expressing the gene if the read count was non-zero, due to the known zero-inflation of single-cell sequencing reads. We considered a gene robustly expressed if more than 20% of cells in that subtype showed non-zero expression, similar to previous work (121). Only one cell type (Glut_Elavl4_Meis2) was found to robustly express both, *Rora* and *Adra2c*. Additionally, the expression of glutamate (*Slc17a6*), as well as classical markers including *Cck* and *Cmip*, which have previously been reported to be associated with *Rora*^{ON} cells in the dorsal horn were examined. Furthermore, control

markers (*Pkcg*, *Pax2*) that are known to be expressed at very low to negligible levels in *Rora*^{ON} cells were included.

CLARITY and 3D-Image acquisition

Tissue was cleared using CLARITY (122). Animals were deeply anesthetized with an i.p. injection of pentobarbital and perfused with 4% PFA. Brain and spinal cords were dissected and post-fixed overnight in 4% PFA at 4°C. The meninges were removed from brain and spinal cord segments and incubated in a bis-free Acrylamide solution (4% acrylamide, 0.25% VA-044 initiator, 0.001M PBS, no PFA) for 24 hours at 4°C with nutation. The tubes were then flushed with nitrogen (N₂) gas for 3 minutes and immediately closed to remove oxygen. Polymerization was then performed by incubating the hydrogel solution with the sample for 2 hours in a water bath at 37°C. Polymerization resulted in a viscous gel that was not solidified, as previously described (122). Excess gel was carefully removed and tissues were washed in 0.001M PBS for 5 minutes. The tissue was placed in the X-CLARITY chamber (Logos Biosystems Inc., South Korea), emerged with an SDS clearing solution (40g sodium dodecyl sulfate (SDS), 200mM boric acid, dH₂O up to 1 L of solution, pH 8.5) and cleared with the following settings: 37°C, 100 RPM, and 1.2A of current. A clearing solution was continually circulating through an adequate chamber and was changed every day following the 4 days after polymerization process. The clarification process lasted 10-15 hours for the spinal cord and about 30 hours for brainstem tissue. After clearing, the samples were placed in PBST (1x PBS, 0.1% (v/v) Triton-X, 0.02% (w/v) sodium azide) under shaking at room temperature for 24 hours.

Prior to imaging, samples were placed in RIMS (40g Histodenz in 30cc 0.02M PBS for a total volume of 48.75cc, pH 7.5, 0.01% sodium azide, refractive index: 1.465) for 24 hours. Imaging was performed using a custom-built COLM microscope as previously described (123). We used a customized sample holder to immerse the spinal cord or brain in a chamber filled up with RIMS. Samples were then imaged using a 4x objective with two light sheets illuminating the sample from the left and the right side. Z-step was set to 5µm in the dorsal-ventral orientation. Images were acquired as 16-bit TIFF files and reconstructed in 3D using the TeraStitcher (124). 3D reconstructions and optical sections of the raw images were produced using Imaris (Bitplane, v.9.0.0).

As the spinal cord lesion is a compact inflammatory tissue, the lesion cavity did not clear entirely and is therefore taken up in all channels. The background noise (scar tissue) is subtracted from the signal channel. The lesion volume was reconstructed using the Imaris Software.

Ex-vivo calcium imaging in mouse DRGs

PV^{Cre}:R26^{LSL-tdTomato} mice were anesthetized using urethane (0.5 - 0.6mg/kg bodyweight, dilution with saline). A laminectomy over the L2 spinal cord level was performed and electrical spinal cord stimulation was applied via acutely implanted electrode for 30 minutes. The following experimental conditions were tested (1) no electrical stimulation; (2) threshold stimulation and (3) supra-threshold stimulation (3x threshold). After stimulation, stimulated (L1-L3) and non-stimulated (T1) dorsal root ganglions (DRG) were dissected and prepared for calcium imaging experiments as previously described (Hutson et al., in preparation). Briefly, Fluo-4 AM (50µg, ThermoFisher, Cat.F14201) was re-suspend in 50µl DMSO (Sigma, Cat. D2650), diluted in 10 ml of HBSS without Ca²⁺ and Mg²⁺ (ThermoFisher, Cat. 14175095), supplemented with 10 mM Hepes (ThermoFisher, Cat. 15630080) and then stored in the dark at -20°C. After acute stimulation experiments, DRGs were extracted and immediately suspended in Fluo-4-AM (10 µM) dissolved in HBSS supplemented with 10 mM Hepes for 1 hour at 37°C, 5% CO₂. The Fluo-4-AM solution was then replaced with HBSS with 10 mM Hepes and the DRGs were washed for 1 hour at 37°C, 5% CO₂. The DRGs were placed into a video-microscopy chamber at 37°C, 5% CO₂ and suspended in HBSS with 10 mM Hepes. Time-lapse recordings were taken with images acquired every second for 5 minutes. Imaging was done on an Olympus XCellence microscope (Olympus, Japan) equipped with a Hamamatsu camera (*ORCA 03G, Japan*) at 20X magnification. After 1 minute of baseline recording, increasing concentrations (50 mM, 100 mM and 150mM) of KCL (Sigma, Cat. P3911, USA) were added to the DRG to elicit depolarisation and induce intracellular Ca²⁺ release. Quantification was done using the Fiji-ImageJ plug-in *Time series analyser*, where the soma of at least 20 neurons per DRG were analysed. To determine the fold-change in Fluo-4 AM intensity after KCL addition, the Fluo-4-AM intensity ratio "F/Fo" was calculated by dividing the average fluorescence intensity after KCL addition "F" with the average intensity of baseline fluorescence "Fo".

Recruitment curves

EES-evoked motor responses were recorded in ankle flexor and extensor muscles in response to single electrical pulses. Rectangular pulses (0.5 ms duration) were delivered at 0.2 Hz through the implanted L2 or S1 electrodes. The intensity of electrical stimulation was applied over a defined range of amplitudes, starting from threshold level and increasing for 200µA. EES-evoked motor potentials were recorded in TA and MG muscles. Animals were awake and hold still during stimulation. Analysis was performed in Matlab. EMG signals (12.207 kHz) were amplified, filtered (1–5000 Hz bandpass), and stored for

off-line analysis. Signals with movement artefacts were excluded. The onset latency and peak amplitude of the different components in compound action potentials were determined through a custom-made software in Matlab (MathWorks).

Electrophysiological and pharmacological experiments

Electrophysiological experiments were performed in awake rats before (baseline condition) and after the administration of various pharmacological agents. The following pharmacological agents were tested: (1) quipazine (5-HT_{2A/C}, 0.2 - 0.3mg/kg) and 8-OH-DPAT (5-HT_{1A/7}, 0.05 - 0.2mg/kg); (2) clonidine (NA₂ agonist, 0.4 - 0.6mg/kg); (3) Guanfacine hydrochloride (alpha_{2a} agonist, 3mg/kg); (4) BRL-44408 (NA_{2a} antagonist, 7 - 7.5mg/kg); (5) JP-1302 (alpha_{2c} antagonist, 7 - 7.5mg/kg) and (6) compound A08 (dual NA_{2a} antagonist/NA_{2c} agonist, 25 - 35mg/kg). All pharmacological agents were injected systemically (i.p.).

Modeling experiments

The neural network is implemented in NEURON (125) using a parallel multi-threaded structure. Afferent fibers are modeled as Poisson point processes with average firing rates estimated from a spindle model and 20% noise level. The latency between action potentials and elicited excitatory postsynaptic potentials (EPSPs) to the target cell follows a normal distribution (mean = 2ms, variance = 0.3ms) accounting for the variability in afferents diameter. A total of 60 Ia- and group-II fibers are implemented for each motor pool (126). Each group-Ia fiber forms excitatory synapses to all motoneurons of the homonymous motor pool (126), while group-II fibers establish excitatory synapses onto each group-II interneuron (127). Each motor pool comprises 169 alpha motoneurons (90,127–129). The membrane potential of each cell is described as a modified Hodgkin- Huxley model comprising sodium, potassium, calcium, and potassiumcalcium gated ion channels (129). To model the effect of 5-HT agonists, which is used with EES to enable locomotion, we lowered the potassium- calcium gated ion channels conductance by 40% (130). Motoneuron morphology consists of a 32 ± 10 -mm-diameter spherical soma connected to an electronic-equivalent dendritic tree of mammalian S type alpha motoneurons (128,131), dendritic sizes adapted to match soma diameter, from cell S-type cell 35/4. The initial segment and efferent axon are implemented with dedicated membrane dynamics (90,129). Inhibitory synapses innervate the soma and behave as alpha functions with a reversal potential $E_{syn} = -75$ mV, a rise time constant $\tau = 1.5$ ms, and a decay time constant $t = 2$ ms. The resulting inhibitory postsynaptic potential (IPSP) at the soma reaches an amplitude of 3mV (109,132). Group-II interneuron excitatory synapses are located along

the dendritic tree with a Poisson distribution (128). Excitatory synapses are modeled by an exponential function with reversal potential $E_{syn} = 0$ mV and decay time constant $t = 0.5$ ms. The conductance of excitatory synapses from group-Ia fibers was tuned to a mean EPSP amplitude = 212 mV (133), increased by 28% to mimic the heteronymous contribution of synergistic innervations (134). The conductance of group-II interneuron synapses was set to one-third the size of group-Ia fiber EPSPs to mimic the smaller impact of group-II fibers on motoneurons (135). Excitatory and inhibitory interneurons were modeled as Integrate and fire cells with membrane time constant $t_m = 30$ ms. Due to the absence of experimental measurements, we tuned the strength of the reciprocal inhibition by comparing the energy of the simulated and experimental EMG signals. We computed a fitness score to measure the amount of alternation in bursting activity of antagonist motor pools during gait:

$$\text{Alternation} = \text{mean} (1 - (\text{EMGenvelope}_{flex} * \text{EMGenvelope}_{ext}))$$

$$\text{EnergyRatio} = (\text{EnergyEMGenvelope}_{flex}) / \text{EnergyEMGenvelope}_{ext} * \\ (\text{EnergyExperimentalEMGenvelope}_{ext}) / \text{EnergyExperimentalEMGenvelope}_{flex}$$

$$\text{Fitness Score} = \text{Alternation} * \text{EnergyRatio}.$$

Synaptic strengths were set to match recordings in healthy rats during stepping (fitness score equal to 1). We performed a robustness test over the chosen value. A variation of 40% in IPSP conductance of Ia-interneurons induced a 37% change in fitness, compared to a total possible maximum change of 1,400% ranging from tonic activation to complete suppression of the motor pool activity. A variation of 56% in EPSP strength resulted in a 10% change in fitness score, showing that the chosen parameters are robust and preserve results over a wide range of values.

Muscle Spindle Model

Instantaneous firing rates of group-Ia and -II afferents fibers were computed using a spindle model (136). Fibers stretch and stretch velocity were linked to the envelope of EMG bursts to mimic the alpha-gamma linkage. The firing rates of the different fibers were computed using the following equations:

$$\text{Ia firing rate} = 50 + 2 * \text{stretch} + 4.3 * \text{sign}(\text{strVelocity}) * \text{strVelocity}^{0.6} \\ + 50 * \text{EMG}_{env}$$

(Equation 1)

$$\text{II firing rate} = 80 + 13.5 * \text{stretch} + 20 * \text{EMG}_{\text{env}}$$

(Equation 2)

Biomechanical Model

Estimation of the muscle fiber stretch during gait was derived from a realistic musculoskeletal model of the rat hindlimb implemented in OpenSim (137) and validated experimentally (138,139). We fed OpenSim with crest, hip, knee, ankle, and metatarsophalangeal joint positions recorded in healthy rats (n = 10 steps) to calculate the corresponding muscle stretch profile of muscles of the ankle.

Coupling with EES

The number of fibers recruited by EES was computed using a validated finite element model of EES (90) with the same geometry and parameters. The coupling between EES and the natural firing rate of afferent fibers is nonlinear. If a depolarization event occurs when the nodes of Ranvier are producing an action potential or during its refractory period, EES may fail to elicit a depolarization, or it may occur at higher thresholds. We modeled afferents fibers as integrate and fire cells with a membrane time constant = 30 ms. EES and natural firing rates were provided as suprathreshold synaptic inputs to each fiber. Firing rates were calculated from the sum of EES frequency and natural firing rate on the cell membrane.

EMG Model

Alpha motoneuron action potentials occurring at the last node of Ranvier were convolved with representative motor unit action potentials (MUAPs), modeled as damped sinusoidal waves with normally distributed amplitude (1 ± 0.2 a.u.) and duration (7.5 ± 2 ms). A latency of 2 ms between each event and the corresponding MUAP was implemented to account for the traveling time of an action potential from the spinal cord to the rat triceps surae (94).

Statistical procedures

All data are reported as mean values \pm s.e.m. Behavioral assays were replicated several times (3 to 10 times depending on the experiments) and averaged per animal. Statistics were then performed over the mean of animals. All statistical analysis was performed in GraphPad Prism, (USA) using two-sided paired or unpaired Student's t-tests, one-way ANOVA for neuromorphological evaluations with more than two groups, and

one- or two-way repeated-measures ANOVA for functional assessments, when data were distributed normally. The post hoc Tukey's or Bonferroni test was applied when appropriate. The significance level was set as $p < 0.05$. The nonparametric Mann-Whitney or Wilcoxon signed-rank tests were used in comparisons of <5 rats or mice.

Data availability

Data are available from the authors upon request.

Acknowledgements

We are grateful to Dr Lutz Hein for providing us the alpha2a and alpha2c knockout mouse lines; Dr Ariel Levine for the fruitful discussion and feedback; Dr Martyn Goulding for providing the $ROR\alpha^{Cre}$ mouse line; Dr Steeve Bourane for his advice and feedback on neonate mouse experiments; Dr Zhigang He for providing viral vectors; Dr Natalia Pavlova, Dr Polina Shkorbatova and Arnaud Bichat for the performed surgeries and Robin Schulz for musical entertainment.

IV. CHAPTER II

Activity-dependent recovery after spinal cord injury involves a druggable epigenetic mechanism

4.1 Abstract

Injured axons fail to regenerate in the adult mammalian central nervous system (CNS), leading to permanent deficits in sensory and motor functions. We found that enhancing the activity of proprioceptive dorsal root ganglion (DRG) neurons through an enriched environment induces a long-lasting increase in their regenerative potential that is dependent on CREB Binding Protein (CBP)-mediated histone acetylation. Delivery of a small molecule activator of CBP acetyltransferase at clinically relevant times after spinal cord injury promoted regeneration and sprouting of sensory and motor axons, together with improvement in both sensory and motor functions. These findings open avenues for therapeutic developments in clinical spinal cord injury.

*Adapted from the submitted manuscript: **Activity-dependent recovery after spinal cord injury involves a druggable epigenetic mechanism.** T. H. Hutson, C. Kathe, I. Palmisano, K. Bartholdi, A. Hervera, F. De Virgiliis, E. McLachlan, L. Zhou, G. Kong, Q. Barraud, M. C. Danzi, A. Medrano-Fernandez, J. Lopez-Atalaya, A. L. Boutillier, S. H. Sinha, A. K. Singh, P. Chaturbedy, L. D. F. Moon, T. K. Kundu, J. L. Bixby, V. P. Lemmon, A. Barco, G. Courtine[#], and S. Di Giovanni[#].*

[#]Co-senior authors

4.2 Introduction

Following spinal cord injury (SCI), motor and sensory axons fail to regenerate, leading to permanent neurological impairments (31,140). Sensory dorsal root ganglia (DRG) neurons convey afferent information from the periphery to the spinal cord in order to modulate motor outputs, and to supraspinal structures for the elaboration of sensorimotor integration and conscious perception. Amongst the DRG, proprioceptive neurons innervate muscle spindles and Golgi tendon organs. They transmit information about the length and tension of muscles, which plays a critical role during sensorimotor execution (12,19). Moreover, proprioceptive afferent feedback plays an important role in directing motor recovery after SCI. Mice lacking functional proprioceptive afferents exhibit a defective rearrangement of descending pathways that prevents recovery after SCI (12). This observation indicates that proprioceptive neurons may deliver molecular cues for axonal regrowth and sprouting after injury. In turn, modulation of proprioceptive afferents with electrical stimulation (76,85) and rehabilitative training (34) augments neuroplasticity and recovery in both animal models and humans after SCI (41). However, the underlying mechanisms remain poorly understood.

Proprioceptors are ideally located for modulation by environmental stimuli. Here, we investigated the impact of environmental enrichment (EE) on proprioceptive DRG neurons, hypothesizing that this would prime them to initiate a regenerative response to a subsequent injury. We show that augmenting the activity of proprioceptive DRG neurons using EE induces a lasting increase in their regenerative potential that is dependent on CREB Binding Protein (CBP)-mediated histone acetylation. In turn, pharmacologically increasing CBP acetyltransferase activity at clinically-relevant times and in clinically-relevant models of SCI promoted regeneration and sprouting of sensory axons and brainstem motor pathways that mediated improvements in both sensory and motor functions. These results show that neuronal activity leads to changes in chromatin environment that boost the regenerative capacity of neurons. Elucidating the mechanisms underlying activity-dependent responses in neurons translated into the identification of a clinically-relevant pharmacotherapy for SCI that warrants evaluation in humans.

4.3 Results

Environmental enrichment induces a lasting increase in the regenerative potential of DRG neurons

To test whether EE can enhance the regenerative potential of DRG neurons, mice were exposed to EE or standard housing (SH) for 1, 3, 6, 10 or 35 days. Neurite outgrowth of DRG neurons was significantly enhanced only after exposure to EE for 10 or 35 days on a growth permissive substrate (**Figure 19A and B**). The extent of neurite outgrowth on myelin was similar to what is observed after a conditioning injury, which represents the benchmark for stimulating DRG axon regeneration (141,142).

EE-dependent neurite outgrowth was abolished when delivering the transcriptional inhibitor actinomycin-D in culture, suggesting a dependence of this response on gene transcription. EE-dependent increase in neurite outgrowth was maintained during a 5-week period of SH after 10 days of EE (**Figure 19C, D and E**), suggesting that EE may trigger long-lasting epigenetic reprogramming. Analyses of growth responses revealed that EE enhanced axon elongation rather than branching, which may translate into axonal regeneration *in vivo*.

Given the multifactorial nature of EE, we decided to discriminate between the relative role of running, and the remaining environmental stimuli (larger cage, increased number of mice, novel objects, and increased nesting material) on DRG outgrowth. Mice were placed either in EE, in SH, in EE with an immobilised wheel or in SH with a running wheel for 10 days. Analysis of neurite outgrowth showed that although the running wheel in SH enhanced outgrowth compared to SH alone, the full complement of EE still induced a significantly higher degree of outgrowth. This result indicated that the full EE is required for maximal enhancement of DRG outgrowth.

We next tested whether EE can also enhance regeneration of axons within the peripheral and the central nervous system. Prior exposure to EE enhanced sciatic nerve regeneration after complete transection and re-anastomosis (**Figure 19F and G**), along with increased muscle re-innervation after a sciatic nerve crush.

We then assessed whether pre-exposure to EE would enhance regeneration of sensory axons in the dorsal columns after a SCI and compared this response to the regeneration observed after a conditioning injury. Three groups of adult mice were exposed to EE or SH for 10 days and then housed in SH, subsequently one SH group received a conditioning sciatic nerve axotomy (SNA) injury and the other SH and the EE groups underwent a sham injury. Next, all the mice received a thoracic (T12) dorsal hemisection. Five weeks later, the retrograde tracer Cholera Toxin subunit B (CTB) was

injected into the sciatic nerves to evaluate the regeneration of ascending dorsal column axons (Figure 1H). The majority of labelled axons from SH Sham mice retracted from the injury site. In contrast, labelled axons from EE Sham mice could be observed within the lesion epicentre. Some regenerating axons even expanded beyond the lesion site, attaining distance up to 800 μm from the lesion border (**Figure 19H and I**). Some of these regenerating axons co-localized with vGlut1, suggesting the formation of putative synapses. In the SH SNA group, we also found as expected axons traversing the lesion (**Figure 19H and I**).

We conducted terminal electrophysiological experiments 6 weeks after injury to evaluate the functionality of these regenerating axons. The dorsal columns were stimulated below the injury at L5, and recorded both below and above the lesion, at L1 and T9, respectively (Figure 1J). In all the animals that underwent EE or SNA, compound action potentials could be recorded above the lesion site. However, the amplitude of these responses was significantly larger for the animals that had been housed in EE compared to SNA (black traces, **Figure 19K and L**), suggesting an increase in neuroplasticity across the lesion. There was no significant difference in the compound action potential recordings below the lesion for any of the groups (blue traces, **Figure 19K**).

To assert that regenerating sensory axons were responsible for the increase in conduction through the lesion site, we specifically silenced these axons using designer receptors exclusively activated by designer drugs (DREADD), using methods that were described previously (143). We injected an AAV-flex-hM4Di into the sciatic nerve to express the Gi receptor into DRG neurons under Cre recombination. Three weeks after SCI, an AAV-Cre was injected rostral to the site at of injury to express the Cre-dependent Gi-coupled DREADD only in those DRG neurons that had extended axons through and beyond the lesion. After 3 additional weeks, mice previously exposed to EE underwent electrophysiological assessment. In all tested mice, compound action potentials could be recorded beyond the lesion. Chemogenetic mediated silencing restricted to regenerated axons (Cre-dependent AAV-flex-hM4Di) significantly reduced conduction across the lesion, establishing causality that was confirmed with a re-transection (**Figure 19K and L**).

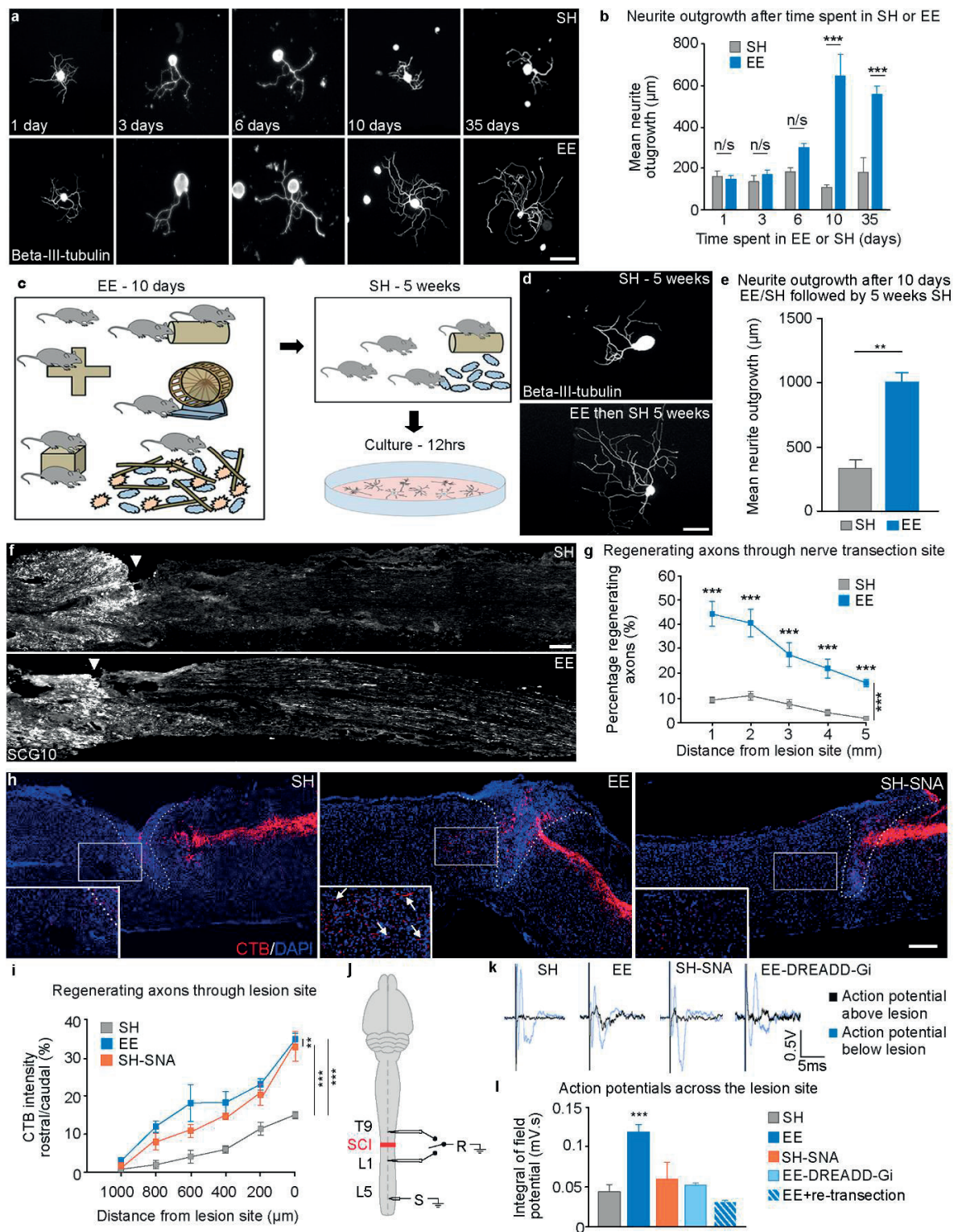


Figure 19 Environmental enrichment induces a lasting increase in the regenerative potential of sensory neurons. **a**, Cultured mouse sciatic DRGs after exposure to EE, stained for Beta-III-tubulin. Scale bar 100 μ m. **b**, Quantification of neurite outgrowth (mean \pm SEM, Unpaired Student's t-tests *** P <0.001, n = 4/group). **c**, Diagram illustrating the experimental design, sciatic DRGs were cultured from mice that had been placed in EE for 10 days and then returned to SH for up to 5 weeks. **d**, Example images of sciatic DRGs from mice that had been in SH or EE for 10 days and then SH for 5 weeks. Scale bar 100 μ m. **e**, Quantification of neurite outgrowth indicated that DRGs from mice that had been exposed to EE still had significantly increased neurite outgrowth compared to SH controls (mean \pm SEM, unpaired Student's t test *** P <0.001, n = 4/group). **f**, Sciatic nerves immunostained for SCG10 after transection and re-anastomosis, Scale bar 500 μ m. **g**, Quantification of regenerating axons (mean \pm SEM, Two-way ANOVA, Holm-Sidak post-hoc, *** P <0.001, ** P <0.01, * P <0.05 n = 6/group). **h**, CTB-traced (red) dorsal column axons after injury, DAPI (blue), lesion site (dashed line). Scale bar, 200 μ m. **i**, Quantification of CTB positive regenerating axons (mean \pm SEM, Two-way repeated measures ANOVA, Tukey's post-hoc ** P <0.01, *** P <0.001, n = 10/group). **j**, Electrophysiological setup. **k**, Compound action potentials recorded below (blue) and above (black) injury. **l**, Quantification of compound action potentials above the lesion (mean \pm SEM, One-way ANOVA, Fisher's LSD post-hoc *** P <0.001, n = 6/group).

Proprioceptive afferent feedback is required for EE-mediated increase in DRG regenerative growth

We next investigated whether a specific type of neurons were implicated in EE-dependent regenerative growth. We injected CTB into the distal sciatic nerve one day after performing a sciatic nerve crush injury. Consequently, only DRG neurons that regenerated an axon across the injury site and into the denervated side would be able to take up the CTB tracer (**Figure 20A**). Two days after the CTB injection, we assessed the number of CTB-positive DRG neurons that co-stained for markers of the main DRG subpopulations (**Figure 20B**). Prior exposure to EE significantly increased the number of CTB positive DRG neurons (**Figure 20C**). The majority of DRG neurons, which regenerated axons through the sciatic nerve crush and were retrogradely labelled with CTB, expressed markers of proprioceptors (parvalbumin) rather than nociceptors (isolectin B4 or substance P) (**Figure 20B and D**), suggesting that EE specifically enhances the regeneration of proprioceptive axons.

Next, we investigated whether the EE-dependent increase in regenerative potential of proprioceptive neurons relied on a muscle spindle proprioceptive mechanism. To this end, we used *Egr3*^{-/-} mice that while retaining a similar number of parvalbumin (PV) DRG neurons compared to WT mice, this mutation abolishes muscle spindle proprioceptive feedback (12,144) (**Figure 20E**). We found that EE- but not sciatic nerve axotomy-dependent DRG outgrowth was abolished in mice lacking intact muscle spindles (*Egr3*^{-/-}) (**Figure 20F and G**). This observation demonstrates that EE-dependent regenerative priming is contingent on intact proprioceptive feedback.

Finally, to further confirm the cell type specificity of the EE mechanism, we assessed neurite outgrowth of DRG neurons from PV-tdTomato mice. Exposure to EE significantly increased the outgrowth of PV^{ON} but not PV^{OFF} DRG neurons (**Figure 20H and I**).

Taken together, these experiments demonstrate that prior exposure to EE specifically primes proprioceptive DRG neurons for enhanced axon regeneration.

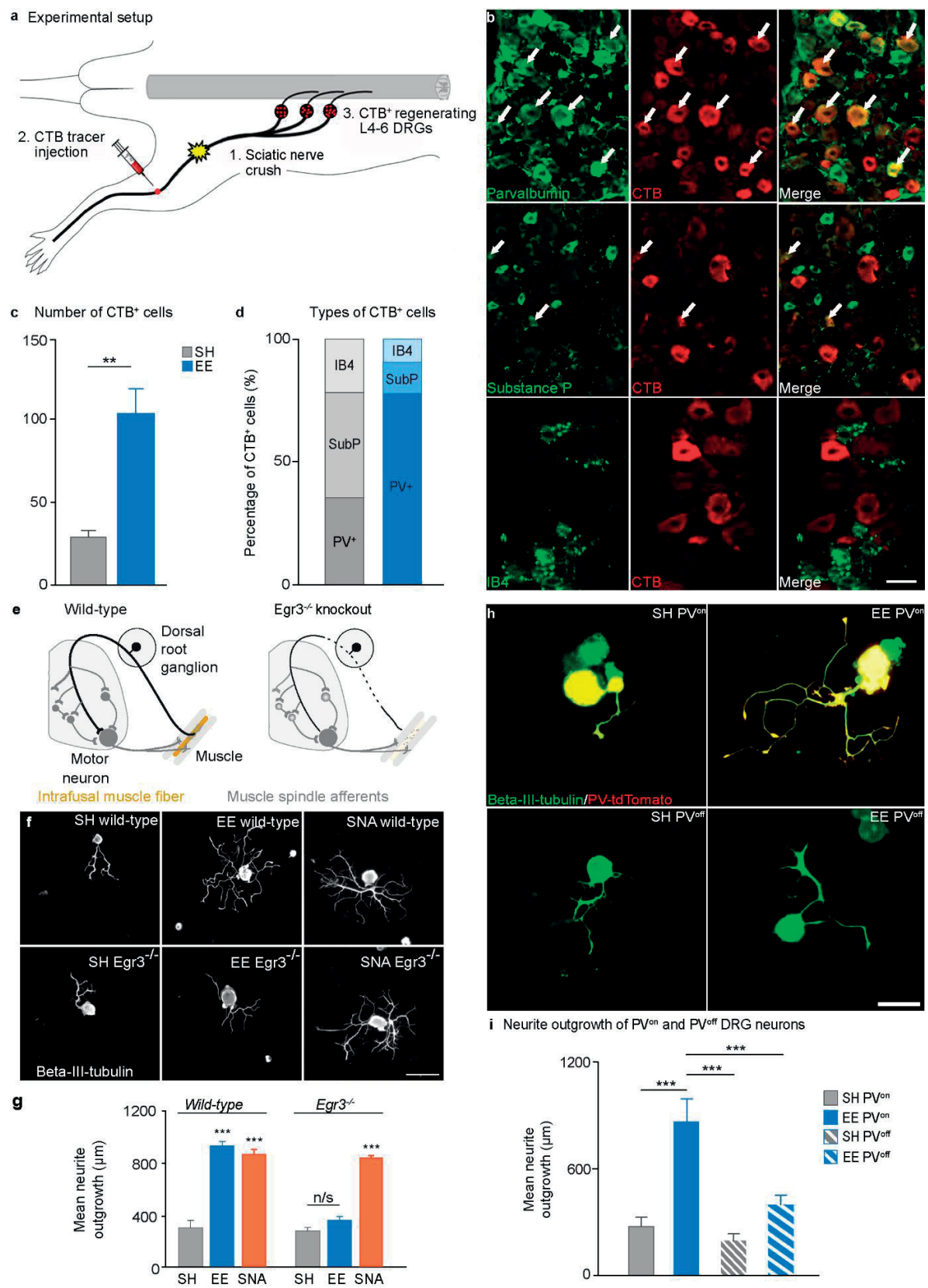


Figure 20 Proprioceptive afferent feedback is required for EE-mediated increase in DRG regenerative growth. **a**, Schematic of the experimental design, after EE and SH exposure mice underwent sciatic nerve crush injury and CTB injection distal to the crush site, axons that regenerate across the injury site take up CTB and retrogradely transport it to the soma. **b**, Representative images of co-localization between parvalbumin, substance P or isolectin B4 (green) and CTB (red) in DRGs from EE mice that had undergone a sciatic nerve crush. Scale bar, 50 μ m. **c**, Quantification of the number of CTB positive DRG neurons suggests EE significantly enhances axon regeneration compared to SH (mean \pm SEM, unpaired Student's t test, ** $P < 0.01$, $n = 3/\text{group}$). **d**, Quantification of the percentage of CTB positive neurons that co-localized with parvalbumin, substance P or isolectin B4 demonstrates high levels of co-localization between CTB and parvalbumin after exposure to EE. **e**, Schematic showing *Egr3* mutation resulting in degeneration of muscle spindles. **f**, Beta-III-tubulin stained sciatic DRGs from WT or *Egr3*^{-/-} mice after exposure to SH or EE. Scale bar 100 μ m. **g**, Quantification of neurite outgrowth. (mean \pm SEM, One-way ANOVA, Tukey's post-hoc, *** $P < 0.001$, $n = 4/\text{group}$). **h**, Example images of tdTomato (red) positive or tdTomato negative DRGs co-stained with beta-III-tubulin (green) cultured from PV-cre x tdTomato mice that had been exposed to either SH or EE for 10 days. Scale bar 100 μ m. **i**, Quantification of neurite outgrowth showed EE significantly increased outgrowth of PV-tdTomato+ DRGs compared to PV-tdTomato- DRGs (mean \pm SEM, One-way ANOVA, Tukey's post-hoc, ** $P < 0.01$, *** $P < 0.001$, $n = 5/\text{group}$).

Environmental enrichment induces signalling pathways involved in neuronal activity, calcium mobilization and the regenerative program of large-diameter DRG neurons

EE and exercise have been shown to increase neurotrophin expression and modify cytokines influencing neuroplasticity (145–147). Surprisingly we found no changes in neurotrophin or cytokines levels in the DRG or in the blood, suggesting that alternative mechanisms may be responsible for EE-dependent DRG regenerative growth.

To uncover EE-dependent molecular mechanisms, we performed RNA sequencing (RNAseq) from whole DRG or laser-captured large-diameter DRG neurons (LDN) and conducted proteomic analysis from sciatic nerve axoplasm after EE or SH. Unsupervised gene expression clustering showed dramatic changes in gene expression of LDN after EE vs SH, but not in the whole DRG, which contains a multitude of different neuronal and glial cell types (**Figure 21A**). These results confirmed that EE specifically modulates gene expression in proprioceptors and potentially mechanoreceptors. EE preferentially increased rather than repressed gene expression in LDN. Similarly, proteomic analysis showed a larger number of up-regulated proteins after EE vs SH (71 vs 49). Importantly, 37 out of 71 significantly up-regulated proteins were also up-regulated at the RNA level, suggesting that gene transcription drove the observed protein changes. Functional classification of EE-dependent gene expression changes in LDNs revealed that EE strongly modulated functionally interconnected molecular pathways involving ion channels, neuronal activity, calcium signalling, energy metabolism and neuronal projection (**Figure 21B**). Combined analysis of the RNAseq and proteomic datasets for protein-protein interactions identified multiple interactions between proteins involved in neuronal activity, calcium signalling and cytoskeletal rearrangements, supporting a role for EE-mediated activity in axon projection and elongation.

These results encouraged us to investigate the role of neuronal activity and calcium release in the EE-mediated increase in DRG regenerative potential. We employed an AAV-mediated chemogenetics approach to inhibit or enhance neuronal activity of DRG neurons using DREADD technology. When activated by the pharmacologically inert ligand clozapine-N-oxide (CNO), Gi-coupled (hM4Di) DREADD receptors inhibit adenylyl cyclase, which silences neuronal activity (148). Instead, activation of Gq-coupled (hM3Dq) DREADD receptors enhance neuronal activity by eliciting IP₃-mediated calcium release from intracellular stores (148). This increase in intracellular calcium levels activates calcium-dependent signalling cascades, which would thus mimic the effects of EE on DRG neurons identified with gene and proteomic analysis.

We injected AAV vectors into the sciatic nerve to express hM4Di, hM3Dq or GFP in DRG neurons. mCitrine/GFP expression confirmed an efficient transduction. Four weeks after injection, mice expressing hM4Di, hM3Dq or GFP were placed in EE or SH. CNO was added in the drinking water to activate the receptors. Ten days later, we performed a sciatic nerve crush, and assessed the extent of regeneration three days post-injury (**Figure 21C and D**).

Gq activation enhanced axon regeneration in SH mice and Gi-dependent inactivation of DRG neurons significantly attenuated axon regeneration of mice exposed to EE, demonstrating the importance of neuronal activity for EE-mediated regeneration (**Figure 21C and D**). Expression of Gi in SH mice or Gq in EE mice did not further impair or promote axon regeneration (**Figure 21C and D**). Similar results were obtained when assessing neurite outgrowth of DRGs cultured after *in vivo* DREADD transduction and EE exposure. Gq expression in DRGs from SH mice significantly increased neurite outgrowth to a similar extent to what was observed in the DRGs of mice exposed to EE, while the expression of Gi in DRG neurons significantly reduced EE-dependent outgrowth.

RNAseq and proteomics data suggests that EE may enhance calcium signalling in proprioceptive DRG neurons. To visualize this induction of activity-dependent signalling pathways in proprioceptive neurons in response to EE, we directly measured intracellular calcium levels in these cells, as an indicator of release from intracellular stores. Transgenic mice that expressed the genetically encoded calcium indicator GCaMP under the PV promoter were exposed to EE or SH. Whole sciatic DRGs were extracted in order to measure the fluorescent signals of proprioceptive neurons *ex vivo* when applying increasing levels of potassium chloride. As anticipated, we found that a prior exposure to EE significantly increased the levels of calcium in DRG neurons at all the potassium chloride concentrations tested compared to calcium levels measured in the DRGs of SH mice (**Figure 21E and F**). These observations show that EE increases calcium signalling in

proprioceptive neurons, which is likely due to the increased solicitation of muscle spindles and force sensors within the enriched environment.

These results provide evidence that EE increases neuronal activity and calcium signalling in proprioceptive DRG neurons and plays an important role in the activity-dependent increase in regenerative potential.

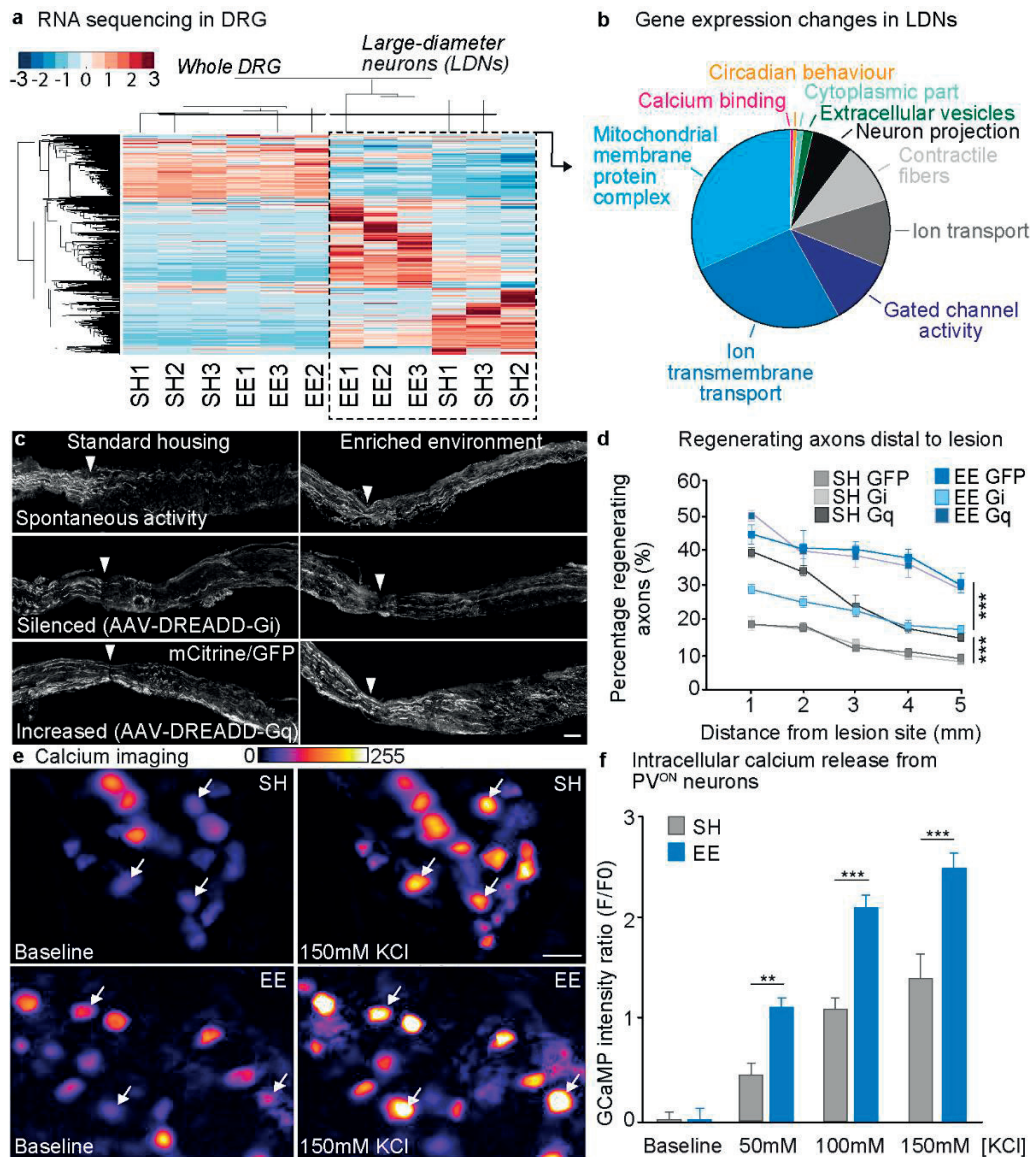


Figure 21 EE induces signalling pathways involved in neuronal activity, calcium mobilization and the regenerative program of large-diameter DRG neurons. **a**, Heatmap of the differentially expressed (DE) genes in whole-DRG and LDN RNA-seq ($P < 0.05$). Color scale represents arbitrary expression units (lowest, blue; highest, red). **b**, Pie chart of genes in each functional group identified by GO analysis of DE genes in LDN. Functional groups are color-coded. **c**, Sciatic nerves transduced with AAV5-GFP, AAV5-hM4Di-mCitrine or AAV5-hM3Dq-mCitrine labeled with mCitrine/GFP after sciatic nerve crush. Arrow-head: lesion site. Scale bar, 500 μ m. **d**, Quantification of axon regeneration (mean \pm SEM, Two-way repeated measures ANOVA, Tukey's posthoc, $***P < 0.001$, $n = 6/\text{group}$). **e**, Time-lapse images of intracellular calcium release from whole-mount PV-GCaMP DRGs before and after addition of 150 mM KCl. Scale bar, 50 μ m. **f**, Quantification of F/F₀ ratio after 50 mM, 100 mM and 150 mM KCl (mean \pm SEM, Two-way ANOVA, Sidak's post-hoc $**P < 0.01$, $***P < 0.001$, $n = 4/\text{group}$).

CBP mediated histone acetylation is required for EE-dependent increase in regeneration potential

We reasoned that EE-dependent modulation of neuronal activity might induce epigenetic modifications enabling active transcription and a lasting increase in regenerative potential. Indeed, we found that EE enhanced H3K27ac and H4K8ac but not H3K9ac, H3K4me2 or H3K4me3 in parvalbumin-positive DRG neurons (**Figure 22A, B and E**). H4K8ac and H3K27ac are both well-established markers of transcriptional activation, which correlated with our RNAseq data where we observed activation of gene expression in the large-diameter sensory neurons after EE. These two histones can be acetylated by CREB-binding protein (CBP) (149,150), a lysine acetyltransferase that contains two calcium-sensitive transactivation domains (151) and involved in activity-dependent neuroplasticity (80,152,153). Acetylation of CBP increases its acetyltransferase activity and facilitates transcription complex formation and acetylation of H4K8 and H3K27, leading to persistent changes in transcriptional activity (154,155). EE significantly increased pCREB (**Figure 22C, D and F**) and active acetylated-CBP (acCBP) expression in parvalbumin-positive DRG neurons (**Figure 22G and H**). Levels of H4K8ac but not pCREB or acCBP remained elevated in PV^{ON} DRG neurons 5 weeks after exposure to EE. The levels of histone acetylation are likely maintained because they do not rely solely upon the histone deacetylase/acetyltransferase equilibrium but on the overall epigenetic configuration of the locus. While this is important for histones, it is unlikely for proteins, such as CBP, whose acetylation status directly depends on the activity of signal transduction pathways. Furthermore, the levels of H4K8ac and acCBP in DRG neurons were enhanced or inhibited by hM3Dq or hM4Di, respectively, linking calcium-dependent neuronal activity to histone acetylation.

To further elucidate the role of CBP in the EE-mediated increase in the regenerative potential of DRG neurons, we used CaMKIIa-creERT2/CBP^{f/f} transgenic mice with tamoxifen inducible CBP deletion in CaMKIIa positive cells (80). This population of neurons includes both large and medium diameter DRG neurons (156). Four weeks after tamoxifen treatment, mice were placed in EE or SH for five weeks prior to the extraction of the sciatic DRG neurons. Neurite outgrowth was then assessed in culture. Importantly, the conditional deletion of CBP in CaMKIIa-positive DRG neurons (80) abolished the EE-dependent increase in neurite outgrowth (**Figure 22I and J**). This data suggests that CBP specifically contributes to mediating the increase in regenerative potential of DRG neurons after EE exposure. We also found that CBP deletion completely abolished the EE-mediated increase in H4K8ac (**Figure 22K**), ruling out a significant role for other histone acetyltransferases.

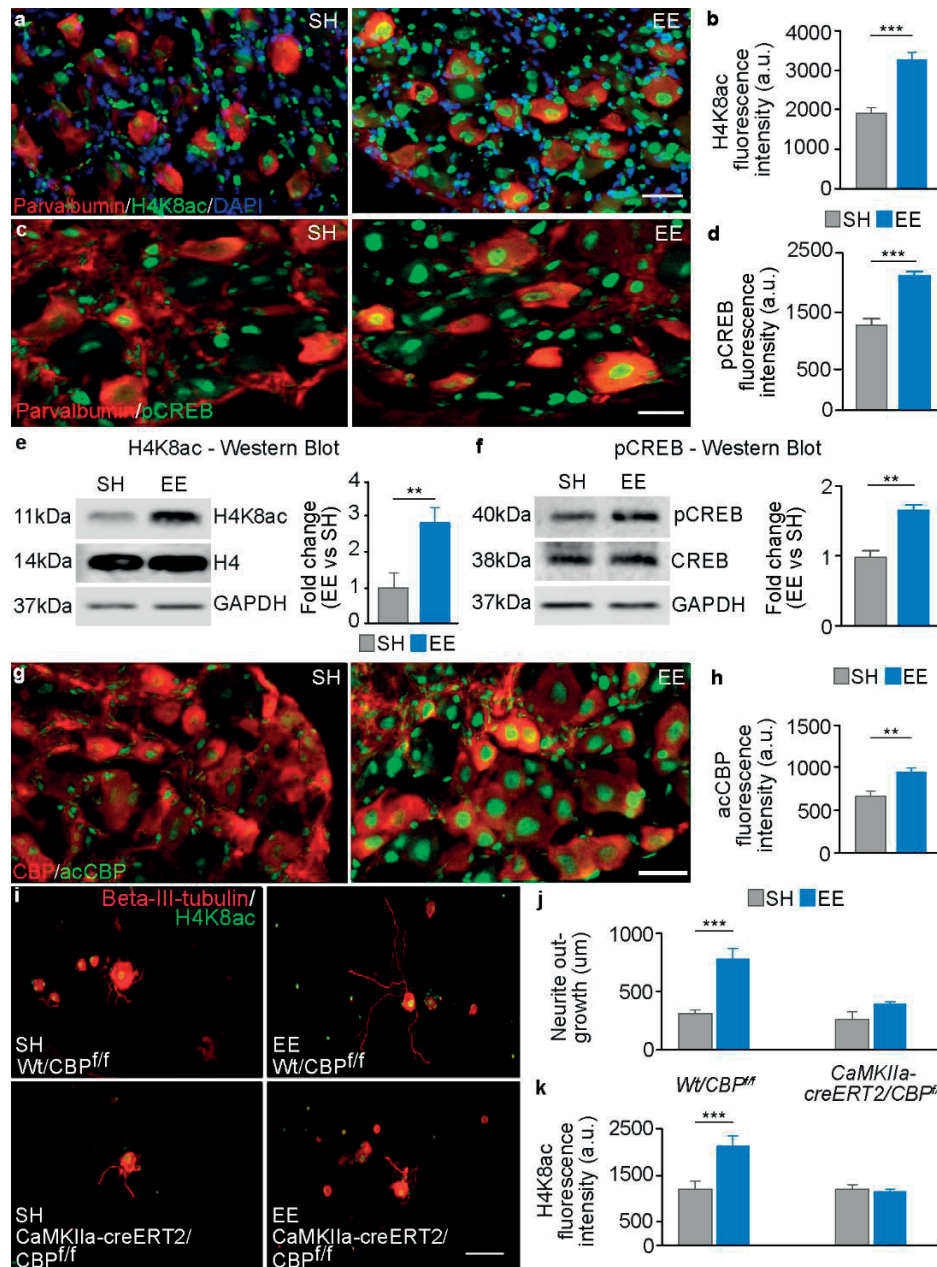


Figure 22 CBP is required for EE-dependent increase in regeneration potential. **a**, DRGs stained for H4K8ac (green), parvalbumin (red) and DAPI (blue). Scale bar, 50 μm. **b**, Quantification of H4K8ac intensity (mean ± SEM, unpaired Student's t test *** $P < 0.001$, $n = 6$ /group). **c**, Examples images of DRGs from mice housed in SH or EE, which were double stained for pCREB (green) and parvalbumin (red). Scale bar, 50 μm. **d**, Quantification of the fluorescence intensity of pCREB in the nuclei of parvalbumin positive DRGs show as significant increase 10 days after EE compared to SH (mean ± SEM, unpaired Student's t test *** $P < 0.001$, $n = 4$ /group). **e**, Immunoblotting analysis for H4K8ac from protein extracts from whole sciatic DRGs after 10 days exposure to SH or EE. Shown is a significant increase in the expression of H4K8ac following exposure to EE (mean ± SEM, unpaired Student's t test, ** $P < 0.01$, $n = 3$ /group). H4K8ac was normalised the levels of H4, while GAPDH was used as a loading control. **f**, Immunoblotting analysis for pCREB from protein extracts of whole sciatic DRGs revealed that exposure to EE significantly increased levels of pCREB compared to SH (mean ± SEM, unpaired Student's t test ** $P < 0.01$, $n = 3$ /group). pCREB was normalised to levels of CREB, while GAPDH was used as a loading control. **g**, DRGs stained for acCBP (green) and total CBP (red). Scale bar, 50 μm. **h**, Quantification of acCBP intensity (mean ± SEM, unpaired Student's t test *** $P < 0.001$, $n = 11$ /group). **i**, Cultured DRG neurons from WT x CBP^{f/f} or CaMKIIa-creERT2 x CBP^{f/f} mice (Beta-III-tubulin, red and H4K8ac, green). Scale bar, 200 μm. **j**, Quantification of neurite outgrowth (mean ± SEM, One-way ANOVA, Tukey's post-hoc *** $P < 0.001$, $n = 5$ /group). **k**, Quantification of H4K8ac intensity (mean ± SEM, One-way ANOVA, Tukey's post-hoc *** $P < 0.001$, $n = 5$ /group).

Pharmacological CBP/p300 activation enhances sprouting of both descending motor and ascending sensory axons leading to functional recovery after contusion SCI in rats

The central role of CBP suggested that the pharmacological activation of CBP might mimic the EE-dependent increase in regenerative growth of DRG neurons. To test this hypothesis, we delivered a small-molecule activator of CBP/p300 (TTK21) after SCI. A recent study has shown that TTK21 is non-toxic, and when conjugated to glucose derived carbon nanospheres (CSP), TTK21 successfully crosses the blood brain barrier, effectively enhances histone acetylation in the hippocampus, and promotes improvements in learning and memory capacities (157). We first confirmed that the addition of CSP-TTK21 to DRG cultures was capable of increasing neurite outgrowth compared to control CSP. Indeed, CSP-TTK21, a pharmacological activator of CBP/p300 (157), triggered a significant increase in neurite outgrowth and H4K8ac in cultured neurons (data not shown).

To substantiate the efficacy of CSP-TTK21 *in vivo*, we evaluated whether CSP-TTK21 could promote anatomical and functional neuroplasticity of motor systems after a more clinically relevant SCI. Adult rats underwent a mid-thoracic spinal cord contusion (220 kdyn). CSP-TTK21 or CSP was administered i.p. 6 hours after SCI, which is a clinically-relevant time point after injury, and repeated weekly thereafter.

To quantify locomotor performance, we applied a principal component (PC) analysis to various parameters calculated from kinematic recordings of quadrupedal walking along a flat corridor. PC1 captured the extent of the recovery, showing that CSP-TTK21 significantly improved locomotor performance compared to CSP-treated rats. Parameters that correlated with improved recovery included reduced paw dragging, increased step height and more frequent plantar steps with weight bearing (**Figure 23A-D**). The number of footfalls occurring during locomotion across a horizontal ladder also decreased significantly. This functional recovery was associated with increased sprouting of descending reticulospinal and serotonergic axons within the lumbar spinal cord (**Figure 23E-J**). Accordingly, CSP-TTK21 enhanced H4K8ac in the reticular formation and raphe nucleus. CSP-TTK21 also augmented the density of vGlut1-positive boutons from proprioceptors onto motoneurons located within lumbar segments below the injury (**Figure 23K and L**), which was associated with increased muscle responses evoked by stimulating proprioceptive afferents (H-reflex, **Figure 23M**). However, CSP-TTK21 did not affect the lesion size or GFAP intensity.

Together, these results show that activating CBP using a small-molecule promotes sprouting of descending pathways and proprioceptive afferents below injury associated with improved recovery of both sensory and motor functions after SCI.

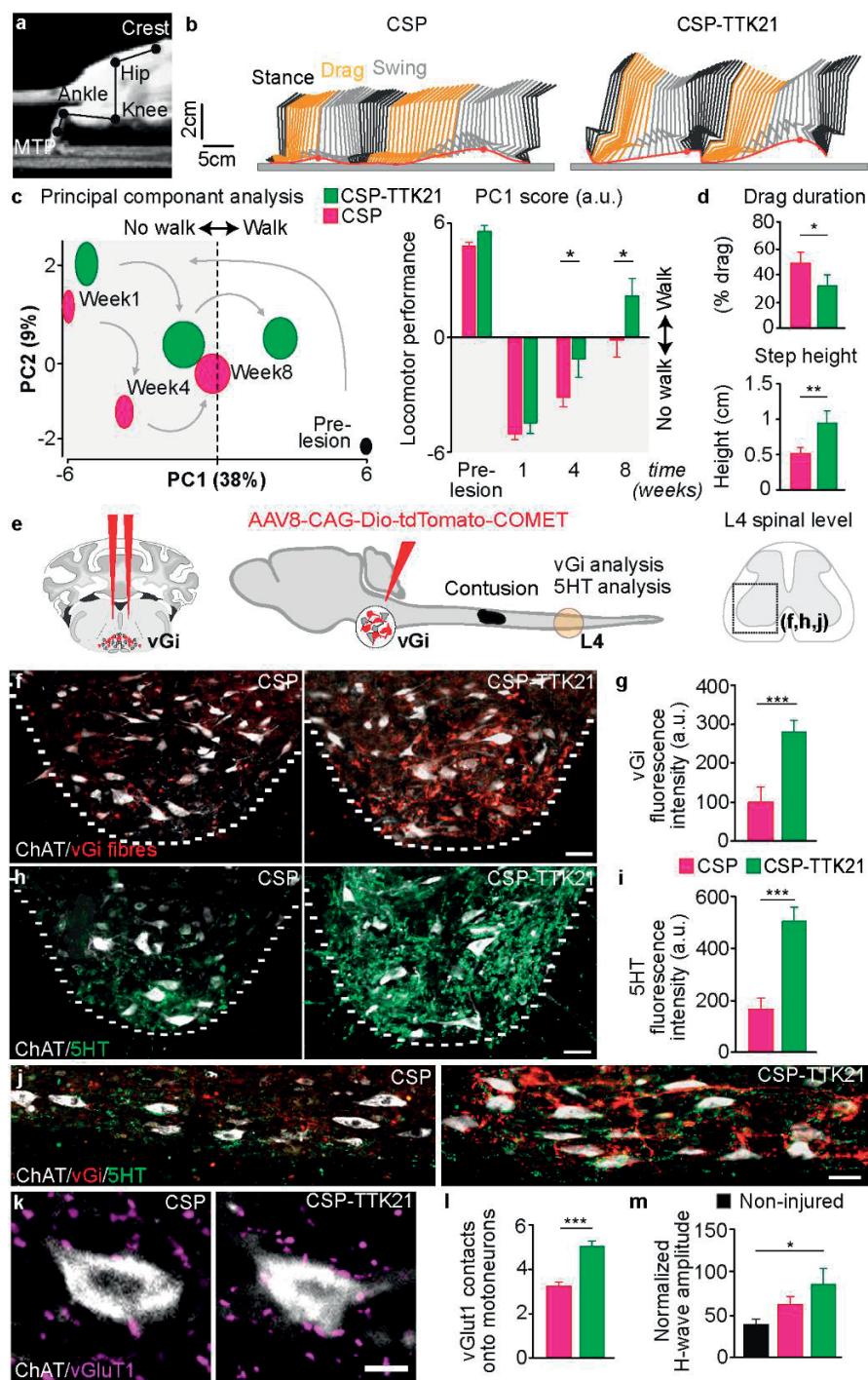


Figure 23 Pharmacological CBP/p300 activation enhances sprouting of both descending motor and ascending sensory axons leading to functional recovery after contusion SCI in rats. **a**, Image showing joints used for reconstruction of hindlimb movements **b**, Representative hindlimb kinematics after treatment with CSP or CSP-TTK21. Black, orange and grey correspond to stance, drag and swing phases of gait, respectively. **c**, PC analysis of gait parameters averaged for each group at weeks 1, 4 and 8 and quantification of average scores on PC1, which quantify the locomotor performance of rats treated with CSP or CSP-TTK21 (mean \pm SEM, Two-way ANOVA, Fisher's LSD post-hoc * $P < 0.05$, $n = 10/\text{group}$). **d**, Bar plots of drag duration and step height show significant improvements after CSP-TTK21 treatment (mean \pm SEM, unpaired Student's t test * $P < 0.05$, ** $P < 0.01$, $n = 10/\text{group}$). **e**, Schematics showing strategy for tracing vGi axons, T9 contusion and the L4 ventral horn analyzed for vGi and 5HT sprouting. **f**, CSP-TTK21 increased sprouting of descending vGi axons (Red) observed around motoneurons (ChAT, Cyan) in the lumbar ventral horn. Scale bar, 50 μm . **g**, Quantification of vGi intensity in the ventral horn (mean \pm SEM, unpaired Student's t test, *** $P < 0.001$, $n = 10/\text{group}$). **h**, CSP-TTK21 increased sprouting of descending 5HT axons (Magenta) was observed around motoneurons (ChAT, Cyan) in the lumbar ventral horn. Scale bar, 50 μm . **i**, Quantification of 5HT intensity in the ventral horn (mean \pm SEM, unpaired Student's t test, *** $P < 0.001$, $n = 10/\text{group}$). **j**, Sagittal sections showing CSP-TTK21 increased sprouting of descending vGi (Red) and 5HT (Green) axons around motoneurons (ChAT, White) below in the injury in the lumbar ventral horn. Scale bar, 50 μm . **k**, vGluT1 positive boutons (yellow) from Group-Ia afferents in proximity to motoneurons (ChAT, Cyan) below the injury (L1-4). Scale bar, 25 μm . **l**, Quantification of vGluT1 positive boutons opposed to motoneurons (mean \pm SEM, unpaired Student's t test *** $P < 0.001$, $n = 10/\text{group}$). **m**, The amplitude of the H-wave significantly increased after treatment with CSP-TTK21 (mean \pm SEM, One-way ANOVA, Tukey's post-hoc * $P < 0.05$, $n = 10/\text{group}$).

4.4 Discussion

Our work demonstrates how increasing the neuronal activity of proprioceptive DRG neurons prior to an injury using EE or chemogenetics elicits CBP-mediated histone acetylation that is required for the enduring increase in axonal regeneration potential. Activating CBP using a small-molecule at clinically relevant time points and in clinically-relevant models of SCI mimicked the effect of increasing neuronal activity. CSP-TTK21 treatment promoted regeneration of ascending sensory axons and sprouting of both sensory and supraspinal motor axons below the lesion. The induced spinal circuit reorganization resulted in significant electrophysiological and behavioural recovery. Here, we discuss the role of activity on enhancing the regeneration potential of proprioceptive neurons as well as the molecular mechanisms underlying these effects before concluding on the implications for spinal cord repair and rehabilitation.

Activity-dependent mechanisms for priming the regeneration potential of proprioceptive neurons

The complete lack of EE-mediated increase in neurite outgrowth observed in DRGs from mice with defective muscle spindle receptors demonstrates the importance of proprioceptive neurons and muscle spindle afferent feedback in triggering the activity-dependent increase in regeneration potential. This finding provides novel evidence and expands upon the recent demonstration that muscle spindle feedback is essential for inducing the correct anatomical reorganisation of projection neurons and functional recovery after spinal cord injury (12). Multiple pieces of evidence emphasised this remarkable cell type specificity. Furthermore, we found that EE drives the expression of genes underlying neuronal activity, calcium signalling and regenerative pathways in large-

diameter DRG neurons. Indeed, this robust gene expression response was largely lost when RNAseq was performed from the whole DRG that contains multiple neuronal populations and glial cells, highlighting the specificity of EE-mediated gene-expression in large-diameter DRG neurons, which are essentially composed of cells innervating proprioceptors. Finally, the impact of neuronal activity on axon regeneration could be reproduced experimentally. We showed that the manipulation of DRG neuronal activity using chemogenetics reproduced or abolished EE-mediated increase in axonal regeneration potential. Indeed, the increase in DRG neuronal activity alone triggered an increase in axon regeneration, further expanding upon what has been observed recently (158,159).

These data suggest that the effects of EE are essentially elicited by proprioceptive feedback signals, which leads to an enhanced activity of proprioceptive DRG neurons that promotes a lasting augmentation of their regenerative potential.

Lasting increase in regeneration potential involves CBP-dependent histone acetylation

Our results provided evidence that the lasting increase in regeneration potential resulted from a CBP-dependent increase in histone acetylation and a dramatic increase in gene expression, including pathways involved in neuronal activity, axonal projection and cytoskeleton remodelling. Specifically, neuronal activity elicited by EE activates CBP and increases the acetylation of H4K8. This enduring increase in histone acetylation likely mediates the long-lasting enhancement in regenerative potential of these DRG neurons that extends for several weeks. The requirement of CBP was confirmed as deletion of CBP completely abrogated the EE-dependent increase in DRG neurite outgrowth and H4K8 acetylation. Furthermore, pharmacological activation of CBP after SCI promoted axonal regeneration and functional recovery. These data show that CBP is necessary for the EE-mediated increase in DRG neurite outgrowth and that its activation promotes functionally relevant axon regeneration and sprouting leading to recovery. These results expand upon recent studies by us and others showing that associated histone acetylation with a transcriptional-dependent enhancement of the regeneration program in neurons (160–165). We previously demonstrated that a conditioning injury activates p300/CBP associated factor (PCAF). Together with HAT p300, PCAF promotes acetylation of the promoters of known regeneration associated genes (RAGs), which facilitate their expression and thereby enhance axon regeneration after injury (160,161,163). The inhibition of HDACs promotes histone acetylation that can also promote axon regeneration (162,164). Similarly, nuclear export of HDAC5 has been shown to be required for peripheral axon regeneration and for the induction of a number of RAGs (165). However, our present results show that EE-dependent histone acetylation does not involve PCAF since H3K9ac is not altered by EE

and it does not require p300, since CBP deletion completely blocked EE-dependent DRG regenerative growth. These observations suggest that a conditioning injury and EE operate via separate signalling mechanisms leading to distinct histone acetylation changes.

Collectively, these studies demonstrate the importance of the chromatin environment to the regenerative capacity of DRG neurons. Identifying and manipulating key histone modifiers that can orchestrate broad changes in gene transcription may lead to significant improvements in axon regeneration.

Implications for spinal cord repair and rehabilitation

The identification of the mechanisms underlying the activity-dependent increase in DRG regenerative growth allowed us to reproduce these effects pharmacologically. We show that the activation of CBP within a clinically relevant time frame after SCI using a non-toxic small molecule promotes axon regeneration and enhanced both electrophysiological and behavioural functional recovery in sensory and motor tests. These findings show that activity-dependent regenerative pathways triggered preceding a SCI can also be successfully targeted to enhance axonal regeneration and sensorimotor recovery after injury.

Rehabilitation strategies including exercises that increase afferent activity in the spinal cord are now well established procedures to augment functional recovery in rodents after SCI (34,166–168). Moreover, modulation of proprioceptive afferent circuits with electrical spinal cord stimulation (74,76,169) augments neuroplasticity and recovery after a SCI. Thus, our results re-emphasized the critical role of proprioceptive neurons in steering the re-organisation of neural pathways that supports functional recovery after SCI.

However, few studies have systematically investigated the impact of task-specific rehabilitation strategies prior to SCI on neuroplasticity and functional recovery. One study demonstrated that voluntary exercise prior to peripheral nerve injury enhances peripheral nerve regeneration (145). This observation is consistent with the robust axon regeneration resulting from an exposure to EE prior to a peripheral nerve injury. The study by Molteni et al reported an increase in neurotrophin mRNA in the DRG after exercise (145). Consequently, they used a pharmacological inhibitor of Trk tyrosine kinase to demonstrate that the exercise-mediated increase in DRG outgrowth was contingent on neurotrophin release. These findings differ from our data, since we did not observe any significant increase in neurotrophin mRNA or protein levels in DRGs after exposure to an EE. Along the same lines, a recent study has shown that exercise after SCI does not change neurotrophin expression in large-diameter DRG neurons (170). It is possible that the pharmacological inhibitor of Trk tyrosine kinase may have off-target effects altering

multiple intracellular signalling pathways that lead to the reduction in DRG outgrowth. Voluntary exercise also prevents the reduction of key signalling molecules that are involved in neuroplasticity including p-synapsin I, p-CREB and p-CaMK in the spinal cord and brain (171). Similarly, we found that EE triggers an increase in calcium related signalling molecules known to be important in gene regulation and inducing neuroplasticity.

Finally, it is worth speculating upon the anecdotal evidence that individuals who had an “active lifestyle” recover to a greater degree after SCI than individuals who lived “less active” lifestyles. In addition to the global benefits associated with a healthy lifestyle, our combined observations prompt us to suggest that neurons are “primed” for axonal regeneration and sprouting, which contribute to this enhanced recovery. It will be useful to collect epidemiological data supporting or refuting this hypothesis.

In summary, we have demonstrated an epigenetic-based mechanism underlying activity-dependent neuronal plasticity. The exploitation of this mechanism allowed to develop a novel pharmacotherapy that enhanced spinal cord repair and functional recovery after SCI, opening a realistic pathway for clinical evaluations.

4.5 Materials and methods

Animal models

All procedures were carried out in accordance with the UK Animals (Scientific Procedures) Act 1986 and approved by the veterinarian and ethical committee of Imperial College and the canton of Vaud and Geneva. Male C57BL/6J mice (Charles River Laboratories, UK) ranging from 6 to 8 weeks of age were used for all experiments except those specifying transgenic mice. Female WT/lox-tdTomato, CaMKIIa-Cre-ERT2/lox-tdTomato, CaMKIIa-Cre-ERT2/CBP^{f/f}, WT/CBP^{f/f} mice with a C57BL/6J genetic background have been previously described¹. For CBP ablation experiments, tamoxifen (T5648; Sigma) was administered to 4 week old CaMKIIa-creERT2/CBP^{f/f} mice using a gastric probe for 5 consecutive days (total consumption ~20 mg per animal); control animals were non-cre recombinase expressing CBP^{f/f} mice (WT/CBP^{f/f}) treated with tamoxifen. PV-cre x GCaMP and PV-cre x tdTomato mice on a C57BL/6J genetic background were provided by the Courtine laboratory. *Egr3*^{-/-} mice containing the *Egr3* mutant allele previously described² were maintained on a C57BL/6J genetic background and provided by the Courtine lab. Adult female Lewis rats (180–220 g body weight, 14–30 weeks of age) were used for the CBP activator experiment.

Animal housing

Animals were kept on a 12 hr light:dark cycle with food and water provided ad libitum. Standard housing for mice consisted of 26x12x18 cm³ cages housing 4 mice with tissue paper for bedding, a tunnel and a wooden chewstick. The enriched environment housing consisted of 36x18x25 cm³ cages housing 8 mice with tissue paper for bedding, a tunnel and a wooden chewstick. EE cages also received additional nesting material which included nestlets, rodent roll and sizzle pet (LBS biotech). EE cages continually contained a hanging plastic tunnel (LBS biotech) and a plastic igloo combined with a fast-track running wheel (LBS-biotech). In addition to this EE cages received a wooden object (cube, labyrinth, tunnel, corner 15) (LBS biotech) that was changed after 5 days to help maintain a novel environment. The EE cages also received 15 g fruity gems (LBS biotech) every 5 days to encourage exploratory and natural foraging behaviour. Rats were housed in standard housing conditions with 3 rats per cage.

DRG culture

Glass coverslips were coated with 100 µg/ml poly-D-lysine (Invitrogen) in H₂O for 2 hours at room temperature. The PDL was removed and washed 3 times with PBS

(Invitrogen, UK), after which they were coated with 2 µg/ml of laminin (Millipore) for 2 hours at 37°C. For the inhibitory myelin substrate, 8 µg/cm² of extracted rat myelin was added to the laminin coated coverslip for 2 hrs at room temperature before removing the myelin and leaving to air dry for 30 mins. L4-L6 DRGs were dissected and collected in Hank's balanced salt solution (HBSS) (Invitrogen) on ice. DRGs then underwent enzymatic digestion (5 mg/ml Dispase II (Sigma), 2.5 mg/ml Collagenase Type II (Worthington) in DMEM (Invitrogen) and incubated at 37°C for 45 min with occasional mixing. DRGs were then transferred to media containing 10% heat-inactivated fetal bovine serum (Invitrogen, UK), B27 (Invitrogen) in DMEM:F12 (Invitrogen) mix and were briefly triturated with a 1 ml pipette to manually dissociate the DRG. After which, the single cell suspension was spun down, re-suspended in media containing 1x B27 and Penicillin/Streptomycin in DMEM:F12 mix and plated at 4,000 cells per coverslip and 4,500 per coverslip for the myelin substrate. The culture was maintained in a humidified incubator at 5% CO₂ and 37°C for 12 or 24 hours before fixing with 4% PFA (Sigma) in PBS (Sigma). For the transcriptional inhibition experiment 0.01 µg/µl or 1 µg/µl Actinomycin-D was added to the culture media at time of DRG plating.

Immunocytochemistry

Cultures were fixed with 4% PFA (Sigma) for 20 mins at room temperature and then washed with 1X PBS (Invitrogen). The cells were blocked with 10% normal donkey serum (Sigma) in PBS + 0.3% Triton-X for 1 hour at room temperature. Primary antibodies used were: Beta-III-tubulin (1:1000, Promega G712A) and H4K8ac (1:1000, Abcam ab15823). Primary antibodies were diluted in 10% normal donkey serum (Sigma) in PBS + 0.3% Triton-X and left incubating with the cells for 4 hours at 4°C. Primary antibodies were removed and the cells washed 3 times in 1X PBS. This was followed by incubation with Alexa Fluor 568-conjugated Donkey anti-mouse and Alexa Fluor 488-conjugated Donkey anti-rabbit (1:1000, Invitrogen) in PBS + 0.3% Triton-X for 2 hours at room temperature. To visualize the nucleus, the cells were stained with DAPI (1:5000, Molecular Probes) in PBS + 0.3% Triton-X.

Sciatic nerve axotomy, crush and reanastomosis

Mice were anaesthetised with 3% isoflurane in 1 L/min oxygen and given a subcutaneous injection of 5 mg/kg Rimadyl and 0.1 mg/kg Buprenorphine for perioperative analgesia. A small incision was performed at the gluteal region and the muscles bluntly dissected to expose the sciatic nerve. For SNA the sciatic nerve was completely transected using micro-scissors (Fine Science Tools). For the crush injury the sciatic nerve was crushed

using no.5 fine forceps (Fine Science Tools) keeping constant firm pressure for 10 seconds. For reanastomosis the nerve was completely transected as above and the two ends were re-anastomosed using two 2.0 sutures. The skin was then closed with two suture clips. For sham surgeries the sciatic nerve was exposed but left uninjured. Regeneration was assessed 1 day after the crush and 3 days after the reanastomosis.

Intramuscular injection

Fourteen days post sciatic nerve crush sensory axons that had re-innervated the muscle were traced by injecting 5 µl of 1% CTB (List Biological Laboratories) diluted in saline into the tibialis anterior and medial gastrocnemius muscles using a 10 µl Hamilton syringe and Hamilton needle (NDL small RN ga34/15mm/pst45°) (Hamilton). 3 days post-tracing, mice were terminally anaesthetised and transcardially perfused with 20 ml PBS (pH 7.4) (Sigma) followed by 20 ml 4% paraformaldehyde in PBS (Sigma).

Dorsal hemisection injury

Surgeries were performed as previously reported³. Briefly, mice were anaesthetised with 3% isoflurane in 1 L/min oxygen and given a subcutaneous injection of 5 mg/kg Rimadyl and 0.1 mg/kg Buprenorphine for perioperative analgesia. A laminectomy at vertebra T9 was performed to expose spinal level T12 and a dorsal hemisection until the central canal was then performed using micro-scissors (Fine Science Tools). For the sham surgery a laminectomy was performed but the dorsal hemisection was not. Any bleeding was stopped and the muscle and skin was sutured closed.

Contusion injury

Rats were anaesthetised with 3% isoflurane in 1 L/min oxygen, a partial laminectomy was made at the T9 vertebra. Contusion injury was produced using a force-controlled spinal cord impactor (IH-0400 Impactor, Precision Systems and Instrumentation). The applied force was set to 220 kdyn (1 dyn = 10 µN). The spinal cord displacement induced by the impact was measured for each animal. Analgesia (buprenorphine, 0.01–0.05 mg/kg, s.c.) and antibiotics (Baytril 2.5%, 5–10 mg/kg, s.c.) were provided for 3 days after surgery

Axonal tracing - Mice

Six weeks post spinal cord injury the sensory axons in the dorsal columns were traced by injecting 3 µl of 1% CTB (List Biological Laboratories) diluted in saline into the sciatic nerve using a 10 µl Hamilton syringe and Hamilton needle (NDL small RN

ga34/15mm/pst45°) (Hamilton). 4 days post-tracing, mice were terminally anaesthetised and transcardially perfused with 20 ml PBS (pH 7.4) (Sigma) followed by 20 ml 4% paraformaldehyde in PBS (Sigma).

Axonal tracing - Rat

Nine weeks post contusion injury an AAV vector was injected (AAV8-CAG-DIO-tdTomato-COMET, titre 1.03×10^{13} vg/ml, kindly provided by Prof. M. Tuszynski) into the ventral gigantocellular (vGi) for tract-tracing was performed in rats. Under isoflurane anesthesia, a craniotomy was performed over the brainstem medulla oblongata. Injection coordinates for rats were -11, -11.5, -12 mm caudal, ± 0.8 mm mediolateral to bregma and 9.5 mm ventral from the surface of the cerebellum (six injections total, 250nl per injection, injected with a Hamilton injection system). The AAV vector was injected at 3nl/s and the needle was held in place for 3 min before being slowly retracted. Five weeks after the AAV injections rats were terminally anaesthetised and transcardially perfused with 200 ml PBS (pH 7.4) (Sigma) followed by 200 ml 4% paraformaldehyde in PBS (Sigma).

Histology and immunohistochemistry

Tissue was post-fixed in 4% paraformaldehyde (PFA) (Sigma) and transferred to 30% sucrose (Sigma) overnight to cryoprotect, the tissue was then embedded in OCT compound (Tissue-Tek) and frozen at -80°C . DRGs were sectioned at 10 μm thickness and mouse spinal cord at 15 μm , rat spinal cord at 30 μm and rat brainstem at 40 μm using a cryostat (Leica). Tissue sections were blocked for 1 h with 10% normal donkey serum (Sigma), 0.3% Triton X-100 (Sigma) in PBS, and then incubated with, and H4K8ac (1:1000, ab15823), H3K27ac (1:500, ab4729), H3K9ac (1:500, Cell Signalling 9671), H3K4me³ (1:500, Abcam ab8580), H3K4me² (1:500, Cell signalling 9726), Parvalbumin (1:1000, Abcam ab64555), Substance P (1:250 ab67006), IB4 (1:250, Invitrogen 121411), CBP (1:50, Abcam ab50702), acCBP (1:1000, Abcam ab61242), pCREB (1:100, Abcam ab32096), SCG-10 (1:500, Novus biologicals NBP1-49461), CTB (1:1000, List biological 703), vGlut1 (1:1000, Synaptic system 135302), 5-HT (1:6000, Sigma S5545), ChAT (1:200 Chemicon), GFAP (1:500, Millipore AB5804) antibodies O/N. This was followed by incubation with Alexa Fluor 568-conjugated donkey anti-mouse and Alexa Fluor 488-conjugated donkey anti-rabbit or Alexa Fluor 568-conjugated donkey anti-rabbit and Alexa Fluor 488-conjugated donkey anti-mouse (1:1000, Invitrogen), respectively. Slides were counterstained with DAPI to visualise nuclei (1:5000, Molecular Probes). Photomicrographs were taken with a Nikon Eclipse TE2000 microscope with a optiMOS scMOS camera using 10x or 20x magnification.

Image analysis

Image analysis was performed using ImageJ (Fiji) software. All analysis was performed by the same experimenter who was blinded to the experimental groups.

Analysis of neurite outgrowth

The mean neurite outgrowth per DRG neuron was manually measured using the NeuronJ plugin for ImageJ. We measured the mean neurite outgrowth of 75 neurons per mouse with at least 4 mice per group and 3 technical replicates per mouse. The EE-mediated increase in DRG outgrowth was also independently verified by our collaborators in Miami, strengthening the reproducibility of this phenotype.

Analysis of immunohistochemistry for epigenetic marks, pCREB, CBP and acCBP

For quantitative analysis of pixel intensity, the nucleus or soma of DRG neurons were manually outlined in images from one series of stained tissue for each mouse. To minimise variability between images pixel intensity was normalized to an unstained area and the exposure time and microscope setting were fixed throughout the acquisition.

Analysis of vGi and 5HT fibres in the ventral horn

Intensity of 5HT immunohistochemistry or tdTomato fluorescent protein labelling of the vGi fibres was measured in the ventral horn of L1-4 spinal sections. Quantification was done using ImageJ, the background was subtracted and then the mean pixel intensity was measured from one series of tissue for each animal.

Analysis of vGlut1 immunohistochemistry in proximity to motor neurons

vGlut1, a pre-synaptic marker labelling proprioceptive or cutaneous sensory afferent terminals was used to identify boutons in close proximity to motor neurons, which had been retrogradely traced with CTB. To determine the number of vGlut1 boutons in close proximity to motor neurons, consecutive confocal images (0.3 μm thick optical sections) were acquired as Z-stacks (total average thickness: 15 μm) using a 40x objective. The Average number of vGlut1 boutons opposed to motor neurons in the ventral horn of L1-3 spinal sections was calculated by analysing at least 20 motor neurons per animal.

Analysis of GFAP intensity and area around the lesion site

GFAP intensity and area was quantified from sagittal spinal cord sections from one series of tissue for each animal. Quantification was done using ImageJ, the background

was subtracted and then the mean pixel intensity and area of immune-reactivity was measured.

Analysis of CTB positive dorsal column axon regeneration in the spinal cord

Regeneration of dorsal column axons were quantified from sagittal spinal cord sections from one series of tissue for each mouse. CTB intensity was quantified using ImageJ software at set distances rostral to injury centre then expressed as a percentage of the CTB intensity caudal to the injury site to control for variations in tracing efficacy. The furthest rostral CTB positive axon was determined relative to the lesion centre and caudal axon retraction was defined as distance the lesioned axon bundle retracted relative to the lesion centre.

Analysis of SCG10 and mCitrine axon regeneration after sciatic nerve injury

The regeneration of peripheral axons in the sciatic nerve was quantified from one series of tissue from each mouse. SCG10 or mCitrine intensity was quantified using ImageJ software at set distances distal to injury site then expressed as a percentage of the pixel intensity proximal to the injury site to control for variations in staining or transduction efficiency.

Behavioural analysis

Mice were trained daily for 2 weeks pre-surgery before baseline measurements and then assessed on day 3 post-surgery and weekly thereafter. All behavioural testing and analysis was done by an observer blinded to the experimental groups.

Gridwalk – Mice crossed a 1 m long horizontal grid 3 times. Videos of the runs were analysed at a later time-point and errors from both hind-limbs were counted. Error values represent the total number of slips made by both hind-limbs over the 3 runs.

Horizontal ladder – Rats walked across a 1 m long horizontal ladder 3 times. Videos of the runs were analysed and errors from both hind-limbs were counted. Error values represent the total number of slips made by both hind-limbs over the 3 runs.

Adhesive tape test – An 8 mm diameter adhesive pad was placed on each hind-paw. The mouse was then placed into plexi-glass box and the time until it first made contact with each of the adhesive pads was recorded, followed by the time until it removed the adhesive pads from each hind-paw. The maximum time allowed for each animal was 5 mins. Each animal was tested twice per time-point and values represent the average time from both hindpaws from both runs.

Kinematic recordings

All procedures used have been detailed previously^{4,5}. Kinematic recordings were obtained from rats walking over-ground along a horizontal runway. Bilateral hindlimb kinematics were captured with a Vicon high-speed motion capture system (Vicon Motion Systems), using 12 infrared cameras (200 Hz). Reflective markers were attached bilaterally at the iliac crest, the greater trochanter (hip joint), the lateral condyle (knee joint), the lateral malleolus (ankle) and the distal end of the fifth metatarsophalangeal joint. The body was modeled as an interconnected chain of rigid segments, and joint angles were generated accordingly. For both the left and right legs, 10 step cycles were extracted randomly over several trials on the runway for each rat at each time point.

Analysis of kinematic recordings

A total of 78 parameters quantifying gait features were computed for each leg and each gait or stroke cycle according to methods described in detail previously^{4,5}. All parameters are reported in Supplementary Table 1. To evaluate differences between experimental conditions and groups, as well as the most relevant parameters to explain these differences, we implemented a multistep statistical procedure based on principal component (PC) analysis. PC analyses were applied to data from all individual gait cycles for all rats together. Data were analysed using the correlation method, which adjusts the mean of the data to 0 and the s.d. to 1. This method of normalization allows the comparison of variables with disparate values (large vs. small values) as well as different variances. Locomotor performance was quantified with the score along PC1, which segregated differences between groups. Factor loading of parameters on PC1, i.e. the correlations between each parameter and PC1 explaining recovery, are reported in Supplementary Table 1.

Electrophysiology

Mice were anaesthetized with an IP injection of 50 mg/kg ketamine and 0.5 mg/kg medetomidine. Their thoracic and lumbar back was shaved and disinfected with chlorhexidine. Mice were kept on a heating blanket throughout the procedure and anaesthesia depth was monitored and the anaesthesia topped up if needed. Laminectomies were performed at vertebrae levels T13, T11 and T7 to expose spinal levels L5, L1 and T9. A concentric bipolar stimulating electrode (FHC CBBPC75) was placed over the dorsal columns at L5 for local surface stimulation (stimulation range: 100 μ sec at 0.1 mA to 0.5 mA, 0.2 Hz). Field potentials were recorded at either L1 (below the injury) or T9 (above the injury) with a fine microneurography electrode (in-house custom made) inserted

superficially into the spinal cord. Recordings were filtered between 300 and 6 kHz; amplified by 4 k. The animals were grounded with a 30 G needle through the skin. The traces had a typical positive-negative-positive waveform corresponding to the compound action potential in the dorsal column⁶ with a conduction velocity of around 25 msec⁷. To capture all components of the compound action potentials, we analysed the area under the curve by measuring the absolute integral of the curves (between 1 and 11 msec). 5 traces were averaged per mouse for analysis and representation at a stimulation intensity that distinctively excites dorsal column fibres controlled for by recording from below the lesion site.

Hoffmann-Reflex Testing

Electrophysiology was performed as previously reported⁸. Briefly, rats were anaesthetized with 30 mg/kg ketamine and 0.1 mg/kg medetomidine and two 24-G needle electrodes were inserted across the lateral side of the ankle for nerve stimulation (via a constant current isolated pulse stimulator, stimulus width 100 μ s). Two recording electrodes were inserted into the medial plantar foot to record electro myograms. The signal was amplified (1000-fold), filtered (10 Hz to 5 kHz), digitized via PowerLab, visualised and analysed with LabChart. The M-wave is evoked by excitation of motor axons. The H-wave is the monosynaptic reflex: Ia proprioceptive afferents synaptically activate motor neurons in the spinal cord. The threshold was determined as the lowest stimulation intensity that elicited a H-wave response in at least 75% of the recordings. First, the responses to increasing stimulus intensities were tested at 0.1 Hz up to 2 x threshold. M-wave and H-wave amplitudes were normalized to the maximum M-wave recorded at higher stimulation intensities.

Laser capture micro-dissection

Sciatic L4-L6 DRGs were extracted from 3 mice per condition. Using RNase-free conditions, DRGs were embedded with Tissue Freezing Medium (Triangle Biomedical Sciences, Inc) and frozen in dry ice-cold 2-methylbutane. 16 μ m thick sections were cut on the cryostat and collected on Leica PEN-membrane slides (Leica). From each animal, 4-6 slides were obtained. Toluidine blue (Sigma) staining was used to identify the DRG neurons. Slides containing sections were dehydrated and stained with ethanol series, as follow: 3 times of 30 seconds in 70% ethanol, 60 seconds in 0.5% Toluidine blue dissolved in 70% ethanol, 2 times for 30 seconds each in 70% ethanol, 1 time for 30 seconds in 90% ethanol, 2 times for 30 seconds in 100% ethanol. Once air-dried the slides underwent laser capture

using a Leica LMD 6000 microscope. From each animal, large diameter neurons with a diameter of ≥ 30 microns were obtained.

Western Blot

Proteins from L4–L6 DRGs were extracted using RIPA buffer with protease and phosphatase inhibitor cocktails (Roche), lysed for 30 min on ice followed by 30 min centrifugation at 4°C. Protein concentration was quantified using Pierce BCA Protein Assay Kit (ThermoScientific). Subsequently, 10–50 μ g protein was loaded in SDS–polyacrylamide gel electrophoresis (PAGE) gels and transferred to polyvinylidene difluoride (PVDF) membranes for 2h. Membranes were blocked with 5% BSA or milk for 1h at room temperature and then incubated with H4K8ac (1:1000, ab15823), H4 (1:1000, Abcam ab10158), CREB (1:500, Abcam ab178322), pCREB (1:500, Abcam ab32096) or GAPDH (1:1000, cell signaling 14C10) antibodies at 4°C overnight. Membranes were then incubated with HRP-linked secondary antibody (GE Healthcare) for 1h at room temperature and developed with ECL substrate.

RNA sequencing

RNA sequencing was performed using RNA from whole DRG tissue and from large diameter laser microdissected DRG neurons in 3 biological replicates. For whole DRG RNAseq, sciatic L4–L6 DRGs were extracted from 2 mice per sample and stored in RNase later (Qiagen). DRG tissue was crushed with RNase free micropestle and RNA was extracted using RNAeasy kit (Qiagen), according to manufacturer's protocol. Residual DNA contamination was removed by on column DNase I treatment (Qiagen) for 15 min at room temperature. RNA concentrations and quality were measured using Agilent 2100 Bioanalyzer (Agilent). RNA with RIN factor above 7.5 was used for library preparation. Libraries were prepared at Ospedale San Raffaele (Milan) using the TruSeq mRNA Sample Preparation kit (Illumina) and sequenced using Illumina HiSeq 2500 100-cycle, pair end sequencing.

For Laser captured DRG neurons, RNA was extracted using Arcturus PicoPure RNA isolation kit (Life Technologies), following manufacturers protocol. RNA concentrations and quality were measured using Agilent 2100 Bioanalyzer (Agilent). RNA with RIN factor between 6 and 7 were used for library preparation. Libraries were prepared using the RiboZero ScriptSeq V2 kit working from the low input protocol using 100 ng of RNA per sample. Libraries were sequenced using Illumina HiSeq 2500 generating 125 bp, paired end reads.

Sequence reads were aligned to the mm10 mouse reference genome sequence using tophat version 2.0.12 running Bowtie2-2.2.3. Gene structure annotations corresponding to the Ensembl annotation of the mm10 genome sequence were used to build a transcriptome index and provided to tophat during the alignment step. The aligned reads were sorted using samtools-0.1.19 and read counts per gene were obtained from mapped reads using HTSeq-0.6.1. EdgeR version 3.8.6 (using limma-3.22.7) in R-3.1.1 was used to identify differentially expressed genes. Read-level quality checking was performed using fastqc-0.10.1 and the fastqc-aggregator (https://github.com/staciaw/fastqc_aggregator) and gene-level quality checking was performed using RSeQC-2.6.1. The gene expression in EE was compared to SH. Heatmap of RNAseq mRNA expression levels of the genes differentially expressed in any sample group ($P < 0.05$) were generated in Matlab R2014b using the dustergram function.

Gene ontology (GO) and KEGG (Kyoto Encyclopedia of Genes and Genomes) were performed on the differentially expressed genes with DAVID (Database for Annotation, Visualization, and Integrated Discovery (<http://david.abcc.ncifcrf.gov/>)) using a threshold of $P < 0.05$. Functional GO clustering was performed using ClueGO in Cytoscape (<http://www.cytoscape.org>): (Bonferroni $P \leq 0.05$) (GO tree interval min3, max8) (GO selection min 4, 1%) (K score 0.3). Differentially expressed proteins and genes that resulted enriched in the GO functional clustering were uploaded into STRING to build a protein-protein interaction network. The network was visualized by Cytoscape, where each node represents a differentially regulated gene (RNA-seq) or protein (proteomic) and edges represent protein-protein interactions.

Axoplasm extraction and proteomics

Sciatic nerves were dissected and the axoplasm was obtained according to the previously published protocol⁹. LC-MS was performed on axoplasmic samples by the Quantitative Biology Center (QBiC) in Tuebingen followed by proteomics analysis. Each axoplasmic extract processed for proteomics was derived by pooling 16 nerves dissected from 8 mice that were housed for 10 days in either SH or EE in biological triplicates and technical duplicates. The raw data was processed with MaxQuant version 1.5.0.25. The protein and peptides intensities were normalized using the "quantile normalization" procedure in R. The differential expression analysis of the proteins and peptide modifications was performed by the means of mixed linear models R (nlme) and ANOVA. The effect of treatment (SH vs EE) on protein expression was modelled as: intensity ~ treatment, with technical replicates nested within biological replicates as random factor. Correction for multiple hypothesis testing was done by R (qvalue) at FDR < 0.05.

Ca imaging

PV-cre x GCaMP mice were housed in EE or SH for 10 days. L4-L6 DRGs were extracted and immediately suspended in HBBS without Ca^{2+} (Thermofisher) with 10 mM Hepes (Thermofisher) at 37°C, 5% CO_2 . The DRGs were then placed into a video-microscopy chamber at 37°C and suspended in HBSS without Ca^{2+} (Thermofisher), to avoid any calcium influx from extracellular medium. Time-lapse recordings were taken with images acquired every 1 second for 5 minutes. Imaging was done on a Nikon Eclipse TE2000 microscope with a optiMOS sCMOS camera using 20X magnification. After 30 seconds of baseline recording, increasing concentrations (50 mM, 100 mM and 150mM) of KCL (Sigma) were added to the DRG to elicit depolarisation and induce intracellular Ca^{2+} release. Quantification was done using the ImageJ plug-in *Time series analyser*, where the soma of all PV neurons were analysed per DRG, 6 DRG's per mouse and 4 mice per condition. To determine the fold-change in GCaMP intensity after KCL addition, the GCaMP intensity ratio "F/Fo" was calculated by dividing the average fluorescence intensity after KCL addition "F" with the average intensity of baseline fluorescence "Fo".

Cytokine Assay

Sciatic L4-L6 DRGs (pool of 4 mice) and serum (pool of 2-4 mice) were collected in 3 biological replicates. 100 µl of serum (corresponding to 1.5 mg of proteins) was run on a Mouse Cytokine Array Panel A (R&D System) and developed according to manufacturer's protocol to quantify cytokine levels. The resulting spots on the membrane were quantified by densitometry and the signal intensity in the EE samples was referred to the SH control.

Neurotrophin ELISA

Levels of neurotrophins were analysed in homogenised L4-6 DRG samples and blood serum. Blood serum was diluted 1:7 to avoid matrix interference, while DRGs were lysed in RIPA buffer and diluted 1:6. 100 µl of serum (corresponding to 0.2 mg of proteins) and 100 µl of lysate (corresponding to 80 mg of proteins) were analysed with the Multi-Neurotrophin Rapid Screening ELISA kit (Biosensis), according to manufacturer's instructions. The absorbance at 450 nm of the samples, obtained using GLoMax plate reader (Promega), was interpolated against the standard curve to calculate the neurotrophin concentration, and referred to mg of proteins.

Synthesis of carbon nanospheres of average size 350nm

5 g of D(+) glucose was dissolved in 50 mL of deionised water to form a clear solution. The solution was placed in a 65 mL teflon lined sealed stainless steel autoclave

and maintained at 180 °C for 12 hr. The products were centrifuged at 10000 rpm for 10 min and were washed with water and ethanol thrice each before being dried in the oven at 60 °C for 4 hr. The final product is a brownish powder which had spheres with an average size of 350 nm.

Synthesis of TTK21

To the Dichloromethane (DCM)solution of 2-Propoxy Benzoic Acid (3.3mmol) one equivalent of thionyl chloride (3.66 mmol) and 4-5 drops of N, N-Dimethylformamide(DMF) were added and the solution was refluxed for 4hr. Thionyl chloride was removed by evaporating the solvent 3-4 times and to that DCM was added (Solution A). To the DCM solution of 4-Chloro-3-(trifluoromethyl) amine (3.1 mmol) a few drops of triethylamine was added at 0 °C and was stirred for 30 min (Solution B). The solution B was added drop-wise to the solution A at 0 °C and after sometime the solution was heated to reflux for 4 hr. Then the solution was evaporated to dryness and was purified by column chromatography. White crystalline solid was obtained.

Conjugation of TTK21 to CSP

CSP suspension in DCM was reacted with one equivalent of SOCl₂ and few drops of DMF. The reaction mixture was refluxed at room temperature for 4hr. Thionyl chloride was removed by evaporating the solvent 3-4 times and to that DCM was added to make the suspension. To that suspension one equivalent TTK21 and few drops of triethylamine were added. The reaction was refluxed for 4 hr. The suspension was filtered and the precipitate was washed with DCM. The conjugated CSP-TTK21 was dried. The conjugation of TTK21 to the nanosphere was analysed by Energy Dispersive X-ray Spectroscopy EDX. The spectrum of CSP-TTK21 shows that wt % of Fluorine is 0.31 which belongs to TTK21 indicating the covalent conjugation of TTK21 to CSP.

CSP-TTK21 administration

Animals were randomised to treatment with the CBP/p300 activator bound to carbon nanospheres (CSP-TTK21) or a control of just carbon nanospheres (CSP) (mice – 20 mg/kg, rats – 10 mg/kg injected IP once a week). Mice received the first IP injection 4 hours after SCI and rats received the first IP injection 6 hours after SCI to simulate a clinically-feasible delay-to-treatment and then once a week thereafter. The optimal dose and time-course for retention of the small molecule-bound nanospheres in the CNS had been previously determined¹⁰. CSP-TTK21 activates CBP 4 fold more potently than p300.

No adverse effects were observed following IP administration of CSP-TTK21 and after histological analysis no obvious cellular toxicity was observed.

AAV-DREADD experiments

Non-Cre dependent DREADD AAV vectors (AAV5-CaMKIIa-EGFP, AAV-CaMKIIa-HA-hM3D(Gq)-IRES-mCitrine, AAV-CaMKIIa-HA-hM4D(Gi)-IRES-mCitrine) were purchased from UNC vector core. Viral titres were matched to 1×10^{13} GC/ml. 3 μ l of non-cre dependent AAV vector was injected in to the sciatic nerve to transduce DRG neurons. 4 weeks later the mice were placed in EE or SH for 10 days and given 0.05 mg/ml CNO with 5mM sucrose in their drinking water each day, mice received approximately 5mg/kg CNO per day.

To determine whether any observed increase in conduction across the lesion site was contingent on regenerating axons. Cre-dependent AAV-DREADD vector (AAV-hSyn-DIO-hM4D(Gi)-mCherry) was purchased from UNC vector core. Titre was 1×10^{13} GC/ml. 3 weeks after a T9 dorsal hemisection 0.5 μ l of cre-dependent AAV5-DREADD-Gi vector was injected in to the spinal cord at T7. 3 weeks later during terminal electrophysiological experiments mice received an I.P. injection of CNO (1.2 mg/kg body weight).

Statistical analysis

Results are expressed as mean values \pm SEM and n values represent number of animals in all experiments. Statistical analysis was carried out using Graphpad Prism 7 (GraphPad, prism software) using two-tailed unpaired Student's *t*-tests, one-way ANOVA for evaluation of experiments with more than two groups, and one- or two-way repeated-measures ANOVA for functional assessments, when data were distributed normally. Tukey's, Sidak's or Fisher's LSD post-hoc tests were applied when appropriate. Behavioral assays were replicated two or three times, depending on the experiment, and averaged per animal. Statistics were then performed over the mean of animals. A threshold level of significance α was set at $P < 0.05$. Significance levels were defined as follows: * $p < 0.05$; ** $p < 0.01$; *** $p < 0.001$.

V. INTEGRATION & PERSPECTIVES

Functional impairments after SCI are the result of the physical interruption of descending connections to spinal cord circuitries located below the level of the lesion. As a consequence, these circuits become isolated from the brain and remain in an inactive state insufficient to generate movement, despite being anatomically and functionally intact (8). Without any interventional therapy, recovery of motor control remains absent. To date, one of the most promising strategies to re-activate spinal circuits below a lesion includes epidural electrical stimulation (EES). There is growing evidence that EES contributes to the improvement of motor function and recovery after spinal cord injury (SCI), especially when combined with physical activity such as locomotor training. Several studies in animal models and human patients reported increased motor control and improved functional recovery when EES was applied over lumbar segments (34,86).

Besides locomotor training enabled by EES, the exposure to enriched environment (EE) represents another activity-based rehabilitation strategy that has been shown to induce plasticity in the adult CNS of experimental animals. Nevertheless, the underlying mechanisms accompanying plastic changes at the spinal and sensory afferent level in response to EE are not well understood.

The two studies presented in this thesis provide direct and conclusive experimental evidence for the mechanistic understanding of EES and EE and how they mediate functional recovery after SCI. Our findings demonstrate the importance of large-diameter afferent fibers in mediating functional recovery and will be important in establishing a framework for the design of neuromodulation therapies after SCI in human patients.

5.1 Refined strategies to modulate proprioceptive feedback after SCI

Our findings in chapter I demonstrate that EES robustly activates proprioceptive neurons concentrated in DRGs through the recruitment of their large-diameter, myelinated fibers. These findings point towards the importance of exploiting muscle spindle feedback in the design of EES-based rehabilitative strategies after SCI. For example, a more specific modulation of proprioceptive feedback circuits during rehabilitation may enhance functional outcomes after SCI. There are several possibilities to achieve a higher specificity in recruiting proprioceptive feedback circuits when applying EES.

One possibility to specifically recruit proprioceptive neurons in DRG consists in applying electrical currents within a defined range of stimulation frequencies (41,76). Based on modeling experiments, spatiotemporal EES patterns applied with a frequency envelope resembling the firing rates of Ia afferent fibers is 'in-phase' with the natural firing pattern of proprioceptive afferent fibers during locomotion. In rodents, this 'in-phase' stimulation approach has been shown to enhance the activity of proprioceptive feedback circuits. Moreover, this stimulation paradigm led to improved motor and sensory outcomes in human patients when combined with daily locomotor training over five months (41).

Another possibility to enhance the activity of proprioceptive feedback circuits after SCI consists in the pharmacological modulation proprioceptive neurons located in DRGs. Pharmacological receptors expressed on proprioceptive neurons may serve as a possible target for pharmacological agents to modify the activity of proprioceptive pathways. As demonstrated in this thesis, noradrenergic receptor subtypes could be a possible target to achieve this goal.

5.2 The role of low-threshold mechanoreceptors in mediating the effects of EES

Besides proprioceptive afferents, we showed that low-threshold mechanoreceptors (LTMRs) involved in the transmission of light touch information are also recruited by EES. Compared to muscle spindle feedback, little is known about the effects of LTMRs on the motor system and how their activation by EES affects motor outcomes. This lack of knowledge may partly explain why many modeling studies, which examined the mechanisms of EES, mainly focused on proprioception but barely on LTMR feedback.

To study the effects of LTMRs on motor outcomes in our computational model, we integrated intraspinal LTMR connections based on the gained anatomical knowledge. These simulations provide important insights about role of LTMRs involved in the generation of locomotion under EES.

Indeed, the role and activation pattern of LTMR afferents is fundamentally different compared to the one of proprioceptive afferents. In contrast to proprioceptive circuits,

LTMRs are activated in a phase-dependent manner, meaning they are activated throughout the entire stance phase of the leg whereas they are inactive during swing phase (25). Our modeling experiments suggested that the continuous activation of LTMR feedback circuits by continuous EES interferes with the natural activity of LTMR circuits and consequently diminishes locomotor outcomes enabled by EES.

Indeed, down-regulating the excitability of LTMRs in combination with an up-regulation of proprioceptive circuits during EES-enabled stepping immediately enhanced locomotor outcomes in spinal rats and mice.

A similar sensory-specific modulation of proprioceptive and cutaneous afferents pathways has recently been described in monkeys (29). During the execution of forearm reaching movements, electrical stimulation was applied to nerves containing either cutaneous or proprioceptive afferents. Whereas cutaneous inputs were suppressed regardless of the type of movement, muscular inputs were specifically facilitated during relevant movements. These outcomes imply that different streams of sensory information are modulated in an individual manner.

In the intact state, this sensory-specific modulation may be directly controlled by the brain. A recent study in monkeys demonstrated the existence of direct supraspinal connections onto cutaneous interneurons within lamina III/IV (26). Supraspinal inputs were found to be mediated by corticospinal tract (CST) fibers which controlled the activity of lamina III/IV interneurons by direct and phase specific inhibition during movements. Similarly, direct CST connections from the brain to cutaneous interneurons in the spinal cord have been shown in mice (21). After SCI, when supraspinal and spinal centers are isolated from each other, this brain-derived inhibition does not exist anymore. Here, by inactivating lamina III/IV interneurons pharmacologically through the injection of the dual $\alpha 2c$ agonist/ $\alpha 2a$ antagonist, we mimicked brain-derived inactivation of these interneurons which is usually provided in the intact state.

5.3 The problematic of noradrenergic receptor modulation

Historically, noradrenergic $\alpha 2$ receptors have been among the first ones targeted to restore locomotion after SCI. In cats with a complete transection of the spinal cord, clonidine has been shown to reliably enhance stepping function after SCI (47,53,54). In contrast, when delivering clonidine in human patients, a depression of locomotor states was observed (48). A similar functional outcome was reported when clonidine was applied in combination with EES in spinal rats (72). These conflicting functional outcomes among

different species may explain why noradrenergic receptor stimulation only received minimal attention as a means to pharmacologically modulate spinal circuits after SCI.

Until now, there was no explanation for the observed interspecies differences in functional outcome in response to clonidine. By using $\alpha 2a^{GFP}$ and $\alpha 2c^{GFP}$ transgenic mouse lines, we found that these two receptor subtypes are expressed on proprioceptive and LTMR feedback circuits. The inactivation of proprioceptive afferent pathways through the activation of $\alpha 2a$ receptors explains why this pharmacological agent abolished locomotor outcomes enabled by EES. Similarly, the inactivation of proprioceptive afferents as a consequence to the administration of clonidine may account for the diminished stepping outcomes observed in human patients. These findings explain why clonidine alone or in combination with EES failed to induce stepping after SCI.

Nevertheless, it is still not clear why clonidine enabled locomotion in cats but not in rats or humans. In order to induce stepping in cats, tail pinching was often applied after the injection of clonidine. Tail pinching is primarily activating cutaneous afferent pathways and is thus activating different afferent feedback circuits compared to EES. Another explanation for the observed differences could be that cats display a different noradrenergic receptor distribution compared to rats and humans.

Having the detailed knowledge about the expression pattern of $\alpha 2a$ and $\alpha 2c$ receptor subtypes, together with the evidence that EES modulates proprioceptive and LTMR afferents, we were able to tailor a targeted neuromodulation strategy to produce stepping after SCI. As electrical and pharmacological stimulation both exert their effects on the same neuronal structures, a direct interaction between the two interventions was observed in functional testing. Electrical or pharmacological intervention alone did not induce plantar and weight-bearing stepping. In contrast, when both interventions were applied simultaneously, all tested rats displayed robust, weight-bearing locomotor movements. This is in contrast to serotonergic or dopaminergic receptor modulation. Even though serotonergic agonists ($5HT_1$, $5HT_{2A}$, $5HT_7$) have been shown to potentiate the effects of EES, such a direct interaction as observed between EES and the dual $\alpha 2a$ antagonist/ $\alpha 2c$ agonist cannot be achieved.

5.4 Activity-dependent mechanisms mediated by enriched environment

Using mice placed in enriched environment (EE) or standard housing (SH), we provided a more detailed insight into activity-dependent mechanisms at the spinal level. We have shown that increased physical activity (in combination with more social interaction) mediates long-term plasticity of proprioceptive afferent neurons in DRG.

Consequently, rats and mice showed improved functional and sensory recovery after injury. The finding that EE primarily engages muscle spindle feedback mechanisms involved in the transmission of proprioceptive information is critically important. Several labs have previously shown that mice lacking functional muscle spindles showed a defective rearrangement of intraspinal pathways involved in the generation of locomotion, which diminished recovery of stepping after SCI (12). Our findings provide a direct link between muscle spindle feedback and neuronal activity to induce plasticity after injury. Overall, we here demonstrate the importance of muscle spindle feedback underlying physical activity and recovery of function after injury. Our findings suggest EE as a way to boost axonal plasticity, i.e. to enhance functional recovery after SCI.

5.5 The detailed mechanistic understanding of the applied neuromodulation allows the design of more precise clinical interventions

Despite lacking mechanistic understanding about how EES mediates its effects to produce locomotion after SCI, functional improvements in patients with relatively simple stimulation protocols have been reported in the past. Nevertheless, there is critical need for the detailed understanding of the underlying mechanisms of the applied therapeutical intervention (114). The mechanistic understanding of EES and EE presented here has the potential to further optimise or combine current stimulation strategies with the goal to enhance functional improvements after SCI.

Furthermore, in patients with a more severe SCI, the effects of EES may need further enhancement in order to induce meaningful functional outcomes. A specific pharmacological intervention targeting large-diameter afferent fibers may help to achieve this enhancement.

Altogether, the findings presented here may lead to more specific therapy interventions in the future and establish a framework to design more efficient neuromodulation strategies to reverse paralysis in humans one day.

PUBLICATIONS & CONTRIBUTIONS

Deconstruction of the sensorimotor circuits engaged by electrical spinal cord stimulation that restore locomotion after paralysis. Kay Bartholdi^{*}, Quentin Barraud^{*}, Andreas Rowald, Emanuele Formento, Nicholas D James, Thomas Hutson, Newton Cho, Claudia Kathe, Jordan Squair, Laetitia Baud, Nathalie Mestdagh, Eric Jnoff, Silvestro Micera, Simone Di Giovanni, Pavel Musienko, Marco Capogrosso & Grégoire Courtine. ^{*}Equally contributing authors. *In preparation*.

I planned and coordinated the experiments for this study under the supervision of Grégoire Courtine and Pavel Musienko. Together with Quentin Barraud and Thomas Hutson I established and performed calcium imaging experiments in DRGs. Together with Laetitia Baud I performed behavioral trainings and recordings in several groups of rats and mice. With Nicholas James I established the DREADD inactivating experiments in PV^{Cre} rats and collected the electrophysiology data presented in this study. I performed CLARITY experiments together with Newton Cho and Quentin Barraud. Together with Claudia Kathe I established the rabies tracing experiments in neonate mice. Anatomical pictures were acquired under the lead of Quentin Barraud. Modeling experiments were conducted by Marco Capogrosso, Emanuele Formento and Andreas Rowald. The single-cell sequencing database was available on-line and the data was analyzed by Jordan Squair. Arnaud Bichat performed the main surgical procedures in rats. Analysis of calcium imaging data was performed by Thomas Hutson at Imperial College London. Reflex analysis was performed by Emanuele Formento, Andreas Rowald and by me. I processed and analyzed all anatomical and functional data presented in this study. I wrote the manuscript, prepared figures and performed statistical analysis on the results shown in this thesis. I am currently preparing additional experiments that will be published together with the here presented results. Together with Grégoire Courtine and Quentin Barraud I am preparing a manuscript for publication for which all authors will contribute to its editing.

Activity-dependent recovery after spinal cord injury involves a druggable epigenetic mechanism. T. H. Hutson, C. Kathe, I. Palmisano, K. Bartholdi, A. Hervera, F. De Virgiliis, E. McLachlan, L. Zhou, G. Kong, Q. Barraud, M. C. Danzi, A. Medrano-Fernandez, J. Lopez-Atalaya, A. L. Boutillier, S. H. Sinha, A. K. Singh, P. Chaturbedy, L. D. F. Moon, T. K. Kundu, J. L. Bixby, V. P. Lemmon, A. Barco, G. Courtine[#], and S. Di Giovanni[#]. [#]Co-senior authors. *In revision*.

For this study, I was involved in establishing calcium imaging experiments in Lausanne for Thomas Hutson, first author of this paper and collaborator from London. Furthermore I maintained and coordinated several transgenic mouse lines described in this paper, such as the *Egr3*^{-/-} knockout or PV^{Cre} mouse lines. I performed reflex recordings in contused rats to evaluate changes in muscle responses after CBP treatment over time. Lastly, I worked on the figures for this paper together with Thomas Hutson and Claudia Kathe, the two first authors of this paper.

LIST OF ABBREVIATIONS

A	AAV	Adeno-associated Virus
	ASIA	American Spinal Injury Association
B	BWS	Body Weight Support
C	CNO	Clozapine-N-Oxide
	CNS	Central Nervous System
D	DoF	Degrees of Freedom
	DREADD	Designer Receptor Exclusively activated by designer drug
E	EES	Epidural electrical stimulation
	EMG	Electromyography
G	GFAP	Glial Fibrillary Acidic Protein
	GFP	Green Fluorescent Protein
M	MTP	Metatarsophalange
N	NA	Noradrenaline
P	PC	Principal Component
S	SCI	Spinal Cord Injury
T	TA	Tibialis Anterior
V	vGlut2	Vesicular Glutamate transporter 2
	VL	Vastus Lateralis
#	5HT	Serotonin

REFERENCES

1. Fawcett JW. Recovery from spinal cord injury: regeneration, plasticity and rehabilitation. *Brain*. 2009 Jun 1;132(6):1417–8.
2. Dobkin BH, Havton LA. Basic Advances and New Avenues in Therapy of Spinal Cord Injury. *Annu Rev Med*. 2004 Feb;55(1):255–82.
3. Dobkin BH, Dobkin BH. The clinical science of neurologic rehabilitation. 2nd ed. New York: Oxford University Press; 2003. 599 p. (Contemporary neurology series).
4. Somers MF. Spinal cord injury: functional rehabilitation. Upper Saddle River, N.J.: Pearson Education; 2010.
5. Gordon T, Mao J. Muscle atrophy and procedures for training after spinal cord injury. *Phys Ther*. 1994 Jan;74(1):50–60.
6. Herman R, He J, D’Luzansky S, Willis W, Dilli S. Spinal cord stimulation facilitates functional walking in a chronic, incomplete spinal cord injured. *Spinal Cord*. 2002 Feb;40(2):65–8.
7. Graupe D, Kohn K. Transcutaneous functional neuromuscular stimulation of certain traumatic complete thoracic paraplegics for independent short-distance ambulation. *Neurol Res*. 1997 Jun;19(3):323–33.
8. Edgerton VR, Tillakaratne NJK, Bigbee AJ, de Leon RD, Roy RR. Plasticity of the spinal neural circuitry after injury. *Annu Rev Neurosci*. 2004 Jul 21;27(1):145–67.
9. Pivetta C, Esposito MS, Sigrist M, Arber S. Motor-Circuit Communication Matrix from Spinal Cord to Brainstem Neurons Revealed by Developmental Origin. *Cell*. 2014 Jan;156(3):537–48.
10. Sherrington CS. Flexion-reflex of the limb, crossed extension-reflex, and reflex stepping and standing. *J Physiol*. 1910 Apr 26;40(1–2):28–121.
11. Courtine G, Gerasimenko Y, van den Brand R, Yew A, Musienko P, Zhong H, et al. Transformation of nonfunctional spinal circuits into functional states after the loss of brain input. *Nat Neurosci*. 2009 Oct;12(10):1333–42.
12. Takeoka A, Vollenweider I, Courtine G, Arber S. Muscle Spindle Feedback Directs Locomotor Recovery and Circuit Reorganization after Spinal Cord Injury. *Cell*. 2014 Dec;159(7):1626–39.
13. Lavrov I, Gerasimenko YP, Ichiyama RM, Courtine G, Zhong H, Roy RR, et al. Plasticity of Spinal Cord Reflexes After a Complete Transection in Adult Rats: Relationship to Stepping Ability. *J Neurophysiol*. 2006 Oct;96(4):1699–710.

14. Lallemand F, Ernfors P. Molecular interactions underlying the specification of sensory neurons. *Trends Neurosci.* 2012 Jun;35(6):373–81.
15. Stuart DG, Hultborn H. Thomas Graham Brown, Anders Lundberg, and the neural control of stepping. *Brain Res Rev.* 2008 Nov;59(1):74–95.
16. Windhorst U. Muscle proprioceptive feedback and spinal networks. *Brain Res Bull.* 2007 Jul;73(4–6):155–202.
17. Kröger S. Proprioception 2.0: novel functions for muscle spindles. *Curr Opin Neurol.* 2018 Aug;1.
18. Jankowska E. Interneuronal relay in spinal pathways from proprioceptors. *Prog Neurobiol.* 1992;38(4):335–78.
19. Akay T, Tourtellotte WG, Arber S, Jessell TM. Degradation of mouse locomotor pattern in the absence of proprioceptive sensory feedback. *Proc Natl Acad Sci.* 2014 Nov 25;111(47):16877–82.
20. Abraira VE, Ginty DD. The Sensory Neurons of Touch. *Neuron.* 2013 Aug;79(4):618–39.
21. Bourane S, Grossmann KS, Britz O, Dalet A, Del Barrio MG, Stam FJ, et al. Identification of a Spinal Circuit for Light Touch and Fine Motor Control. *Cell.* 2015 Jan;160(3):503–15.
22. Koch SC, Del Barrio MG, Dalet A, Gatto G, Günther T, Zhang J, et al. ROR β Spinal Interneurons Gate Sensory Transmission during Locomotion to Secure a Fluid Walking Gait. *Neuron.* 2017 Dec;96(6):1419–1431.e5.
23. Bouyer LJG, Rossignol S. Contribution of Cutaneous Inputs From the Hindpaw to the Control of Locomotion. II. Spinal Cats. *J Neurophysiol.* 2003 Dec;90(6):3640–53.
24. Duysens J, Pearson KG. The role of cutaneous afferents from the distal hindlimb in the regulation of the step cycle of thalamic cats. *Exp Brain Res.* 1976 Jan 26;24:245–55.
25. Leem JW, Willis WD, Chung JM. Cutaneous sensory receptors in the rat foot. *J Neurophysiol.* 1993 May;69(5):1684–99.
26. Seki K, Perlmutter SI, Fetz EE. Sensory input to primate spinal cord is presynaptically inhibited during voluntary movement. *Nat Neurosci.* 2003 Dec;6(12):1309–16.
27. Bourane S, Duan B, Koch SC, Dalet A, Britz O, Garcia-Campmany L, et al. Gate control of mechanical itch by a subpopulation of spinal cord interneurons. *Science.* 2015 Oct 30;350(6260):550–4.
28. Peirs C, Williams S-PG, Zhao X, Walsh CE, Gedeon JY, Cagle NE, et al. Dorsal Horn Circuits for Persistent Mechanical Pain. *Neuron.* 2015 Aug;87(4):797–812.

29. Confais J, Kim G, Tomatsu S, Takei T, Seki K. Nerve-Specific Input Modulation to Spinal Neurons during a Motor Task in the Monkey. *J Neurosci*. 2017 Mar 8;37(10):2612–26.
30. Todd AJ. Neuronal circuitry for pain processing in the dorsal horn. *Nat Rev Neurosci*. 2010 Dec;11(12):823–36.
31. Anderson MA, O'Shea TM, Burda JE, Ao Y, Barlatey SL, Bernstein AM, et al. Required growth facilitators propel axon regeneration across complete spinal cord injury. *Nature*. 2018 Sep;561(7723):396–400.
32. Dobkin B, Barbeau H, Deforge D, Ditunno J, Elashoff R, Apple D, et al. The Evolution of Walking-Related Outcomes Over the First 12 Weeks of Rehabilitation for Incomplete Traumatic Spinal Cord Injury: The Multicenter Randomized Spinal Cord Injury Locomotor Trial. *Neurorehabil Neural Repair*. 2007 Jan;21(1):25–35.
33. Ichiyama RM, Gerasimenko YP, Zhong H, Roy RR, Edgerton VR. Hindlimb stepping movements in complete spinal rats induced by epidural spinal cord stimulation. *Neurosci Lett*. 2005 Aug;383(3):339–44.
34. van den Brand R, Heutschi J, Barraud Q, DiGiovanna J, Bartholdi K, Huerlimann M, et al. Restoring Voluntary Control of Locomotion after Paralyzing Spinal Cord Injury. *Science*. 2012 Jun 1;336(6085):1182–5.
35. Fuentes R, Petersson P, Siesser WB, Caron MG, Nicolelis MAL. Spinal Cord Stimulation Restores Locomotion in Animal Models of Parkinson's Disease. *Science*. 2009 Mar 20;323(5921):1578–82.
36. Limousin P, Krack P, Pollak P, Benazzouz A, Ardouin C, Hoffmann D, et al. Electrical Stimulation of the Subthalamic Nucleus in Advanced Parkinson's Disease. *N Engl J Med*. 1998 Oct 15;339(16):1105–11.
37. Cameron T. Safety and efficacy of spinal cord stimulation for the treatment of chronic pain: a 20-year literature review. *J Neurosurg*. 2004 Mar;100(3 Suppl Spine):254–67.
38. Minassian K, McKay WB, Binder H, Hofstoetter US. Targeting Lumbar Spinal Neural Circuitry by Epidural Stimulation to Restore Motor Function After Spinal Cord Injury. *Neurotherapeutics*. 2016 Apr;13(2):284–94.
39. Capogrosso M, Milekovic T, Borton D, Wagner F, Moraud EM, Mignardot J-B, et al. A brain–spine interface alleviating gait deficits after spinal cord injury in primates. *Nature*. 2016 Nov 9;539(7628):284–8.
40. Minassian K, Jilge B, Rattay F, Pinter MM, Binder H, Gerstenbrand F, et al. Stepping-like movements in humans with complete spinal cord injury induced by epidural stimulation of the lumbar cord: electromyographic study of compound muscle action potentials. *Spinal Cord*. 2004 Jul;42(7):401–16.

41. Wagner FB, Mignardot J-B, Le Goff-Mignardot CG, Demesmaeker R, Komi S, Capogrosso M, et al. Targeted neurotechnology restores walking in humans with spinal cord injury. *Nature*. 2018 Nov;563(7729):65–71.
42. Musienko PE, Bogacheva IN, Gerasimenko YP. Significance of peripheral feedback in the generation of stepping movements during epidural stimulation of the spinal cord. *Neurosci Behav Physiol*. 2007 Feb;37(2):181–90.
43. Wenger N, Moraud EM, Gandar J, Musienko P, Capogrosso M, Baud L, et al. Spatiotemporal neuromodulation therapies engaging muscle synergies improve motor control after spinal cord injury. *Nat Med*. 2016 Feb;22(2):138–45.
44. Hentall ID, Mesigil R, Pinzon A, Noga BR. Temporal and Spatial Profiles of Pontine-Evoked Monoamine Release in the Rat's Spinal Cord. *J Neurophysiol*. 2003 Jun;89(6):2943–51.
45. Agnati LF, Guidolin D, Guescini M, Genedani S, Fuxe K. Understanding wiring and volume transmission. *Brain Res Rev*. 2010 Sep;64(1):137–59.
46. Musienko P, van den Brand R, Maerzendorfer O, Larmagnac A, Courtine G. Combinatory Electrical and Pharmacological Neuroprosthetic Interfaces to Regain Motor Function After Spinal Cord Injury. *IEEE Trans Biomed Eng*. 2009 Nov;56(11):2707–11.
47. Forssberg H, Grillner S. The locomotion of the acute spinal cat injected with clonidine i.v. *Brain Res*. 1973 Feb 14;50(1):184–6.
48. Dietz V, Wirz M, Colombo G, Curt A. Locomotor capacity and recovery of spinal cord function in paraplegic patients: a clinical and electrophysiological evaluation. *Electroencephalogr Clin Neurophysiol Mot Control*. 1998 Apr;109(2):140–53.
49. Philipp M, Brede M, Hein L. Physiological significance of α_2 -adrenergic receptor subtype diversity: one receptor is not enough. *Am J Physiol-Regul Integr Comp Physiol*. 2002 Aug;283(2):R287–95.
50. Kanagy NL. α_2 -adrenergic receptor signalling in hypertension. *Clin Sci*. 2005 Nov 1;109(5):431–7.
51. Ahlquist RP. A study of the adrenotropic receptors. *Am J Physiol-Leg Content*. 1948 Jun;153(3):586–600.
52. Bylund DB. Subtypes of alpha2-adrenoceptors: pharmacological and molecular biological evidence converge. *Trends Pharmacol Sci*. 1988 Oct;9(10):356–61.
53. Barbeau H, Norman KE. The effect of noradrenergic drugs on the recovery of walking after spinal cord injury. *Spinal Cord*. 2003 Mar;41(3):137–43.
54. Chau C, Barbeau H, Rossignol S. Early Locomotor Training With Clonidine in Spinal Cats. *J Neurophysiol*. 1998 Jan;79(1):392–409.

55. Docherty JR. Subtypes of functional alpha1- and alpha2-adrenoceptors. *Eur J Pharmacol.* 1998 Nov 13;361(1):1–15.
56. Surprenant A, North RA. Mechanism of synaptic inhibition by noradrenaline acting at alpha 2-adrenoceptors. *Proc R Soc Lond B Biol Sci.* 1988 Jun 22;234(1274):85–114.
57. Shen KZ, North RA, Surprenant A. Potassium channels opened by noradrenaline and other transmitters in excised membrane patches of guinea-pig submucosal neurones. *J Physiol.* 1992 Jan;445:581–99.
58. Bylund DB, Blaxall HS, Iversen LJ, Caron MG, Lefkowitz RJ, Lomasney JW. Pharmacological characteristics of alpha2-adrenergic receptors: comparison of pharmacologically defined subtypes with subtypes identified by molecular cloning. *Mol Pharmacol.* 1992 Jul;42(1):1–5.
59. Uhlen S, Lindblom J, Tiger G, Wikberg JES. Quantification of alpha2a and alpha2c adrenoceptors in the rat striatum and in different regions of the spinal cord. *Acta Physiol Scand.* 1997 Aug;160(4):407–12.
60. Nicholas AP, Hökfelt T, Pieribone VA. The distribution and significance of CNS adrenoceptors examined with in situ hybridization. *Trends Pharmacol Sci.* 1996 Jul;17(7):245–55.
61. Huang Y, Stamer WD, Anthony TL, Kumar DV, St John PA, Regan JW. Expression of alpha(2)-adrenergic receptor subtypes in prenatal rat spinal cord. *Brain Res Dev Brain Res.* 2002 Feb 28;133(2):93–104.
62. Rosin DL, Zeng D, Stornetta RL, Norton FR, Riley T, Okusa MD, et al. Immunohistochemical localization of alpha 2a-adrenergic receptors in catecholaminergic and other brainstem neurons in the rat. *Neuroscience.* 1993 Sep;56(1):139–55.
63. Gold MS, Dastmalchi S, Levine JD. Alpha2-adrenergic receptor subtypes in rat dorsal root and superior cervical ganglion neurons. *Pain.* 1997 Jan;69(1–2):179–90.
64. Rosin DL, Talley EM, Lee A, Stornetta RL, Gaylinn BD, Guyenet PG, et al. Distribution of alpha2c-adrenergic receptor-like immunoreactivity in the rat central nervous system. *J Comp Neurol.* 1996 Aug 12;372(1):135–65.
65. Nicholas AP, Pieribone V, Hökfelt T. Distributions of mRNAs for alpha2-adrenergic receptor subtypes in rat brain: An in situ hybridization study: ALPHA-2 RECEPTOR mRNA SUBTYPES IN RAT BRAIN. *J Comp Neurol.* 1993 Feb 22;328(4):575–94.
66. Stone LS, Broberger C, Vulchanova L, Wilcox GL, Hökfelt T, Riedl MS, et al. Differential distribution of alpha2A and alpha2C adrenergic receptor immunoreactivity in the rat spinal cord. *J Neurosci Off J Soc Neurosci.* 1998 Aug 1;18(15):5928–37.

67. Hein L, Altman JD, Kobilka BK. Two functionally distinct α 2-adrenergic receptors regulate sympathetic neurotransmission. *Nature*. 1999 Nov;402(6758):181–4.
68. Brede M. α 2-adrenergic Receptor Subtypes. Novel Functions Uncovered in Gene-Targeted Mouse Models. *Biol Cell*. 2004 Jun;96(5):343–8.
69. Riddell JS, Jankowska E, Eide E. Depolarization of group II muscle afferents by stimuli applied in the locus coeruleus and raphe nuclei of the cat. *J Physiol*. 1993 Feb;461:723–41.
70. Chau C, Barbeau H, Rossignol S. Effects of Intrathecal α 1- and α 2-Noradrenergic Agonists and Norepinephrine on Locomotion in Chronic Spinal Cats. *J Neurophysiol*. 1998 Jun;79(6):2941–63.
71. Lavrov I, Dy CJ, Fong AJ, Gerasimenko Y, Courtine G, Zhong H, et al. Epidural Stimulation Induced Modulation of Spinal Locomotor Networks in Adult Spinal Rats. *J Neurosci*. 2008 Jun 4;28(23):6022–9.
72. Musienko P, van den Brand R, Marzendorfer O, Roy RR, Gerasimenko Y, Edgerton VR, et al. Controlling Specific Locomotor Behaviors through Multidimensional Monoaminergic Modulation of Spinal Circuitries. *J Neurosci*. 2011 Jun 22;31(25):9264–78.
73. Ladenbauer J, Minassian K, Hofstoetter US, Dimitrijevic MR, Rattay F. Stimulation of the Human Lumbar Spinal Cord With Implanted and Surface Electrodes: A Computer Simulation Study. *IEEE Trans Neural Syst Rehabil Eng*. 2010 Dec;18(6):637–45.
74. Moraud EM, Capogrosso M, Formento E, Wenger N, DiGiovanna J, Courtine G, et al. Mechanisms Underlying the Neuromodulation of Spinal Circuits for Correcting Gait and Balance Deficits after Spinal Cord Injury. *Neuron*. 2016 Feb;89(4):814–28.
75. Danner SM, Hofstoetter US, Freundl B, Binder H, Mayr W, Rattay F, et al. Human spinal locomotor control is based on flexibly organized burst generators. *Brain*. 2015 Mar;138(3):577–88.
76. Formento E, Minassian K, Wagner F, Mignardot JB, Le Goff-Mignardot CG, Rowald A, et al. Electrical spinal cord stimulation must preserve proprioception to enable locomotion in humans with spinal cord injury. *Nat Neurosci* [Internet]. 2018 Oct 31 [cited 2018 Nov 9]; Available from: <http://www.nature.com/articles/s41593-018-0262-6>
77. van Praag H, Kempermann G, Gage FH. Neural consequences of environmental enrichment. *Nat Rev Neurosci*. 2000 Dec;1(3):191–8.
78. Kempermann G, Kuhn HG, Gage FH. More hippocampal neurons in adult mice living in an enriched environment. *Nature*. 1997 Apr;386(6624):493–5.

79. Alwis DS, Rajan R. Environmental enrichment and the sensory brain: the role of enrichment in remediating brain injury. *Front Syst Neurosci* [Internet]. 2014 Sep 2 [cited 2018 Oct 12];8. Available from: <http://journal.frontiersin.org/article/10.3389/fnsys.2014.00156/abstract>
80. Lopez-Atalaya JP, Ciccarelli A, Viosca J, Valor LM, Jimenez-Minchan M, Canals S, et al. CBP is required for environmental enrichment-induced neurogenesis and cognitive enhancement: CBP and environment-induced neurogenesis. *EMBO J*. 2011 Oct 19;30(20):4287–98.
81. Nithianantharajah J, Hannan AJ. Enriched environments, experience-dependent plasticity and disorders of the nervous system. *Nat Rev Neurosci*. 2006 Sep;7(9):697–709.
82. de Groot PCE, Hjeltnes N, Heijboer AC, Stal W, Birkeland K. Effect of training intensity on physical capacity, lipid profile and insulin sensitivity in early rehabilitation of spinal cord injured individuals. *Spinal Cord*. 2003 Dec;41(12):673–9.
83. Teeter L, Gassaway J, Taylor S, LaBarbera J, McDowell S, Backus D, et al. Relationship of physical therapy inpatient rehabilitation interventions and patient characteristics to outcomes following spinal cord injury: The SCIRehab project. *J Spinal Cord Med*. 2012 Nov;35(6):503–26.
84. Dominici N, Keller U, Vallery H, Friedli L, van den Brand R, Starkey ML, et al. Versatile robotic interface to evaluate, enable and train locomotion and balance after neuromotor disorders. *Nat Med*. 2012 Jul;18(7):1142–7.
85. Asboth L, Friedli L, Beauparlant J, Martinez-Gonzalez C, Anil S, Rey E, et al. Cortico–reticulo–spinal circuit reorganization enables functional recovery after severe spinal cord contusion. *Nat Neurosci*. 2018 Apr;21(4):576–88.
86. Shealy CN, Mortimer JT, Reswick JB. Electrical inhibition of pain by stimulation of the dorsal columns: preliminary clinical report. *Anesth Analg*. 1967 Aug;46(4):489–91.
87. Cameron T. Safety and efficacy of spinal cord stimulation for the treatment of chronic pain: a 20-year literature review. *J Neurosurg*. 2004 Mar;100(3 Suppl Spine):254–67.
88. Angeli CA, Boakye M, Morton RA, Vogt J, Benton K, Chen Y, et al. Recovery of Over-Ground Walking after Chronic Motor Complete Spinal Cord Injury. *N Engl J Med*. 2018 Sep 27;379(13):1244–50.
89. Gill ML, Grahm PJ, Calvert JS, Linde MB, Lavrov IA, Strommen JA, et al. Neuromodulation of lumbosacral spinal networks enables independent stepping after complete paraplegia. *Nat Med*. 2018 Nov;24(11):1677–82.

90. Capogrosso M, Wenger N, Raspopovic S, Musienko P, Beauparlant J, Bassi Luciani L, et al. A Computational Model for Epidural Electrical Stimulation of Spinal Sensorimotor Circuits. *J Neurosci*. 2013 Dec 4;33(49):19326–40.
91. Danner SM, Shevtsova NA, Frigon A, Rybak IA. Computational modeling of spinal circuits controlling limb coordination and gaits in quadrupeds. *eLife* [Internet]. 2017 Nov 22 [cited 2018 Nov 26];6. Available from: <https://elifesciences.org/articles/31050>
92. Mayer WP, Murray AJ, Brenner-Morton S, Jessell TM, Tourtellotte WG, Akay T. Role of muscle spindle feedback in regulating muscle activity strength during walking at different speed in mice. *J Neurophysiol*. 2018 Nov;120(5):2484–97.
93. Arber S, Ladle DR, Lin JH, Frank E, Jessell TM. ETS Gene *Er81* Controls the Formation of Functional Connections between Group Ia Sensory Afferents and Motor Neurons. *Cell*. 2000 May;101(5):485–98.
94. Gerasimenko YP, Lavrov IA, Courtine G, Ichiyama RM, Dy CJ, Zhong H, et al. Spinal cord reflexes induced by epidural spinal cord stimulation in normal awake rats. *J Neurosci Methods*. 2006 Oct;157(2):253–63.
95. Philipp M, Hein L. Adrenergic receptor knockout mice: distinct functions of 9 receptor subtypes. *Pharmacol Ther*. 2004 Jan;101(1):65–74.
96. Altman JD, Trendelenburg AU, MacMillan L, Bernstein D, Limbird L, Starke K, et al. Abnormal regulation of the sympathetic nervous system in α_2A -adrenergic receptor knockout mice. *Mol Pharmacol*. 1999 Jul;56(1):154–61.
97. Jnoff E, Christophe B, Collart P, Coloretti F, Debeuckelaere A, De Ryck M, et al. Discovery of Selective α_2C Adrenergic Receptor Agonists. *ChemMedChem*. 2012 Mar 5;7(3):385–90.
98. Delaunois A, De Ron P, Dedoncker P, Rosseels M-L, Cornet M, Jnoff E, et al. Advantageous safety profile of a dual selective α_{2C} agonist/ α_{2A} antagonist antinociceptive agent. *Fundam Clin Pharmacol*. 2014 Aug;28(4):423–38.
99. Gong S, Zheng C, Doughty ML, Losos K, Didkovsky N, Schambra UB, et al. A gene expression atlas of the central nervous system based on bacterial artificial chromosomes. *Nature*. 2003 Oct;425(6961):917–25.
100. Häring M, Zeisel A, Hochgerner H, Rinwa P, Jakobsson JET, Lönnerberg P, et al. Neuronal atlas of the dorsal horn defines its architecture and links sensory input to transcriptional cell types. *Nat Neurosci*. 2018 Jun;21(6):869–80.
101. Quevedo J, Stecina K, Gosgnach S, McCrea DA. Stumbling Corrective Reaction During Fictive Locomotion in the Cat. *J Neurophysiol*. 2005 Sep;94(3):2045–52.

102. Burke RE, Degtyarenko AM, Simon ES. Patterns of Locomotor Drive to Motoneurons and Last-Order Interneurons: Clues to the Structure of the CPG. *J Neurophysiol*. 2001 Jul;86(1):447–62.
103. McCREA DA. Neuronal Basis of Afferent-evoked Enhancement of Locomotor Activity. *Ann N Y Acad Sci*. 1998 Nov;860(1 NEURONAL MECH):216–25.
104. Arber S. Motor Circuits in Action: Specification, Connectivity, and Function. *Neuron*. 2012 Jun;74(6):975–89.
105. Alvarez FJ, Jonas PC, Sapir T, Hartley R, Berrocal MC, Geiman EJ, et al. Postnatal phenotype and localization of spinal cord V1 derived interneurons. *J Comp Neurol*. 2005 Dec 12;493(2):177–92.
106. Molgaard S, Ulrichsen M, Boggild S, Holm M-L, Vaegter C, Nyengaard J, et al. Immunofluorescent visualization of mouse interneuron subtypes. *F1000Research* [Internet]. 2014 Nov 20 [cited 2018 Oct 9]; Available from: <http://f1000research.com/articles/3-242/v2>
107. Angeli CA, Edgerton VR, Gerasimenko YP, Harkema SJ. Altering spinal cord excitability enables voluntary movements after chronic complete paralysis in humans. *Brain*. 2014 May;137(5):1394–409.
108. Liu Y, Latremoliere A, Li X, Zhang Z, Chen M, Wang X, et al. Touch and tactile neuropathic pain sensitivity are set by corticospinal projections. *Nature*. 2018 Sep;561(7724):547–50.
109. Pratt CA, Jordan LM. Ia inhibitory interneurons and Renshaw cells as contributors to the spinal mechanisms of fictive locomotion. *J Neurophysiol*. 1987 Jan;57(1):56–71.
110. Zhang J, Lanuza GM, Britz O, Wang Z, Siembab VC, Zhang Y, et al. V1 and V2b Interneurons Secure the Alternating Flexor-Extensor Motor Activity Mice Require for Limbed Locomotion. *Neuron*. 2014 Apr;82(1):138–50.
111. D. Laflamme O, Akay T. Excitatory and inhibitory crossed reflex pathways in mice. *J Neurophysiol* [Internet]. 2018 Oct 10 [cited 2018 Nov 26]; Available from: <https://www.physiology.org/doi/10.1152/jn.00450.2018>
112. Kim YS, Anderson M, Park K, Zheng Q, Agarwal A, Gong C, et al. Coupled Activation of Primary Sensory Neurons Contributes to Chronic Pain. *Neuron*. 2016 Sep;91(5):1085–96.
113. Valjent E, Bertran-Gonzalez J, Hervé D, Fisone G, Girault J-A. Looking BAC at striatal signaling: cell-specific analysis in new transgenic mice. *Trends Neurosci*. 2009 Oct;32(10):538–47.
114. Arber S, Costa RM. Connecting neuronal circuits for movement. *Science*. 2018 Jun 29;360(6396):1403–4.

115. Lähdesmäki J, Sallinen J, MacDonald E, Kobilka BK, Fagerholm V, Scheinin M. Behavioral and neurochemical characterization of alpha(2A)-adrenergic receptor knockout mice. *Neuroscience*. 2002;113(2):289–99.
116. Musienko P, Courtine G, Tibbs JE, Kilimnik V, Savochin A, Garfinkel A, et al. Somatosensory control of balance during locomotion in decerebrated cat. *J Neurophysiol*. 2012 Apr 15;107(8):2072–82.
117. Mestre C, Péliissier T, Fialip J, Wilcox G, Eschaliier A. A method to perform direct transcutaneous intrathecal injection in rats. *J Pharmacol Toxicol Methods*. 1994 Dec;32(4):197–200.
118. De la Calle JL, Paíno CL. A procedure for direct lumbar puncture in rats. *Brain Res Bull*. 2002 Nov 30;59(3):245–50.
119. Gu Z, Kalambogias J, Yoshioka S, Han W, Li Z, Kawasawa YI, et al. Control of species-dependent cortico-motoneuronal connections underlying manual dexterity. *Science*. 2017 Jul 28;357(6349):400–4.
120. Sathiyamurthy A, Johnson KR, Matson KJE, Dobrott CI, Li L, Ryba AR, et al. Massively Parallel Single Nucleus Transcriptional Profiling Defines Spinal Cord Neurons and Their Activity during Behavior. *Cell Rep*. 2018 Feb;22(8):2216–25.
121. Zeisel A, Hochgerner H, Lonnerberg P, Johnsson A, Memic F, van der Zwan J, et al. Molecular architecture of the mouse nervous system. 2018 Apr 6 [cited 2018 Dec 7]; Available from: <http://biorxiv.org/lookup/doi/10.1101/294918>
122. Lee E, Choi J, Jo Y, Kim JY, Jang YJ, Lee HM, et al. ACT-PRESTO: Rapid and consistent tissue clearing and labeling method for 3-dimensional (3D) imaging. *Sci Rep* [Internet]. 2016 May [cited 2018 Nov 28];6(1). Available from: <http://www.nature.com/articles/srep18631>
123. Tomer R, Ye L, Hsueh B, Deisseroth K. Advanced CLARITY for rapid and high-resolution imaging of intact tissues. *Nat Protoc*. 2014 Jul;9(7):1682–97.
124. Bria A, Iannello G. TeraStitcher - A tool for fast automatic 3D-stitching of teravoxel-sized microscopy images. *BMC Bioinformatics*. 2012;13(1):316.
125. Hines ML, Carnevale NT. The NEURON simulation environment. *Neural Comput*. 1997 Aug 15;9(6):1179–209.
126. Segev I, Fleshman JW, Burke RE. Computer simulation of group Ia EPSPs using morphologically realistic models of cat alpha-motoneurons. *J Neurophysiol*. 1990 Aug;64(2):648–60.
127. Stienen AHA, Schouten AC, Schuurmans J, van der Helm FCT. Analysis of reflex modulation with a biologically realistic neural network. *J Comput Neurosci*. 2007 Dec;23(3):333–48.

128. Jones KE, Bawa P. Computer Simulation of the Responses of Human Motoneurons to Composite 1A EPSPs: Effects of Background Firing Rate. *J Neurophysiol.* 1997 Jan;77(1):405–20.
129. McIntyre CC, Richardson AG, Grill WM. Modeling the Excitability of Mammalian Nerve Fibers: Influence of Afterpotentials on the Recovery Cycle. *J Neurophysiol.* 2002 Feb;87(2):995–1006.
130. Booth V, Rinzel J, Kiehn O. Compartmental Model of Vertebrate Motoneurons for Ca²⁺-dependent Spiking and Plateau Potentials Under Pharmacological Treatment. *J Neurophysiol.* 1997 Dec;78(6):3371–85.
131. Fleshman JW, Segev I, Burke RB. Electrotonic architecture of type-identified alpha-motoneurons in the cat spinal cord. *J Neurophysiol.* 1988 Jul;60(1):60–85.
132. McIntyre CC, Grill WM. Extracellular Stimulation of Central Neurons: Influence of Stimulus Waveform and Frequency on Neuronal Output. *J Neurophysiol.* 2002 Oct;88(4):1592–604.
133. Harrison PJ, Taylor A. Individual excitatory post-synaptic potentials due to muscle spindle Ia afferents in cat triceps surae motoneurons. *J Physiol.* 1981 Mar;312:455–70.
134. Scott JG, Mendell LM. Individual EPSPs produced by single triceps surae Ia afferent fibers in homonymous and heteronymous motoneurons. *J Neurophysiol.* 1976 Jul;39(4):679–92.
135. Munson JB, Fleshman JW, Sybert GW. Properties of single-fiber spindle group II EPSPs in triceps surae motoneurons. *J Neurophysiol.* 1980 Oct;44(4):713–25.
136. Prochazka A, Gorassini M. Ensemble firing of muscle afferents recorded during normal locomotion in cats. *J Physiol.* 1998 Feb;507(1):293–304.
137. Delp SL, Anderson FC, Arnold AS, Loan P, Habib A, John CT, et al. OpenSim: Open-Source Software to Create and Analyze Dynamic Simulations of Movement. *IEEE Trans Biomed Eng.* 2007 Nov;54(11):1940–50.
138. Johnson WL, Jindrich DL, Roy RR, Reggie Edgerton V. A three-dimensional model of the rat hindlimb: Musculoskeletal geometry and muscle moment arms. *J Biomech.* 2008;41(3):610–9.
139. Johnson WL, Jindrich DL, Hui Zhong, Roy RR, Edgerton VR. Application of a Rat Hindlimb Model: A Prediction of Force Spaces Reachable Through Stimulation of Nerve Fascicles. *IEEE Trans Biomed Eng.* 2011 Dec;58(12):3328–38.
140. He Z, Jin Y. Intrinsic Control of Axon Regeneration. *Neuron.* 2016 May;90(3):437–51.

141. Neumann S, Bradke F, Tessier-Lavigne M, Basbaum AI. Regeneration of sensory axons within the injured spinal cord induced by intraganglionic cAMP elevation. *Neuron*. 2002 Jun 13;34(6):885–93.
142. Neumann S, Woolf CJ. Regeneration of dorsal column fibers into and beyond the lesion site following adult spinal cord injury. *Neuron*. 1999 May;23(1):83–91.
143. Wahl AS, Omlor W, Rubio JC, Chen JL, Zheng H, Schroter A, et al. Asynchronous therapy restores motor control by rewiring of the rat corticospinal tract after stroke. *Science*. 2014 Jun 13;344(6189):1250–5.
144. Tourtellotte WG, Milbrandt J. Sensory ataxia and muscle spindle agenesis in mice lacking the transcription factor *Egr3*. *Nat Genet*. 1998 Sep;20(1):87–91.
145. Molteni R, Zheng J-Q, Ying Z, Gomez-Pinilla F, Twiss JL. Voluntary exercise increases axonal regeneration from sensory neurons. *Proc Natl Acad Sci*. 2004 Jun 1;101(22):8473–8.
146. Ickes BR, Pham TM, Sanders LA, Albeck DS, Mohammed AH, Granholm A-C. Long-Term Environmental Enrichment Leads to Regional Increases in Neurotrophin Levels in Rat Brain. *Exp Neurol*. 2000 Jul;164(1):45–52.
147. Rattazzi L, Piras G, Brod S, Smith K, Ono M, D'Acquisto F. Impact of Enriched Environment on Murine T Cell Differentiation and Gene Expression Profile. *Front Immunol* [Internet]. 2016 Sep 30 [cited 2018 Dec 15];7. Available from: <http://journal.frontiersin.org/Article/10.3389/fimmu.2016.00381/abstract>
148. Roth BL. DREADDs for Neuroscientists. *Neuron*. 2016 Feb;89(4):683–94.
149. Jin Q, Yu L-R, Wang L, Zhang Z, Kasper LH, Lee J-E, et al. Distinct roles of GCN5/PCAF-mediated H3K9ac and CBP/p300-mediated H3K18/27ac in nuclear receptor transactivation: Histone acetylation and gene activation. *EMBO J*. 2011 Jan 19;30(2):249–62.
150. Henry RA, Kuo Y-M, Andrews AJ. Differences in Specificity and Selectivity Between CBP and p300 Acetylation of Histone H3 and H3/H4. *Biochemistry*. 2013 Aug 27;52(34):5746–59.
151. Hu SC, Chrivia J, Ghosh A. Regulation of CBP-mediated transcription by neuronal calcium signaling. *Neuron*. 1999 Apr;22(4):799–808.
152. Chrivia JC, Kwok RPS, Lamb N, Hagiwara M, Montminy MR, Goodman RH. Phosphorylated CREB binds specifically to the nuclear protein CBP. *Nature*. 1993 Oct;365(6449):855–9.
153. Alarcón JM, Malleret G, Touzani K, Vronskaya S, Ishii S, Kandel ER, et al. Chromatin Acetylation, Memory, and LTP Are Impaired in CBP+/- Mice. *Neuron*. 2004 Jun;42(6):947–59.

154. Thompson PR, Wang D, Wang L, Fulco M, Pediconi N, Zhang D, et al. Regulation of the p300 HAT domain via a novel activation loop. *Nat Struct Mol Biol.* 2004 Apr;11(4):308–15.
155. Yuan LW, Giordano A. Acetyltransferase machinery conserved in p300/CBP-family proteins. *Oncogene.* 2002 Mar;21(14):2253–60.
156. Bangaru MLY, Meng J, Kaiser DJ, Yu H, Fischer G, Hogan QH, et al. Differential expression of CaMKII isoforms and overall kinase activity in rat dorsal root ganglia after injury. *Neuroscience.* 2015 Aug;300:116–27.
157. Chatterjee S, Mizar P, Cassel R, Neidl R, Selvi BR, Mohankrishna DV, et al. A Novel Activator of CBP/p300 Acetyltransferases Promotes Neurogenesis and Extends Memory Duration in Adult Mice. *J Neurosci.* 2013 Jun 26;33(26):10698–712.
158. Lim J-HA, Stafford BK, Nguyen PL, Lien BV, Wang C, Zukor K, et al. Neural activity promotes long-distance, target-specific regeneration of adult retinal axons. *Nat Neurosci.* 2016 Aug;19(8):1073–84.
159. Jaiswal PB, English AW. Chemogenetic enhancement of functional recovery after a sciatic nerve injury. Chan Y-S, editor. *Eur J Neurosci.* 2017 May;45(10):1252–7.
160. Tedeschi A, Nguyen T, Puttagunta R, Gaub P, Di Giovanni S. A p53-CBP/p300 transcription module is required for GAP-43 expression, axon outgrowth and regeneration. *Cell Death Differ.* 2009 Apr;16(4):543–54.
161. Gaub P, Joshi Y, Wuttke A, Naumann U, Schnichels S, Heiduschka P, et al. The histone acetyltransferase p300 promotes intrinsic axonal regeneration. *Brain.* 2011 Jul;134(7):2134–48.
162. Gaub P, Tedeschi A, Puttagunta R, Nguyen T, Schmandke A, Di Giovanni S. HDAC inhibition promotes neuronal outgrowth and counteracts growth cone collapse through CBP/p300 and P/CAF-dependent p53 acetylation. *Cell Death Differ.* 2010 Sep;17(9):1392–408.
163. Puttagunta R, Tedeschi A, Sória MG, Hervera A, Lindner R, Rathore KI, et al. PCAF-dependent epigenetic changes promote axonal regeneration in the central nervous system. *Nat Commun [Internet].* 2014 Dec [cited 2019 Jan 29];5(1). Available from: <http://www.nature.com/articles/ncomms4527>
164. Cho Y, Cavalli V. HDAC5 is a novel injury-regulated tubulin deacetylase controlling axon regeneration: HDAC5 controls axon regeneration. *EMBO J.* 2012 Jul 18;31(14):3063–78.
165. Cho Y, Sloutsky R, Naegle KM, Cavalli V. Injury-Induced HDAC5 Nuclear Export Is Essential for Axon Regeneration. *Cell.* 2013 Nov;155(4):894–908.

166. Rossignol S, Frigon A. Recovery of Locomotion After Spinal Cord Injury: Some Facts and Mechanisms. *Annu Rev Neurosci*. 2011 Jul 21;34(1):413–40.
167. Sandrow-Feinberg HR, Houle JD. Exercise after spinal cord injury as an agent for neuroprotection, regeneration and rehabilitation. *Brain Res*. 2015 Sep;1619:12–21.
168. Starkey ML, Bleul C, Kasper H, Mosberger AC, Zörner B, Giger S, et al. High-Impact, Self-Motivated Training Within an Enriched Environment With Single Animal Tracking Dose-Dependently Promotes Motor Skill Acquisition and Functional Recovery. *Neurorehabil Neural Repair*. 2014 Jul;28(6):594–605.
169. Jiang Y-Q, Zaimi B, Martin JH. Competition with Primary Sensory Afferents Drives Remodeling of Corticospinal Axons in Mature Spinal Motor Circuits. *J Neurosci*. 2016 Jan 6;36(1):193–203.
170. Keeler BE, Liu G, Siegfried RN, Zhukareva V, Murray M, Houle JD. Acute and prolonged hindlimb exercise elicits different gene expression in motoneurons than sensory neurons after spinal cord injury. *Brain Res*. 2012 Feb;1438:8–21.
171. Gomez-Pinilla F, Ying Z, Zhuang Y. Brain and Spinal Cord Interaction: Protective Effects of Exercise Prior to Spinal Cord Injury. Adlard PA, editor. *PLoS ONE*. 2012 Feb 22;7(2):e32298.

CURRICULUM VITAE

Name/ First name Bartholdi Kay-Alexander

Address Tälligstrasse 9a,
8570 Weinfelden, CH

Phone +41 (0)79 512 36 37

E-Mail kay.bartholdi@epfl.ch

Nationality Swiss

Date of birth November 26th 1986

Education

2014-present PhD candidate in neuroscience, Swiss Federal institute of Technology, Geneva (EPFL), Switzerland

2009-2011 Master in sport physiology, ETH Zurich
Mentor: Professor Dr. Grégoire Courtine

2006-2009 Bachelor in Life sciences and Technology, ETH Zurich

2001-2005 Kantonsschule Frauenfeld, Frauenfeld, Switzerland

Professional experience

2014-present PhD candidate in neuroscience, Swiss Federal institute of Technology, Geneva (EPFL), Switzerland

2012-2013 Research associate, Swiss Federal Institute of Technology, Lausanne (EPFL), Switzerland

2011-2012 Research associate, University of Zurich, Zurich, Switzerland

Languages

German Native

English Fluent

French Basic

Spanish Basic

Management skills

Project management of a team with several people with different backgrounds

Experience in presenting scientific data to large and diverse audiences

Time-management skills developed in a high-pressure environment

Publications

Deconstruction of the sensorimotor circuits engaged by electrical spinal cord stimulation that restore locomotion after paralysis. **Kay Bartholdi***, Quentin Barraud*, Andreas Rowald, Emanuele Formento, Nicholas D James, Thomas Hutson, Newton Cho, Claudia Kathe, Jordan Squair, Laetitia Baud, Nathalie Mestdagh, Eric Jnoff, Silvestro Micera, Simone Di Giovanni, Pavel Musienko, Marco Capogrosso & Grégoire Courtine. *Equally contributing authors. *In preparation.*

Activity-dependent recovery after spinal cord injury involves a druggable epigenetic mechanism. T. H. Hutson, C. Kathe, I. Palmisano, **K. Bartholdi**, A. Hervera, F. De Virgiliis, E. McLachlan, L. Zhou, G. Kong, Q. Barraud, M. C. Danzi, A. Medrano-Fernandez, J. Lopez-Atalaya, A. L. Boutillier, S. H. Sinha, A. K. Singh, P. Chaturbedy, L. D. F. Moon, T. K. Kundu, J. L. Bixby, V. P. Lemmon, A. Barco, G. Courtine[#], and S. Di Giovanni[#]. [#]Co-senior authors. *In revision.*

Restoring voluntary control of locomotion after paralyzing spinal cord injury. Rubia van den Brand, Janine Heutschi, Quentin Barraud, Jack DiGiovanna, **Kay Bartholdi**, Michèle Hürlimann, Lucia Friedli, Isabel Vollenweider, Eduardo Martin Moraud, Simone Duis, Nadia Dominici, Silvestro Micera, Pavel Musienko, Grégoire Courtine. *Science*, 2012.

Poster presentations

Poster at SfN in San Diego, 2018

Poster at ISRT in London, 2017 (winner of the ISRT poster price)

Poster at SfN in San Diego, 2016

Poster at SfN in Washington, 2014

Oral presentations

'Mechanisms through which epidural electrical stimulation restores locomotion after spinal cord injury'. Brain Mind Institute research day (June 2016), EPFL Lausanne, Switzerland.

